The use of fluorescence to probe the morphology changes in complex polymers

By

Marehette le Grange

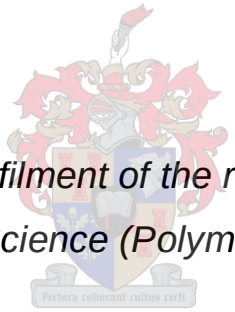

Thesis presented in partial fulfilment of the requirements for the degree of Master of Science (Polymer Science)

Supervisor: Prof Albert van Reenen
Co-supervisor: Dr Marietjie Lutz

University of Stellenbosch
Department of Chemistry and Polymer Science

March 2015

DECLARATION

By submitting this thesis/dissertation electronically, I declare that the entirety of the work contained therein is my own, original work, that I am the sole author thereof (save to the extent explicitly otherwise stated), that reproduction and publication thereof by Stellenbosch University will not infringe any third party rights and that I have not previously in its entirety or in part submitted it for obtaining any qualification.

March 2015

ABSTRACT

Impact polypropylene copolymers (IPC) are commercially used in a variety of applications. They are very complex materials and extensive studies have been conducted to understand the relationship between their chemical structure, morphology and impact properties. The distribution of ethylene propylene rubber (EPR) within IPC has drawn much attention but visualization of the morphology is difficult. In this study a fluorescent marker was used to probe the distribution of EPR within the crystalline and semi-crystalline fraction.

The EPR was removed from a commercial IPC and labelled with a fluorescent marker. In this study a method utilizing the hydrophilic nature of cellulose nanowhiskers (CNW) was developed to label the EPR. CNW were labelled with fluorescein-5'-isothiocyanate (FITC) and rhodamine B (RhB) using a one-step procedure. The labelled CNW were incorporated into the EPR by means of sonication. The mobility of the labelled CNW within the EPR film was investigated by confocal fluorescence microscopy (CFM), and showed that the labelled whiskers did not move within the EPR, thus substantiating the validity of this approach. The labelled EPR was recombined with the crystalline fraction by means of injection moulding and was analysed by CFM, and the distribution of the labelled EPR was evaluated. Confocal fluorescence microscopy showed an even distribution of the labelled rubber throughout the injection moulded sample.

The miscibility of two EPRs within the IPC matrix in the melt was also investigated using this technique. CFM showed that the technique has promise to prove miscibility or the lack thereof when chemically similar materials are combined in the presence of morphologically different matrix materials.

OPSOMMING

Impak polipropileen kopolimere (IPK) word kommersieel gebruik in ‘n wye reeks produkte. Die samestelling van hierdie kopolimere is baie ingewikkeld en uitgebreide studies is al gedoen om hul chemiese samestelling op molekulêre vlak te verstaan. Baie studies met betrekking tot die verspreiding van die etileen-propileen rubber (EPR) binne in hierdie impak polipropileen kopolimere is al gedoen, maar visualisering van die morfologie is moeilik en beperk. Hierdie kennis kan bydra tot die verbetering van hul chemiese eienskappe en toepassings. In hierdie studie word ’n fluorosserende merker gebruik om die verspreiding van die EPR binne die kristallyne en semi-kristallyne fraksie te ondersoek.

Die EPR is verwyder vanuit 'n kommersiële IPK en is gemerk met 'n fluoresserende merker. In hierdie studie is 'n metode ontwikkel om die EPR te merk deur gebruik te maak van die hidrofiliese eienskap van sellulose nanovesels (SNV). Die SNV is gemerk met fluoressien-5'-isotiosianaat (FITC) en rhodamien B (RhB) met behulp van 'n eenstap proses. Die gemerkte SNV is deur middel van sonikasie in die EPR versprei. Die mobiliteit van die gemerkte SNV binne-in die EPR film is ondersoek deur gefokusde fluoressensie mikroskopie (GFM) en het getoon dat die gemerkte vesels nie binne die EPR beweeg nie. Dit bevestig dus die geldigheid van hierdie benadering. Die gemerkte EPR is herkombineer met die kristallyne fraksie deur middel van spuitgiet en is geanaliseer deur GFM en die verspreiding van die gemerkte EPR is geëvalueer. GFM het 'n eweredige verspreiding van die gemerkte rubber regdeur die moster wat gespuitgiet is getoon.

Die mengbaarheid van twee EPRs binne-in die IPK matriks is ook ondersoek deur gebruik te maak van hierdie tegniek. GFM het getoon dat hierdie tegniek waarde inhou om te bewys dat twee produkte mengbaar is of nie, al word hulle geherkombineer word met ‘n matriks wat morfologiese van hul verskil.

DEDICATION:

In loving memory of my parents Nico and Sarie le Grange, for their support, sacrifices and love through all the years.

ACKNOWLDGEMENTS

While my name may be on the front cover, the rest of this thesis would not exist were it not for the input of some remarkable individuals.

Prof. Albert van Reenen, my promoter, study leader and reliable source of critique and encouragement. Without the financial support you secured, this thesis would never have been. Thank you so much for your guidance and leadership during this project, it has been a privilege to work with you.

Dr. Marietjie Lutz, for your guidance and support as my co-promotor. Your insight was invaluable, and your encouragement made a major difference to me.

Dr. Maggie Brand, Divann Robertson, Madeleine du Toit and the rest of the olefins and nanowhiskers group. Thank you for your friendship, help and support. It was an honour working with you.

Kobie Bisschoff, for your tremendous support this year in helping me manage a full time job and a masters and come out relatively unscathed.

My family, for their support through and encouragement, who have never been further than a phone call away (if not closer). Thank you for everything you are to me**,** I love you all very much.

My **dearest loving husband**, for all the coffee and tea, and for making the guest room your own when I needed the space to work. Thanks for your love and support and words cannot describe my appreciation.

Lastly, I would like to thank the following people for their vital contributions to this thesis:

1. Sasol polymers for funding and polymers
2. Mr. Mohamed Jaffer (UCT, for your assistance on the TEM)
3. Lize Engelbrecht and her team at the CAF Cell imaging unit
4. Dr. R. Bucher, iThemba Labs (WAXD)
5. The Department of Chemistry and Polymer Science

God, the author of my breath and sustainer of my being. All honour and acknowledgement belongs to You.

TABLE OF CONTENTS

LIST OF FIGURES

LIST OF TABLES

LIST OF EQUATIONS

LIST OF ABBREVIATIONS

BC	Bacterial cellulose
BODIPY	4,4-difluoro-4-bora-3a,4a-diaza-s-indacenes
CFM	Confocal fluorescent microscopy
CN	Cellulose nanocrystals
CNW	Cellulose nanowhiskers
CNW/FITC	Cellulose nanowhiskers labelled with FITC
CNW/RhB	Cellulose nanowhiskers labelled with rhodamine B
DSC	Differential scanning calorimetry
EPC	Ethylene propylene copolymers
EPR	Ethylene-propylene rubber
EPR (com)	Ethylene propylene rubber extracted from commercial impact polypropylene copolymer
FITC	Fluorescein-5'-isothiocyanate
I_{α}	Alpha cellulose
I_{β}	Beta cellulose
I_{004}	Crystallite indice parallel to fibre axis
I_{110}	Crystallite indice perpendicular to tot fibre axis
$I_{11\bar{0}}$	Crystallite indice perpendicular to tot fibre axis
I_{200}	Crystallite indice perpendicular to tot fibre axis
$I_{amorphous}$	Amorphous index
IPC	Impact polypropylene copolymers
iPP	Isotactic polypropylene
MA	Maleic anhydride
MCC	Microcrystalline cellulose
PEPNP	Polyoxyethylene (9) nonylphenyl ether
PP	Polypropylene
PE	Polyethylene
RBITC	Rhodamine B isothiocyanate.
RhB	Rhodamine B
TEM	Transmission electron microscopy
T_c	Crystallization temperature
Tg	Glass transition temperature
T_m	Melting temperature
wt%	Weight percentage
X_c	Percentage crystallinity of CNW
XRD	X-ray diffraction

CHAPTER 1

Introduction and objectives

1.1 Introduction

Cellulose is one of the most ubiquitous and abundant biological polymers. Over the last decade much research has been done in this field due to the wide range of applications it offers. They are composed of long glucose molecules; these chains form an intricate web which consists of cellulosic fibres that provide structure and support.[1] Cellulose fibres consist of chains that are highly organized and packed, as well as regions which are randomly orientated. The organized area is known as the crystalline region and the disorganized area is known as the amorphous part of these cellulose fibres. The crystalline regions of this polymer, when isolated as nano-sized artifacts, have proven to be of great value. These nanocrystalline materials have shown significant promise in the field of nanocomposites.[2] The nanocrystals can be isolated through methods such as acid hydrolysis[3] and sonication[4] of micro crystalline cellulose (MCC). The most effective method described thus far is the use of 64% sulphuric acid.[5]. The nanocrystals are known by many different terms in literature. They are most commonly referred to as cellulose nanocrystals, or cellulose nanowhiskers (CNW).The name comes from the rod-like nanoparticles, which were characterized using transmission electron microscopy (TEM).[5]

Producing effective nanocomposites of hydrophobic polymers with CNW is a big challenge, as compatibility of CNW with hydrophobic polymers is difficult to achieve. The CNW form stable aqueous dispersions due to hydrogen bonding.[2,6] Alternative routes have been explored to use CNW in non-aqueous and non-polar systems. . The surface of the CNW can be modified to obtain non-flocculated dispersions in an appropriate organic medium. This can be done by coating the surface of CNW with surfactants that have polar heads and long hydrophobic tails, or by grafting hydrophobic chains to the CNW surfaces.[7] The most common method is to mix the aqueous suspension with a surfactant such as a phosphoric ester of polyoxyethylene (9) nonylphenyl ether (PEPNP).[8] The CNW can then be incorporated into an organic solvent like toluene.

Impact polypropylene copolymers (IPC) are very complex materials. IPCs are commercially used in a wide range of applications such as automotive applications, household electric goods, packaging etc.[9] These complex copolymers consist of an isotactic polypropylene (iPP) matrix, a semi-crystalline mixture of ethylene-propylene copolymers, and an amorphous phase consisting of ethylene-propylene rubber (EPR). These components and their dispersion within the material have an effect on the morphology and complexity of the overall product. The different components

influence the properties and overall performance of the products directly. Extensive studies have been conducted to investigate the relationship between chemical structure, morphology and the properties of IPC, but the morphology on macroscopic levels is still not clear.[10-12]

Fluorescent dyes have been used widely in different applications, and are known for their ability to act as fluorescent markers, especially for cell imaging. The fluorophores can either associate with certain molecules or be attached through covalent bonds.[13] Fluorescein-5'-isothiocyanate (FITC) is an important fluorophore in applications involving confocal fluorescent microscopy (CFM) due to the dye's excellent fluorescent quantum yield, high molar absorptivity and fair solubility in water.[14] Another commonly used fluorescent marker is rhodamine B (RhB). Together with FITC, these markers have been used to label CNW[15,16] to investigate their dispersion in nano-composites. The homogeneity of the labelled whiskers can be evaluated by the fluorescent intensity by means of a fluorescent microscopy.[17,18] Attaching fluorescent markers to polyolefins is usually quite a strenuous process. The microstructure of maleic anhydride (MA) grafted onto ethylene propylene copolymers (EPC) was observed by looking at the distribution of MA which was labelled with a fluorescent dye.[19]

As previously mentioned, IPC are extremely complex and numerous studies have been conducted to investigate their morphology, especially the EPR distribution, to gain a better understanding of these materials.[20] In this study a fluorescent marker was used to probe the dispersion of EPR within the iPP matrix and semi-crystalline regions.

1.2 Objectives

The objective of this study was to incorporate a fluorescent marker into EPR to create a method for tracking the EPR dispersion within the crystalline phase. If successful, this will contribute to a better understanding of the morphology of IPCs. As it is unlikely for a fluorescent molecule to attach to a hydrocarbon like EPR, the hydrophobic nature of CNW was utilized to achieve this goal. The fluorescent marker FITC was attached to the CNW, after which the labelled whiskers were incorporated into EPR. The fluorescently marked EPR was then recombined with the crystalline and semi-crystalline fractions using injection moulding. The goal was to ascertain an idea of where the EPR particles migrate to within the crystalline fraction through the use of fluorescent microscopy. Additionally, the miscibility of two different molecular weight EPRs was also investigated by incorporating two different fluorescent markers. In order to achieve this objective, the project was divided into different sections:

1. Isolating the CNW.
2. Labelling the CNW with FITC.

3. Extracting the EPR from IPC.
4. Developing a method for the incorporation of labelled CNW into extracted EPR.
5. Recombining the fluorescent marked EPR with the crystalline fraction using injection moulding.
6. Evaluating the labelling method using an alternative EPR fraction.
7. Evaluating the miscibility of the two different molecular weight EPRs through fluorescent labelling.

1.3 Thesis outline

The following is an overview of the structure of the thesis.

Chapter 1: Presents the introduction and objective of this study.

Chapter 2: Discusses the history and background of the materials and analytical techniques.

Chapter 3: Gives a full overview of the experimental procedures and techniques which were used in this study.

Chapter 4: Discusses the results and characterization of the cellulose nanowhiskers.

Chapter 5: Discusses the results of the extracted of the ethylene propylene rubber from IPC648, the labelling of the rubber and the recombination of the two fractions**.**

Chapter 6: Discusses the results from the alternative ethylene propylene rubber and the miscibility of the two different rubber fractions.

Chapter 7: Deals with the conclusion and future recommendations

1.4 References

1. Fleming K, Gray DG, Matthews S. Chemistry-A European Journal 2001; 7(9):1831-1836.

2. Siró I, Plackett D. Cellulose 2010; 17(3):459-494.

3. Camacho F, Gonzalez-Tello P, Jurado E, Robles A. Journal of Chemical Technology and Biotechnology 1996; 67(4):350-356.

4. Capadona JR, Shanmuganathan K, Trittschuh S, Seidel S, Rowan SJ, Weder C. Biomacromolecules 2009; 10(4):712-716.

5. Bondeson D, Mathew A, Oksman K. Cellulose 2006; 13(2):171-180.

6. Dufresne A. Molecules 2010; 15(6):4111-4128.

7. Kamel S. Express Polymer Letters 2007; 1(9):546-575.

8. Bonini C, Heux L, Cavaillé J, Lindner P, Dewhurst C, Terech P. Langmuir 2002; 18(8):3311- 3314.

9. Mncwabe S, Luruli N, Marantos E, Nhlapo P, Botha L. Macromolecular Symposia 2012; 313(1):33-42.

10. Zhang C, Shangguan Y, Chen R, Wu Y, Chen F, Zheng Q, Hu G. Polymer 2010; 51(21):4969-4977.

11. Simonazzi T, Cecchin G, Mazzullo S. Progress in Polymer Science 1991; 16(2–3):303-329.

12. Van Reenen A, Basson N. Express Polymer Letters 2012; 6(5): 427-436

13. Dong S, Roman M. Journal of the American Chemical Society 2007; 129(45):13810-13811.

14. Gonçalves MST. Chemical reviews 2008; 109(1):190-212.

15. JunkeráNielsen L, Eyley S, Thielemans W, Aylott J. Chemical Communications 2010; 46(47):8929-8931.

16. Yang Q, Pan X. Journal of Applied Polymer Science 2010; 117(6):3639-3644.

17. Huang J, Li C, Gray DG. American Chemical Society Sustainable Chemistry & Engineering 2013; 1(9):1160-1164.

18. Aloisi G, Costantino U, Latterini L, Nocchetti M, Camino G, Frache A. Journal of Physics and Chemistry of Solids 2006; 67(5):909-914.

19. Zhang M, Duhamel J, van Duin M, Meessen P. Macromolecules 2004; 37(5):1877- 1890.

20. Macko T, Ginzburg A, Remerie K, Bruell R. Macromolecular Chemistry and Physics 2012; 213(9):937-944.

CHAPTER 2

Relevant background

2.1 Propylene homo- and copolymers

Polypropylene (PP) is a polyolefin, and is one of the most extensively used polymers for the fabrication of plastic articles. One of the major advantages of PP is its high performance to cost ratio. PP has excellent mechanical properties, such as high strength, heat resistance and processability. One major limitation of PP is the low impact resistance especially at low temperatures. [1,2]

The word olefin comes from the word 'olefiant', which means oil-forming gas. Dutch chemists first used this word to describe ethylene gas that produced oil when chlorine was added to it. Polypropylene was polymerized for the first time by Berthelot in 1869 through a reaction involving concentrated sulphuric acid, but the product was considered of no importance at the time. In 1894 a linear, low molecular weight polyethylene (PE) was produced by von Pechman through the decomposition of diazomethane.[3,4] The cationic polymerization of polypropylene was attempted by Fontana in 1952, but the resultant product was of little use as a structural material. The following year Ziegler managed to produce high molecular weight polyolefins, as well as high density PE. In 1954, crystalline PP was first synthesized by Natta, followed shortly by Ziegler, using organo-metallic catalysts, which are based on aluminium and titanium.[5,6] Crystalline (isotactic) PP was commercially first produced in 1957 by Hercules, Montecatini and Farbwerke-Hoechst. Today, PP is one of the most commercially used polymers.[3,5]

In industry, PP is divided into two types. The first type is PP homopolymer, and the second random and block copolymers. A wide variety of PP with various molecular weight distributions is being produced depending on the numerous applications. [7] PP homopolymer can further be described in terms of stereoregularity, which can also be referred to as tacticity. Head-to-tail addition of the monomer units result in an even distribution of the methyl groups along the polymer chain. When the methyl groups have the same relative configuration (facing in the same direction) in relation to the polymer backbone it is called isotactic PP. Syndiotactic PP is also a result of head-to-tail addition, but here the methyl groups have an alternating relative configuration with regards to the polymer backbone. When there is no consistent configuration of the methyl

distribution PP is said to be atactic.[5,6] In isotactic PP, the orientation of the methyl groups enable the polymer chains orientate and form close packed highly ordered crystal structures, making isotactic PP more crystalline compared to syndiotactic and atatic PP.

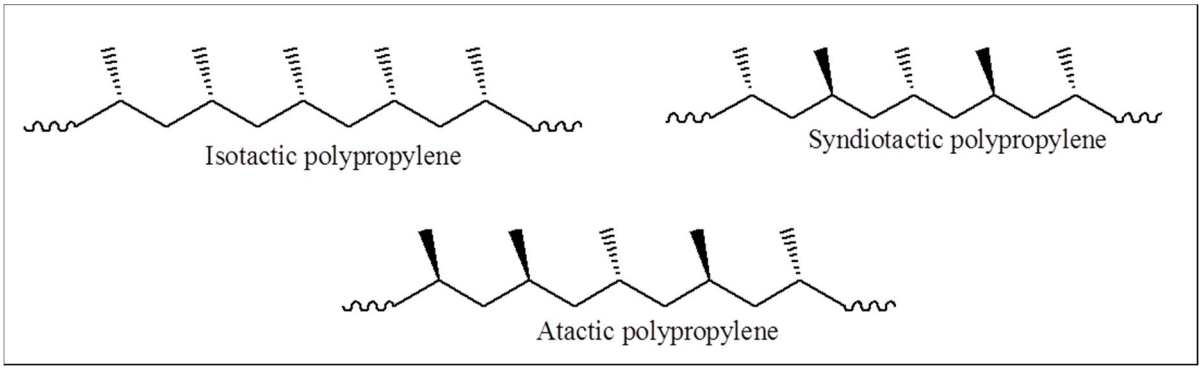

Figure 2.1: Different relative orientation of the methyl groups in polypropylene

The overall crystallinity of iPP, which relates both to stereoregularity and molecular weight, contributes to the high melting temperature which allows the exploitation of its properties over a wide temperature range.[8] However, due to a fairly high glass transition temperature (Tg), PP homopolymer is too brittle for applications with temperatures below 0 ^{o}C and lacks transparency. The range of applications can be expanded if the clarity and flexibility of PP can be improved.[1,2,7] The second type of PP is the random and block copolymers. These polymers are manufactured by the addition of a second monomer or monomers to the propylene. This has an effect of lowering of the Tg of the final product. The monomer that would be typically added is ethylene. The most commonly used comonomer is ethylene. The addition of ethylene could lead to the formation of (a) semicrystalline propylene-ethylene copolymers (also called “randoms”), (b) ethylene-propylene rubber, or, if the ethylene is added in a sequential fashion after the initial propylene polymerization, (c) impact polypropylene copolymers (IPCs).[2,9,10]

2.1.1 Impact polypropylene copolymers

Commercially, IPC are some of the most widely used polymers due to their very unique properties. They fall under a unique group of polyolefins which is classed as “in reactor polymer blends,” the aim of which is to improve the impact strength of polypropylene, especially at low temperatures. This is done by the synthesis of a rubbery ethylene-propylene copolymer (EPR) directly in the reactor.[11-13] The rubber particles play an active role in distributing the stress around the particles, through rubber cavitation and plastic deformation. This helps rigid PP to improve its impact strength.[1]

IPCs are also known as heterophasic ethylene/propylene copolymers and consist of a crystalline PP matrix (major component), an EPR phase, and a variety of propylene and ethylene-rich copolymers which make the chemical composition and molecular architecture very complex.[12-14] The crystalline PP matrix is also referred to as the continuous phase, with the EPR uniformly dispersed within the matrix. It is important that the EPR is homogenously dispersed, and the size is controlled to obtain the right balance between toughness and impact strength.[5,15]

IPC are made either by blending PP homopolymer with rubber, or sequential copolymerization. Producing IPC through copolymerization has more advantages with regards to the control of the reaction and final properties.[16,17] In the production of random copolymers, the ethylene co-monomer units are incorporated randomly, leading to defects in the long PP chains. This leads to a decrease in the isotactic segments and improves the thermal and processing properties compared to PP homopolymer. This synthesis takes place in a single reactor. However, the most common methods of synthesizing IPC are sequential copolymerization. The polymerization consists of two phases. In the first reactor iPP is synthesized with the help of a Ziegler-Natta catalyst. The second stage is a gas-phase fluidised reactor with a mixture of ethylene and propylene. The iPP, along with unreacted monomer and catalyst, is transferred to the second stage after a predetermined time. The EPR is produced here within the iPP matrix. The process occurring in the second reactor forms a very important part in determining the morphology which influences the final properties. The resultant copolymer system includes iPP, EPR, a series of EP segmented copolymers with different lengths of ethylene and propylene, and an ethylene homopolymer. This highly complex mixture is largely due to the heterogeneous catalyst used in the process. It is worth noting that the reactor build-up and stickiness during the second stage of the process is prevented by the iPP formed in the first reactor.[9,17,18]

As mentioned before, the final properties of IPC are strongly dependant on their microstructure.[11] The morphology of the heterophasic polymer particles can be described in terms of the relative amounts and nature of each polymeric phase. The growing polymer must be produced at the catalyst surface, and therefore depends on the morphology of the microparticles.[19] The complex nature of IPCs has been well documented, but not a lot has been reported on the physical relationship between the molecular structure and the chemical composition.[20] Previous investigations on the composition and microstructure of IPC have shown a multiphase copolymeric system consisting of PP homopolymer, different length PE-PP block copolymers, random copolymers of ethylene-propylene, and to a much lesser extent, small amounts of PE homopolymer. PE and PP are generally immiscible in blend, and research has proposed that the ethylene-propylene copolymers act as compatibilizer between the disperse phase and the iPP matrix.[13,16,21]

Kakugo *et al.*[22] proposed that in the first reactor iPP forms a double grain structure. Debling and Ray based their model on this finding. According to Debling and Ray's model, the iPP particles form a few mesoparticles, called polymer globules by Kakugo *et al*.[18,19,19,22,23] The mesoparticles formed by the primary polymer particles contain catalyst crystallites. These structures also contain macropores, which separates the mesoparticles and micropores from the microparticles. In the second reactor, where the EPR is formed, the EPR expands progressively into the small micropores and finally into the larger macropores. [18]

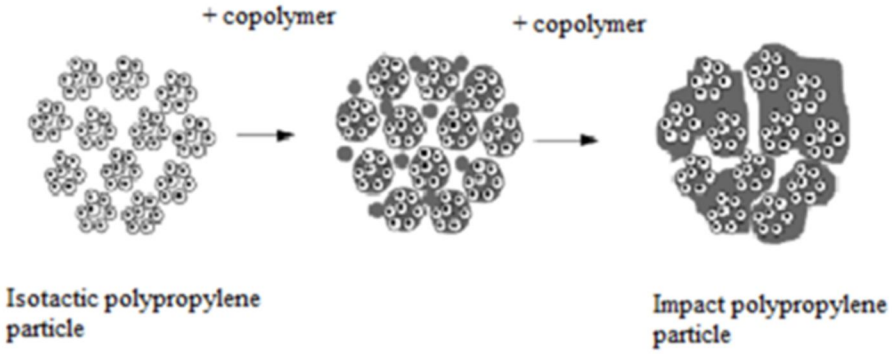

Figure 2.2: Proposed model for the particle growth in impact polypropylene [24]

Kittilsen and McKenna proposed that the EPR initially forms inside the PP homopolymer, then seeps out to partially fill the micropores and macropores of the matrix, and finally onto the surface of the polymer particles. The EPR layer creates stresses in the viscoelastic PP homopolymer, which leads to the formation of cracks through which the EPR can flow into the pores.[25] According to Cecchin *et al*.[26] the PP particles formed in the first reactor are composed of a number of polymer mesoparticles. They proposed that the catalyst fragments are located at the surface of these mesoparticles due to segregation during hompolymerization. This leads to EPR polymerizing at the surface of the mesoparticles and filling the pores between them, hence the continuous EPR network within the PP matrix.[27] Urdampilleta *et al*.[18] investigated the particle morphology before and after the gas phase reaction. They found that the iPP particles were formed by a small number of mesoparticles. These particles were bigger in size than those observed by Kakugo *et al*.[22] They also showed that most of the EPR was finely dispersed within the mesoparticles, while some EPR broke the iPP matrix and flowed into the macropores between the mesoparticles, smoothing the surface of the iPP as polymerization occurs.[18,27]

Chen *et al*.[27] first investigated the morphology of iPP in the first reactor and later the effect of thermal treatment on the morphology of IPCs. They concluded that the iPP particles exhibit a tertiary architecture which consists out of many secondary subglobules, which are in turn formed by a number of primary globules. The large macropores between the subglobules and finely

distributed micropores forms a network of pores inside the IPP particles. The ethylene-propylene co-monomers can diffuse into the macro and micropores, which contain distributed fragments of catalyst, leading to the formation of the elastomeric phase inside.[27] When the IPCs were exposed to thermal treatment they found a multiple-layered core-shell structure of the dispersed EP phase. The core was formed of PE-rich polymer, with EPR as an intermediate layer and an outer shell comprised of EP block copolymer. This indicated that the performance of IPC was dependent on both the architecture of the original IPC particles and the subsequent melt-process.[28] In 2009 Zhou *et al*.[13] proved the existence of a quaternary structure (nascent particle). The proposed structure is seen in Figure 2.3. According to their findings, the control of the iPP produced in the first stage together with the design of the catalyst structure is crucial to obtain the morphology required for IPCs to have the desired balance of stiffness and toughness.[29]

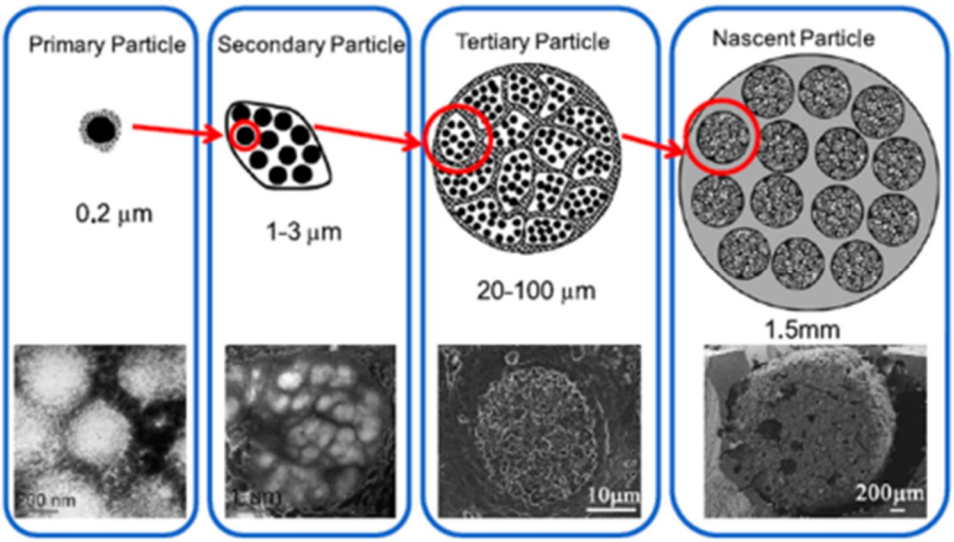

Figure 2.3: The architecture of a nascent particle of impact polypropylene with quaternary structure [29]

Extensive research has been done on the morphology, composition and phase structure of IPCs. Although progress has been made in this field, there are still fundamental aspects of these complex polymers that are not known.[13,20,29] It is clear that the size and distribution of the rubber particles after processing influences the impact properties. It should also be mentioned that the final morphology of the polymer can be influenced by the processing parameters.[13,20,28] Therefore, detailed analysis of the microstructure of IPC is needed to achieve a better understanding of the location and function of each component. This will lead to a better understanding of the final product and its properties.

2.2 Cellulose

Cellulose is one of the most abundant biological polymers on earth and was first discovered and isolated from green plants by Anselme Payen in 1838.[30] [31] Cellulose is a support structure for plants on a cellular level, and is also present in bacteria, fungi, algae and even some animals.[32] Although wood is the most commercially exploited natural resource of cellulose, cellulose can also be produced by non-plant species. One such example is bacterial cellulose (BC), which is produced by the gram-negative bacteria, *Acetobacter xylimum*. It produces cellulose with a higher degree of crystallinity, purity and mechanical properties, and has shown great potential in biomedical applications.[33] Extracting pure cellulose from wood pulp is a twofold process which involves extracting and bleaching.[34,35]

Before cellulose was discovered as the "sugar of the plant cell wall", it was widely used as an energy source for building materials and clothing. Cellulose was first used as a chemical raw material by the Hyatt Manufacturing Company, who produced the first thermoplastic polymer, Celluloid, through the chemical modification of cellulose in 1870.[36] Cellulose is naturally organized as microfibrils linked together to form an intricate web of cellulose fibers, which helps with structure and support.[37] They fall into the class of carbohydrates with a chemical formula consisting of carbon, hydrogen and oxygen ($C_6H_{10}O_5$), as first determined by Herman Staudinger in 1920. In 1992, Kobayashi and Shoda were the first to chemically synthesize cellulose.[36]

The difference between the properties of cellulose, and carbohydrates with low molecular masses, is due to the intermolecular interactions, chain lengths, cross-linking reactions and the distribution of the repeat units. A linear homopolysaccharide composed of two anhydroglucose rings, joined via a β-1,4 glycosidic linkage form the basic repeat unit, of the cellulose polymer shown in Figure 2.4.[32,36]

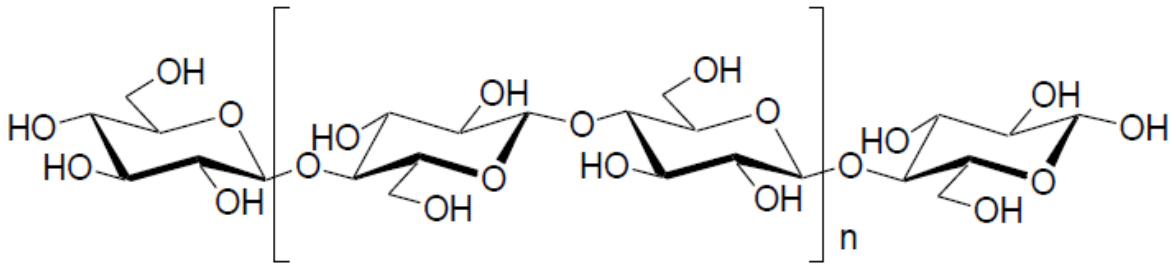

Figure 2.4: Cellulose repeat unit [32]

There are three hydroxyl groups on each monomer and their ability to form hydrogen bonds plays a significant role in the physical properties of cellulose.[38] This molecular structure contributes to

the hydrophilicity, degradability, chirality and functionalization of the hydroxyl group. To accommodate these hydroxyl groups, the pyranose rings are orientated to follow the chair conformation with the hydroxyl groups in an equatorial position.[31] Cellulose does not occur in nature as isolated individual molecules, but occurs as assemblies of individual cellulose chain forming fibres. The morphological hierarchy of cellulose is as follows; the elementary fibrils cluster together to form microfibrils which assembles into fibres.[36,39,40] The individual microfibrils have diameters ranging from 2 to 20 nm and can be considered as a string of cellulose crystals joined by disordered amorphous regions.[32] The distinct fiber morphology determines the biological function of cellulose as well as the various end applications.[32,38]

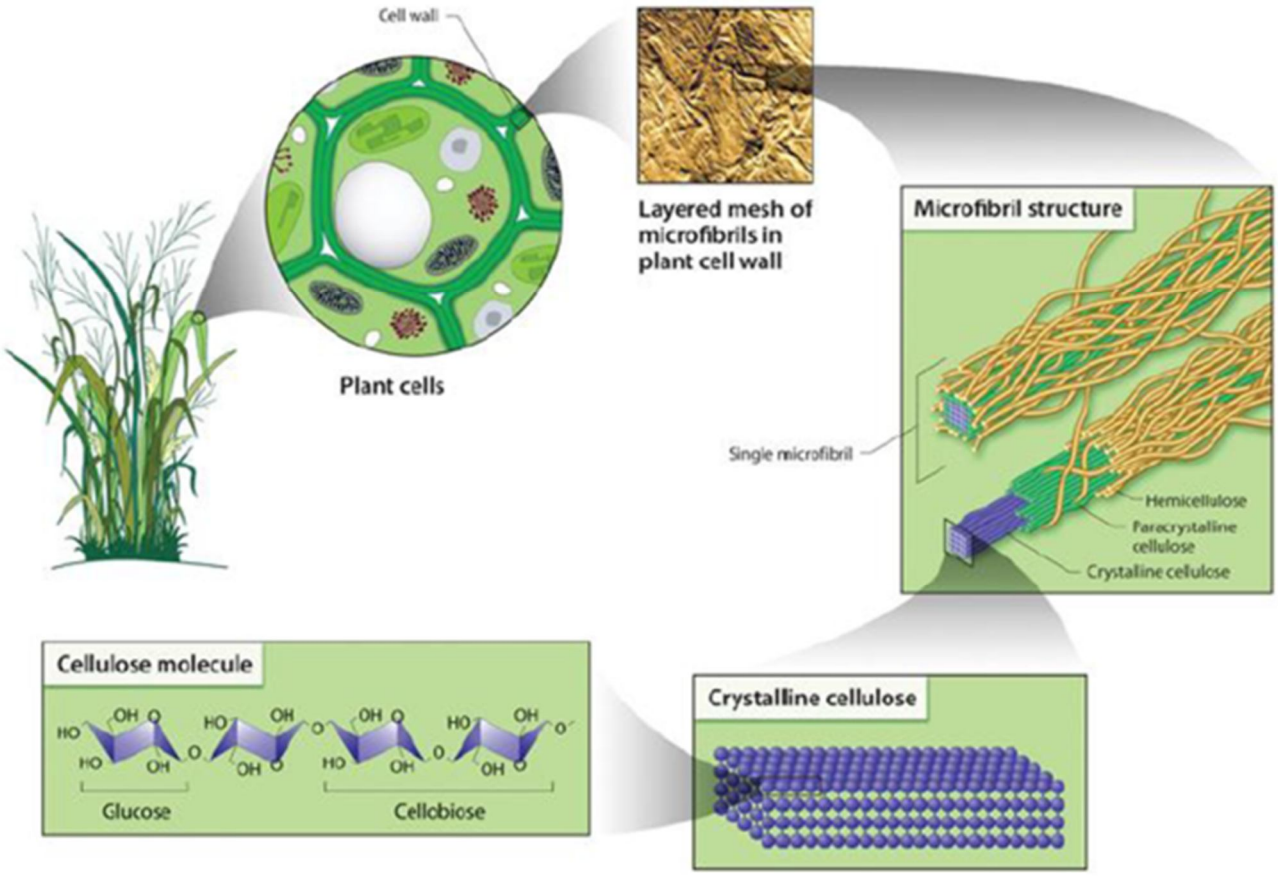

Figure 2.5: The hierarchical structure of cellulose in plants[32]

The inter- and intra-molecular interaction networks and the molecular orientation of the crystalline regions can differ, and gives rise to cellulose polymorphs and allomorphs.[40] There are six documented polymorphs of cellulose (I, II, III_I, III_{II}, IV_I and IV_{II}), which can be interchangeable depending on the chemical treatment and source as shown in Figure 2.6.[32,40]

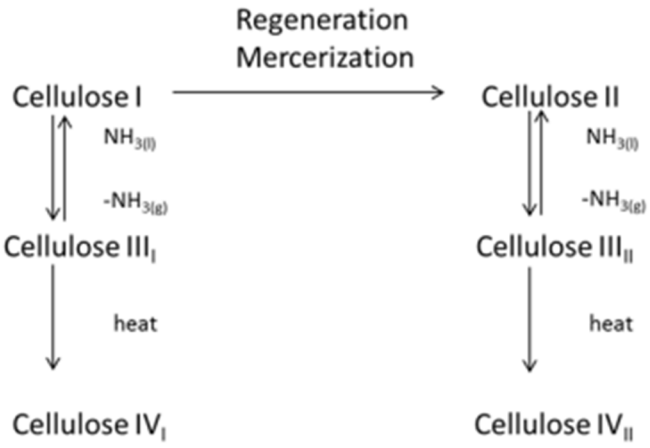

Figure 2.6: Interconversion of cellulose polymorphs [31]

In the 1980s, Attala and Vanderhart were the first to establish that Cellulose I, also known as native cellulose, has two different crystalline forms; alpha cellulose and beta cellulose (I_α and I_β).[41] The conformation of their polysaccharide chains is similar, although the pattern of the hydrogen bonding is different; I_α has a parallel configuration and I_β has an antiparallel configuration. The ratio of these polymorphs (I_α/I_β) depends on the origin of the cellulose. Cellulose I has a high modulus and crystallinity and exhibits the best mechanical properties but is thermodynamically less stable than cellulose II.[32,36,42]

Cellulose I has a crystal nature which is referred to as monoclinic sphenodic structure. As mentioned earlier, the hydrogen bonds play a significant role in directing the crystalline packing. Solid cellulose forms microcrystalline structures with areas of higher order crystallinity and areas with a lower order of crystallinity.[38] The amorphous regions are dispersed as chain dislocations on segments along the elementary fibril. In these regions the microfibrils are distorted by internal strain leading to unordered packing. Cellulose is resistant to strong alkali but the amorphous regions of the structures are susceptible to acid hydrolysis.[38,43] The breakdown of the amorphous regions releases microcrystalline regions as monocrystallites, which are also referred to as cellulose nanowhiskers. The moncrystallite cellulose has diameter of 5 – 20 nm and lengths between 100 – 300 nm.[33,44]

2.2.1 Cellulose Nanowhiskers

Cellulose nanowhiskers (CNW) have garnered a great deal of interest in applications like nano-composites due to their mechanical properties and renewability. Developing bionanocomposites from renewable biomass is a viable supplement to materials produced from mineral and fossil fuels.[45] CNW have shown great potential as a reinforcing material. The name, CNW, is attributing

to their needle-like or rod-like structure. The term “whiskers” in CNW was designated due to these elongated crystal structures, but they can also be referred to as nanocrystals (NC), nanoparticles etc.[39,46]

The most common method used to produce CNW from cellulose fibres is through acid hydrolysis. Other methods such as mechanical disintegration and enzymatic hydrolysis have also been used.[47] The first report of controlled sulphuric acid-catalysed degradation of cellulose fibres was in 1950, and the first cellulose crystals in solution were reported by Ranby and Noe in 1961. [48,39,43] The amorphous regions within the cellulose fibres are more susceptible to acid hydrolysis than the crystalline regions. The diffusion of hydronium ions into the amorphous areas is assisted by free volume effects. Degradation of the crystalline regions will follow if time, temperature or acid concentration permits hydrolysis. The hydrolysis conditions and the effect on the properties of the resulting CNW were first researched by Dong *et al*.[49,50] [32,43,45,51] The controlled acid hydrolysis of the amorphous region of cellulose results in highly crystalline monocrystals referred to as CNW. Although CNW can be obtained through hydrochloric acid and sulphuric acid hydrolysis, it has been proven by Araki *et al*.[52,53] that the dispersibility of the CNW in water is better for the whiskers obtained from the sulphuric acid. The negatively charged sulphate groups on the surface of the whiskers provide electrostatic stabilization in aqueous solutions.[32,46] Figure 2.7 shows the esterification of the hydroxyl groups on the surface of the CNW.[54] Later Marchessault *et al*.[55] demonstrated that the electrostatic forces enable the whiskers to form a chiral nematic liquid through self-ordering.[39,46]

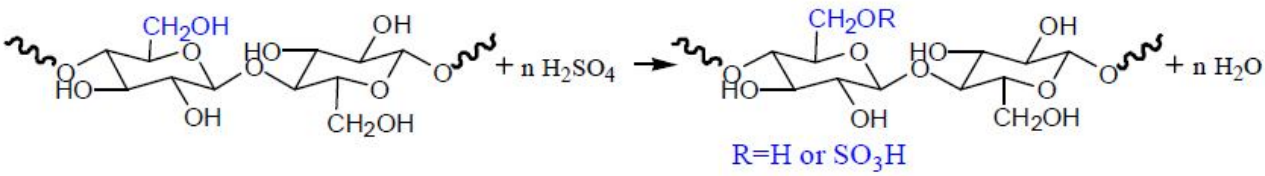

Figure 2.7: Illustration of the sulfation of cellulose hydroxyl groups during sulphuric acid hydrolysis.[54]

Transmission electron microscopy (TEM) analysis of dry CNW suspensions revealed the rod-like structure morphology of the whiskers. X-ray diffraction (XRD) was utilized in 1953 to confirm the dimensions of CNW, and atomic force microscopy (AFM) was later used to characterize the structure of CNW.[56,39,57]

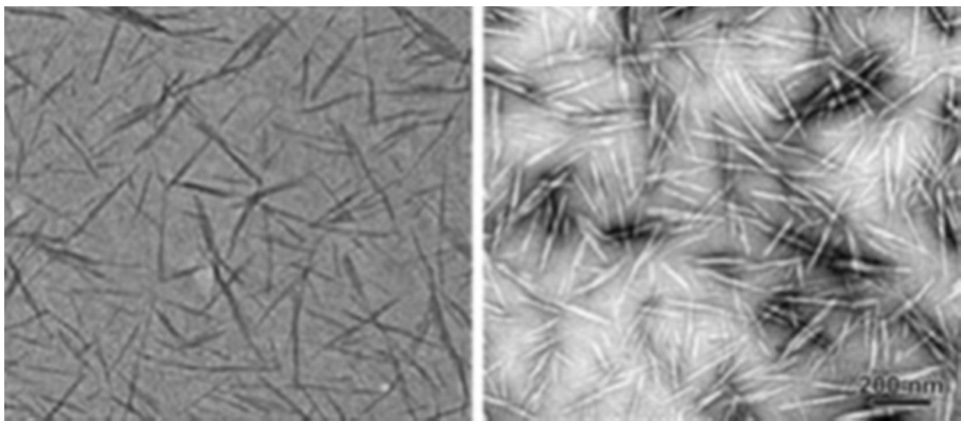

Figure 2.8: TEM images of CNW obtained from acid hydrolysis of cotton (left) and ramie (right).[43]

The dimensions of CNW are heavily influenced by both the origin and the process used. CNW have diameters between 3 nm and 20 nm and lengths ranging from 100 nm to 300 nm. The high aspect ratio (length/diameter) enables CNW to transfer stress through the matrix and act as a reinforcing material in composites.[43,47,51] CNW also exhibit electrical, optical and magnetic properties which are different to native cellulosic fibers.[58]

The high crystallinity and unique structure of CNW contribute to the high mechanical properties. Experimental and theoretical approaches have shown that CNW display an elastic modulus of 100-160 GPa. The high aspect ratio, nano-scale structural dimensions and great mechanical properties of CNW opened up a field to exploit the whiskers in nano-composites.[54,59,60] In 1995 Favier *et al*.[61] were the first to report on the use CNW in composite materials. They studied the percolation of CNW from tunicates and found that the CNW enhance stress transfer, which increases the final composite modulus compared to other micron-sized fillers.[43,61] The self-association due to the strong interaction of the hydroxyl groups leads to the formation of load-bearing percolating architectures within the host polymer matrix.[59] Using CNW as a reinforcing phase has several advantages over other types of nanofillers: They are easily modified, inexpensive, renewable and biocompatible.[45,62]

The primary obstacle in creating effective CNW nanocomposites is their homogeneous dispersion within a polymeric matrix. The high stability of CNW in aqueous suspensions due to their strong hydrogen bonds makes it extremely difficult to obtain well dispersed suspensions in non-polar solvents.[32] CNW are ideal for nanocomposites with hydrophilic polymers but not nanocomposites that require organic solvents. The dispersion of the CNW is crucial for the fabrication of nanocomposites, and aggregation of CNW within a polymer matrix can lead to a decrease in the overall modulus.[32,43,47,59] Surface functionalization of CNW became important for compatibilization and dispersibility. Different methods have been developed to improve the compatibility of CNW

with non-polar polymer matrices. This includes surface modification through chemical means, grafting or the use of surfactants. The most commonly used method was the creation of hydrophobic surfaces on sulphuric-hydrolysed CNW.[46] Alternative methods such as intensive ultrasonication for diluted whiskers in organic solvents were also utilized. Heux *et al*.[63] used a phosphoric ester surfactant to form stable CNW suspensions in toluene and cyclohexane.[47]

2.3. Fluorescence

Fluorescent dyes have been used widely as fluorescent sensors. In biochemistry and life sciences fluorescent dyes are generally used as a tracking agent to help with analysis of biological molecules, and in bio-imaging applications.[64] Fluorescent molecules emit light after being excited by a light source. Every fluorescent molecule will absorb and emit light at specific wavelengths which stretches from the ultraviolet to near-infrared region of the electromagnetic spectrum.

Labelling with a fluorescent molecule can extend over a wide range of wavelengths using fluorescent proteins, semiconductor nanocrystals or organic molecules. Covalent or non-covalent linkages can form between the organic fluorophores and the sample to be analysed. The linkages produce the respective complexes or conjugates to show fluorescence from short to long wavelengths, depending on the marker used.[65] Fluorescein is one of the most commonly used fluorescent markers and falls in the class of organic fluorophores, together with rhodamine, squaraines, cyanines and 4,4-difluoro-4-bora-3a,4a-diaza-s-indacenes (BODIPY dyes).

2.3.1 Fluorescein

Fluorescein is a polycyclic fluorophore with maximum absorption of λ_{abs} 490 nm in water and fluorescence of λ_{em} 512 nm in water, in the visible region of the electromagnetic spectra. The advantage of using fluorescein lies in its' excitation maximum of 494 nm, which is close to the 488 nm spectral line of the argon laser which is used in confocal laser-scanning microscopy and flow cytometry. Fluorescein has a few derivatives, but fluorescein isothiocyanate (FITC) is by far the most commonly used.[65,66]

Labelling CNW with a fluorescent marker can determine the location of the whiskers in biological systems. A three-step method was proposed by Dong *et al*.[66] for the labelling of CNW with FITC. This method was simplified when JunkeráNielsen *et al*.[67] explored a simple procedure used by Vieira Ferreira. Vieira reacted FITC with the free hydroxyl groups on the surface of the

microcrystalline cellulose (MCC) in a basic solution. JunkeráNielsen *et al*. used this method to dual-label the whiskers with FITC and RBITC.[68,67,69]

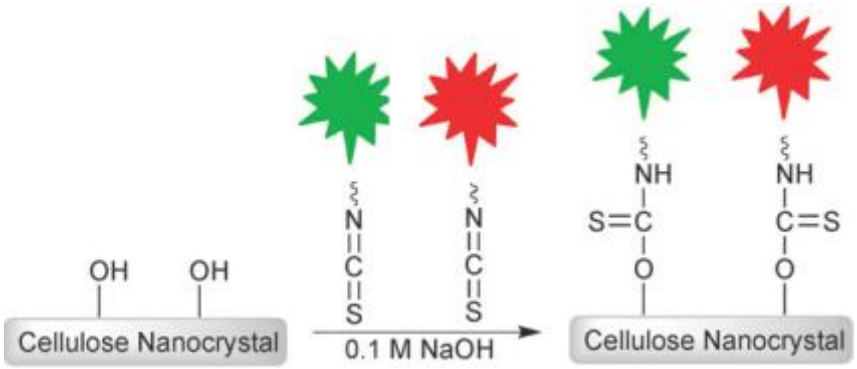

Figure 2.9: Schematic representation of cellulose nanowhiskers labelled with isothiocyanate fluorescent dyes.[67]

The fluorescent dye covalently bonds to the hydroxyl group on the surface of CNW. However, attaching a fluorescent marker covalently to polyoefins is a difficult process. This can be done by modifying the polymer. Zhang *et al*.[70] used a fluorescent dye to observe the distribution of maleic anhydride (MA), which was grafted onto ethylene propylene copolymers.

2.3.2 Rhodamine B

Rhodamine B belongs to the xanthene class of dyes and is amongst the oldest synthetic dyes used in the dyeing of fabrics. Rhodamine B (RhB) is a derivate of rhodamine and is specifically used in bioanalysis.[65] Rhodamine B is also frequently used as a fluorescent standard assisting with the determination of the quantum yields.[71] Rhodamine dyes are easily detectable and not very expensive. The rhodamine B dyes absorb at a long wavelength, at about 556 nm, and emits fluorescence at 574 nm.[72]

2.4 Characterization techniques used in this study

2.4.1 Transmission electron microscopy (TEM)

TEM is a very important analytical technique for structure characterization, which works on a similar basis to a light microscope. A beam of electrons passes through a material. The electrons which are transmitted interact with the material and create an image. The image is focused and magnified onto an imaging device or a sensor detector. TEM analysis can assist in identifying and

quantifying the chemical and electron structures of individual nanocrystals.[73] The use of TEM for structural analysis of CNW from different sources has been well documented.[32,43] CNW is suspended in water and deposited onto a carbon-coated electron microscope grid, after which it is negatively stained with uranyl acetate. Staining with uranyl acetate enhances the contrast between different phases, which allows for better observation of the size, shape and crystal aggregation.[39]

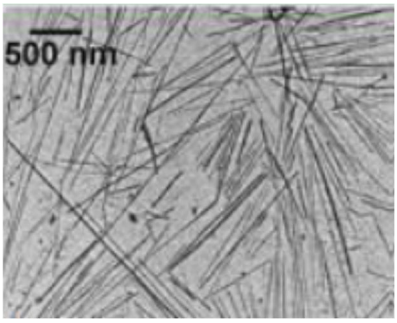

Figure 2.10: Images of dried cellulose nanowhiskers dispersions derived from tunicin.[32]

2.4.2 X-ray diffraction (XRD)

X-ray diffraction (XRD) is an analytical technique used to probe the crystalline structure of a solid material. The technique is primarily used for phase identification of crystalline material providing information about the unit cell dimensions. It can be used as a fingerprint characterization and determination of the crystalline structure. Each crystalline solid has a very unique X-ray diffraction pattern. XRD is non-constructive and is one of the most important characterization techniques in solid state chemistry and material science. XRD is based on the interference of monochromatic X-rays and a crystalline sample which is then analysed by using Bragg's Law ($n\lambda = 2dsin\theta$). A cathode ray tube generates X-rays, which is filtered to produce monochromic radiation, which is then directed towards the sample. The crystalline atoms in the sample cause the incident rays to diffract into many directions, and Bragg's law is used to explain the diffraction pattern of the scattered X-rays. The law relates the wavelength of the scattered X-rays to the angle and lattice spacing of the crystalline sample.

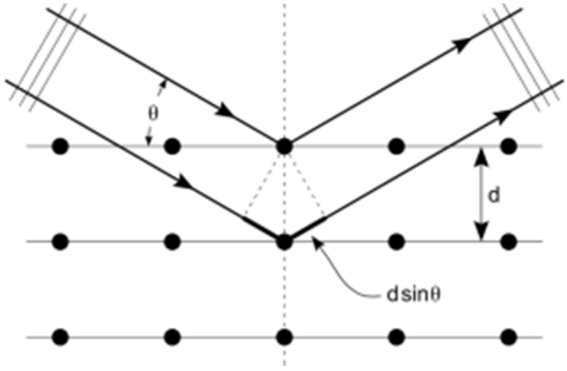

Figure 2.11: Schematic presentation illustrating Bragg's law.

The sample is scanned through a range of two-theta (2θ) angles to account for all possible diffraction directions. The first report utilizing XRD to ascribe lateral dimensions to CNW was published in 1953 by Mukherjee and Woods.[56] They investigated the change in crystallinity of cellulose when CNW was prepared by acid hydrolysis.[33,47,74]

2.4.3 Flow birefringence

Birefringence flow is a simple hydrodynamic technique for measuring the rotation and orientation of particles in suspension. This technique was first used by Marchessault *et al*.[55] to show the chiral nematic behaviour of CNW. Birefringence characterization was later employed to investigate the dispersion and isolation of CNW in a suspension.[33,39,75,76] Two polarizing filters are placed on opposite sides of the suspension at 90 degrees to each other. The light source will shine through the first polarized filter, then through the suspension followed by the second polarized filter. Stirring the suspension will allow the CNW to align in the direction of flow. The flow causes macro domains which are observed through the polarized filter as a distinct light pattern. This pattern is called flow birefringence.[62]

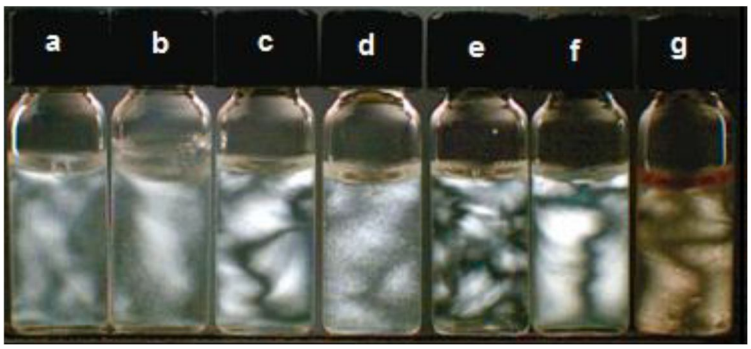

Figure 2.12: Photographs of 5.0 mg/mL dispersions of CNW viewed through cross polarizers and with different solvents[39]

2.4.4 Differential scanning calorimetry (DSC)

DSC is one of the most commonly used thermoanalytical techniques to study the melting and crystallization temperatures of polymers.[11] DSC measures the difference in the amount of heat required to increase the temperature of the sample compared to the reference, as a function of temperature. The technique is based on the principle that when the sample has a phase transition, it will need more or less energy than the reference for both to maintain the same temperature. DSC results have provided valuable information about the crystallinity, melting points, glass transition temperatures and polydispersity of polymer samples. The sample is heated at a certain rate with a heating profile, which is programmed manually. DSC has been used to evaluate IPC for many years. Characterization with DSC of fractionated IPC has revealed valuable information about the copolymer fractions, as Chen *et al*.[27,28] showed. Chen *et al*.[28] showed that the 30 ^{o}C fraction is mostly non-crystalline, while the fractions at higher temperature become more and more crystalline.[77-79]

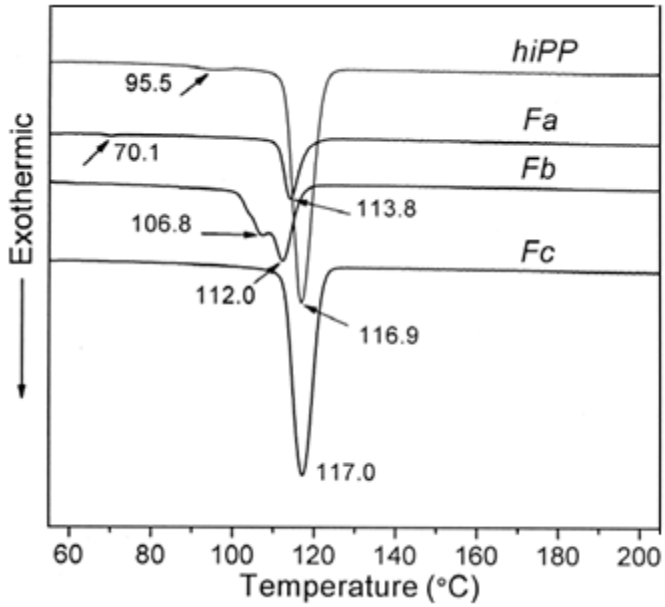

Figure 2.13: DSC cooling curves at 10 °C/min of high impact polypropylene (hiPP), the rubbery fraction (Fa), 100 °C soluble fraction (Fb) and the remained fraction (Fc).[28]

2.4.5 Confocal fluorescence microscopy (CFM)

CFM is still fairly new in the field of polymer characterization, although wide field fluorescence has been used for years. CFM is a microscopic technique which provides an accurate three-dimensional optical resolution. The name confocal originates from the fact that a pinhole is placed in front of the detector to eliminate any out-of-focus signals. In CFM, the sample is excited by a laser which is reflected by a dichroic mirror and focused by a microscope objective onto a small area of the sample. The fluorophores in the sample emit light after absorbing the light from the laser. The emitted light passes through the dichroic mirror where the shorter wavelengths are reflected and the longer wavelengths are focused at the pinhole. The light passing through the pinhole is measured by a detector, like a photomultiplier tube. Through scanning different sections in the sample, a very clean three-dimensional image can be generated by the detector.

As mentioned earlier, fluorescence dyes are often use in different fields as molecular markers. Fluorescent microscopy has been used to investigate the homogenous dispersion of fluorescently labelled CNW. CFM analysis can distinguish between CNW agglomerates by the fluorescent intensities.[64,66,67]

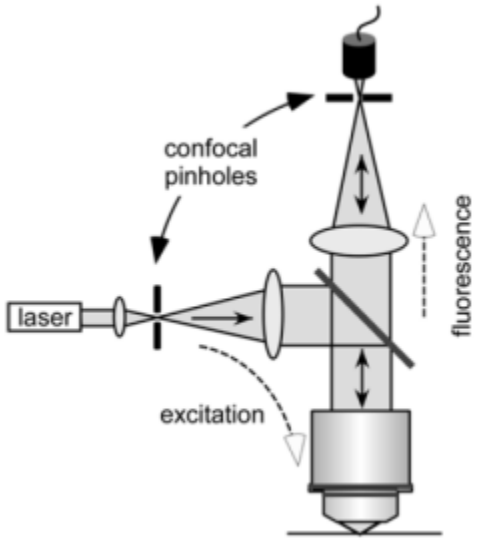

Figure 2.14: Schematic diagram illustrating the excitation of a sample by a laser in CFM.[70]

2.5 References

1. Jung W, Weon J. Journal of Material Science 2013; 48(3):1275-1282.

2. Rungswang W, Saendee P, Thitisuk B, Pathaweeisariyakul T, Cheevasrirungruang W. Journal of Applied Polymer Science 2012; 128(5):3131-3140

3. Welch MB, Hsieh HL, Vasile C, Seymour RB. Degradation and decomposition, Handbook of Polyolefins. New York: Marcel Dekker, 1993.

4. Grinshpun V, O'driscoll K, Rudin A. Journal of Applied Polymer Science 1984; 29(4):1071-1077.

5. Simonazzi T, Cecchin G, Mazzullo S. Progress in Polymer Science 1991; 16(2–3):303-329.

6. Moore EP. Polypropylene Handbook. New York: Hanser/Gardner Publications, 1996.

7. Xu J, Jin W, Fu Z, Fan Z. Journal of Applied Polymer Science 2005;98(1):243-246.

8. Schnauß A. Chemie Ingenieur Technik 1991;63(2):188-188.

9. Mncwabe S, Luruli N, Marantos E, Nhlapo P, Botha L. Macromolecular Symposia 2012; 313(1):33-42.

10. Nomura T, Nishio T, Fujii T, Sakai J, Yamamoto M, Uemura A, Kakugo M. Polymer Engineering & Science 1995; 35(16):1261-1271.

11. de Goede E, Mallon P, Pasch H. Macromolecular Materials and Engineering 2010; 295(4):366-373.

12. Basson NC, van Reenen A. Macromolecular Symposia 2012; 315(1):30-34.

13. Tian Z, Feng L, Fan Z, Hu G. Industrial and Engineering Chemistry Research 2014; 53(28) 11345-11354.

14. Grein C, Gahleitner M, Bernreitner K. Express Polymer Letters 2012; 6(9):688-696.

15. Vestberg T, Denifl P, Wilén C. Journal of Polymer Science Part A: Polymer Chemistry 2013; 51(9) 2040-2048.

16. Jancar J, Tochacek J. Polymer Degradation and Stability 2011; 96(9):1546-1556.

17. Mirabella Jr FM. Polymer 1993; 34(8):1729-1735.

18. Urdampilleta I, González A, Iruin JJ, de La Cal JC, Asua JM. Macromolecules 2005; 38(7):2795-2801.

19. Debling JA, Ray WH. Industrial and Engineering Chemistry Research 1995; 34(10):3466-3480.

20. Van Reenen A, Basson N. Express Polymer Letters 2012; 6(5): 427-436.

21. Xue Y, Fan Y, Bo S, Ji X. European Polymer Journal 2011; 47(8):1646-1653.

22. Kakugo M, Sadatoshi H, Yokoyama M, Kojima K. Macromolecules 1989; 22(2):547-551.

23. Kakugo M, Sadatoshi H, Sakai J, Yokoyama M. Macromolecules 1989; 22(7):3172-3177.

24. Debling JA, Ray WH. Journal of Applied Polymer Science 2001; 81(13):3085-3106.

25. Kittilsen P, McKenna T. Journal of Applied Polymer Science 2001; 82(5):1047-1060.

26. Cecchin G, Marchetti E, Baruzzi G. Macromolecular Chemistry and Physics 2001; 202(10):1987-1994.

27. Chen Y, Chen Y, Chen W, Yang D. Polymer 2006; 47(19):6808-6813.

28. Chen Y, Chen Y, Chen W, Yang D. European Polymer Journal 2007; 43(7):2999-3008.

29. Zhou Y, Niu H, Kong L, Zhao Y, Dong J, Wang D. Polymer 2009; 50(19):4690-4695.

30. Visakh P, Thomas S. Waste and Biomass Valorization 2010; 1(1):121-134.

31. O'Sullivan A. Cellulose 1997; 4(3):173-207.

32. Siqueira G, Bras J, Dufresne A. Polymers 2010; 2(4):728-765.

33. Eichhorn S. Soft Matter 2011; 7(2):303-315.

34. Loader N, Robertson I, Barker A, Switsur V, Waterhouse J. Chemical Geology 1997; 136(3):313-317.

35. Rinne K, Boettger T, Loader NJ, Robertson I, Switsur V, Waterhouse J. Chemical Geology 2005; 222(1):75-82.

36. Klemm D, Heublein B, Fink H, Bohn A. Angewandte Chemie International Edition 2005; 44(22):3358-3393.

37. Fleming K, Gray D, Matthews S. Chemistry-A European Journal 2001; 7(9):1831-1836.

38. John M, Thomas S. Carbohydrate Polymers 2008; 71(3):343-364.

39. Habibi Y, Lucia L, Rojas O. Chemical Reviews 2010; 110(6):3479-3500.

40. Brinchi L, Cotana F, Fortunati E, Kenny J. Carbohydrate Polymers 2013; 94(1):154-169.

41. Atalla RH, Vanderhart DL. Science 1984; 223(4633):283-285.

42. Morán JI, Alvarez VA, Cyras VP, Vázquez A. Cellulose 2008; 15(1):149-159.

43. Eichhorn S, Dufresne A, Aranguren M, Marcovich NE, Capadona JR, Rowan SJ, Weder C, Thielemans W, Roman M, Renneckar S. Journal of Material Science 2010; 45(1):1-33.

44. Dufresne A. Molecules 2010; 15(6):4111-4128.

45. Liu H, Song J, Shang S, Song Z, Wang D. American Chemical Society Applied Materials & Interfaces 2012; 4(5):2413-2419.

46. Hasani M, Cranston ED, Westman G, Gray DG. Soft Matter 2008; 4(11):2238-2244.

47. Li Y, Ragauskas AJ. Algae 2011; 75(80):10-15.

48. Rånby B, Noe R. Journal of Polymer Science 1961; 51(155):337-347.

49. Dong XM, Kimura T, Revol J, Gray DG. Langmuir 1996; 12(8):2076-2082.

50. Dong XM, Revol J, Gray DG. Cellulose 1998; 5(1):19-32.

51. Heath L, Thielemans W. Green Chemistry 2010; 12(8):1448-1453.

52. Araki J, Wada M, Kuga S, Okano T. Colloids and Surfaces A: Physicochemical and Engineering Aspects 1998; 142(1):75-82.

53. Araki J, Wada M, Kuga S. Langmuir 2001; 17(1):21-27.

54. Li Y. PhD Dissertation; Georgia Institute of Technology 2012.

55. Marchessault R, Morehead F, Walter N. Nature 1959; 184(4686):632-633.

56. Mukherjee S, Woods H. Biochimica et Biophysica Acta 1953; 10:499-511.

57. Rusli R, Eichhorn SJ. Applied Physics Letters 2008; 93(3):033111.

58. Azizi Samir, My Ahmed S, Alloin F, Dufresne A. Biomacromolecules 2005; 6(2):612-626.

59. Capadona JR, Shanmuganathan K, Trittschuh S, Seidel S, Rowan SJ, Weder C. Biomacromolecules 2009; 10(4):712-716.

60. Ludueña LN, Vecchio A, Stefani PM, Alvarez VA. Fibers and Polymers 2013; 14(7):1118-1127.

61. Favier V, Chanzy H, Cavaille J. Macromolecules 1995; 28(18):6365-6367.

62. Dong H, Strawhecker KE, Snyder JF, Orlicki JA, Reiner RS, Rudie AW. Carbohydrate Polymers 2012; 87(4):2488-2495.

63. Heux L, Chauve G, Bonini C. Langmuir 2000; 16(21):8210-8212.

64. Yang Q, Pan X. Journal of Applied Polymer Science 2010; 117(6):3639-3644.

65. Gonçalves MST. Chemical Reviews 2008; 109(1):190-212.

66. Dong S, Roman M. Journal of the American Chemical Society 2007; 129(45):13810-13811.

67. JunkeráNielsen L, Eyley S, Thielemans W, Aylott J. Chemical Communications 2010; 46(47):8929-8931.

68. Vieira Ferreira L, Cabral P, Almeida P, Oliveira A, Reis M, Botelho do Rego A. Macromolecules 1998; 31(12):3936-3944.

69. Huang J, Li C, Gray DG. American Chemical Society Sustainable Chemistry & Engineering 2013; 1(9):1160-1164.

70. Zhang M, Duhamel J, van Duin M, Meessen P. Macromolecules 2004; 37(5):1877-1890.

71. Karstens T, Kobs K. The Journal of Physical Chemistry 1980; 84(14):1871-1872.

72. Yang X, Guo X, Zhao Y. Talanta 2002; 57(5):883-890.

73. Wang Z. The Journal of Physical Chemistry B 2000; 104(6):1153-1175.

74. Kvien I, Sugiyama J, Votrubec M, Oksman K. Journal of Materials Science 2007; 42(19):8163-8171.

75. Rusli R, Shanmuganathan K, Rowan SJ, Weder C, Eichhorn SJ. Biomacromolecules 2011; 12(4):1363-1369.

76. Bondeson D, Mathew A, Oksman K. Cellulose 2006; 13(2):171-180.

77. Cheruthazhekatt S, Pijpers TF, Harding GW, Mathot VB, Pasch H. Macromolecules 2012; 45(15):5866-5880.

78. Hongjun C, Xiaolie L, Dezhu M, Jianmin W, Hongsheng T. Journal of Applied Polymer Science 1999; 71(1):93-101.

79. Tan H, Li L, Chen Z, Song Y, Zheng Q. Polymer 2005; 46(10):3522-3527.

CHAPTER 3

Experimental

3.1 Materials

The microcrystalline cellulose (MCC) used to produce the CNW was provided by JRS Pharma under the product name VIVAPUR101. Concentrated sulphuric acid (96 wt%) was supplied by Merck. Deionized water was produced in-house by an Elga Purelab instrument. The 5(6)-fluorescein isothiocyanate mixed isomer (FITC) and Rhodamine B (RhB) used to label the CNW were purchased from Sigma-Aldrich. Sodium hydroxide used in the labelling process and neutralization of the CNW produced by acid hydrolysis, was also purchased from Merck. IPC648 (ethylene content 12%, MFI = 8.5 g/10 min) was supplied by SASOL Polymers. An ethylene-propylene copolymer sample (non-commercial laboratory material, Mw 724000 g/mol) was obtained and was used in the evaluation of miscibility of EPR materials. The solvent used for the extraction of the EPR and the incorporation of the labelled whiskers into the EPR was Xylene, a mixture of isomers produced by Kimix. A mixture of Irganox 1010 and Irgafos 168 was used as a stabilizer during the injection moulding process and was supplied by Ciba. All chemicals were used as received.

3.2 Methods

3.2.1 Preparation of cellulose nanowhiskers by means of acid hydrolysis

The CNW were isolated by means of acid hydrolysis of MCC following a similar procedure to that used by Bonderson *et al*.[1] A 64 wt% sulphuric acid solution was used in a ratio of 1 g MCC to 8.75 ml (64 wt%) sulphuric acid. The sulphuric acid was added drop-wise to the MCC, stirred vigorously, and the MCC was kept in an ice bath to prevent an increase in reaction temperature, which can cause cross-linking. After the addition of the sulphuric acid, the ice bath was removed and the temperature was increased to 45 °C and the suspension was stirred at 800 rpm for 120 minutes. The suspension was diluted tenfold with deionized water to cool the suspension and to end the hydrolysis process. Centrifugation and solvent exchange were used to remove the

remaining acid and dissolved amorphous regions from the MCC. Deionised water was used as solvent to replace the supernatant after centrifugation. This step was repeated until the supernatant became turbid. The turbid suspension was collected and the centrifugation process was continued together with the collection of the turbid suspension until the supernatant became clear again. The collected turbid suspension containing the CNW was then washed by means of dialysis for a few days until the pH was five to ensure that any trace amounts of acid was removed. A few drops of 0.1 M sodium hydroxide were added, while the suspension was slowly stirred. When the pH reached a value between seven and eight the suspension was placed on dialysis to remove any excess sodium hydroxide and salt. The neutralised suspension was freeze dried to isolate the CNW in a powder form.

3.2.2 Preparation of cellulose nanowhiskers by means of sonication

The sonication method used by Capadona *et al.* was followed.[2] Deionized water was added to the MCC at a ratio of 21 mg MCC to 1 ml deionized water. The MCC suspension was sonicated for 6 hours. The MCC suspension was left for 24 hours to settle and the top turbid layer was decanted. The decanted suspension was freeze dried to isolate the CNW in powder form.

The percentage yield of the CNW produced by means of sonication, as described above, was investigated in an attempt to increase the percentage yield obtained. This was done by using different sonication times and stirring between the time intervals. The MCC suspensions were sonicated for 4 hours, after which the suspensions were stirred every 30 minutes for a total of 6 hours, 7 hours and 8 hours respectively. All three suspensions were left to settle for 24 hours, decanted and then freeze dried to obtain the resultant powder form of the CNW.

3.2.3 Fluorescent labelling of the cellulose nanowhiskers

The cellulose nanowhiskers were labelled with FITC and RhB respectively following the one-step procedure used by JunkeráNielsen *et al*.[3] The CNW were labelled using 250 mg CNW and 10.8 mg FITC in a 25 ml 0.1 M sodium hydroxide solution. The solution was stirred for 72 hours in the dark to ensure that the FITC attached to the CNW. The reaction scheme is illustrated below.

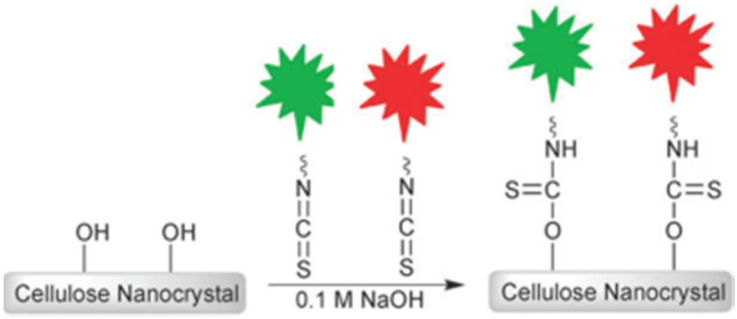

Figure 3.1: Schematic representation of cellulose nanowhiskers labelled with isothiocyanate fluorescent dyes.[3]

The suspension was centrifuged and washed with 0.1 M sodium hydroxide to remove the excess dye. The step was repeated extensively until the supernatant became clear. Once the supernatant was clear this step was repeated twice, after which the suspension was dialysed for a few days to remove any traces of unattached FITC and salts. It is important that the excess dye is removed from the solution, which is done by the extensive washing of the labelled whiskers through centrifugation and dialysis. The suspension was freeze dried to isolate the CNW/FITC. The same procedure was followed for the labelling of the CNW with RhB, and the esterification process is illustrated in Figure 3.2.

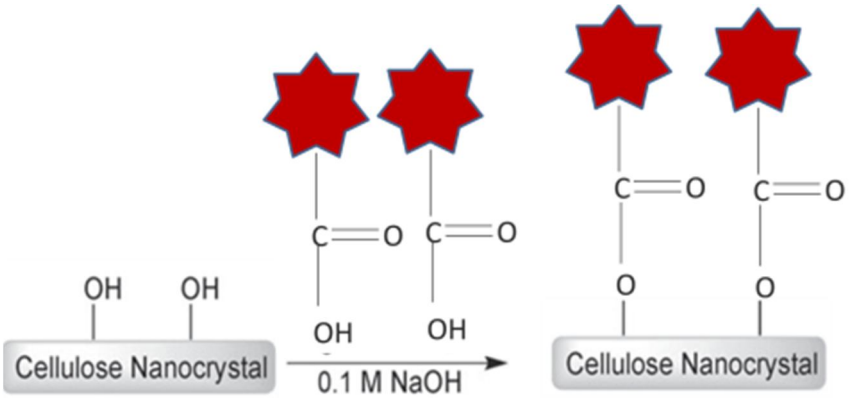

Figure 3.2: Schematic representation of the base catalysed esterification of CNW and RhB.

3.2.4 Extraction of the ethylene propylene rubber

IPC648 was dissolved in xylene at 135 °C under reflux for 4 hours, after which the solution was left over night to cool down and allow the semi-crystalline and isotactic polypropylene to slowly crystallize out of solution. The ratio of the IPC648 to xylene was 1 g to 700 ml.[4,5] The xylene-insoluble fraction (semi-crystalline and isotactic polypropylene) and the xylene-soluble fraction (EPR) were separated by means of filtration. The filtration was done at room temperature and the

insoluble fraction (crystalline fraction) was washed with xylene to make sure that all the EPR was removed from between the polymer particles. The xylene solution containing the EPR was poured into a petri dish to allow isolation of the EPR after solvent evaporation. The crystalline fraction was also placed in a petri dish to dry. The dry crystalline fraction formed white hard brittle clumps and the dry EPR formed a rubbery film.

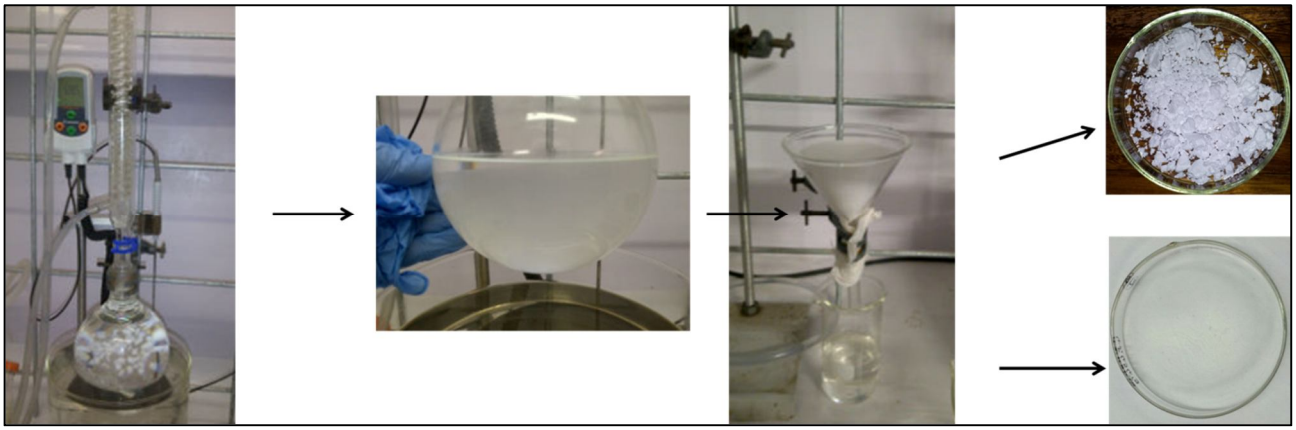

Figure 3.3: Schematic illustration of the extraction process.

The laboratory ethylene-propylene copolymer was separated and fractionated by following the same procedure and ratios as was used for the IPC648. Initially, the ethylene-propylene copolymer did not dissolve properly at 135 °C, and the temperature was increased to 140 °C. After 4 hours there were still small traces of undissolved polymer, so the time was extended to 6 hours. The reason for the increase in temperature and time can be ascribed to the increase in molecular weight.

3.2.5 Incorporation of labelled whiskers into the rubbery EPR fraction

The procedure described in this section was applied to both EPR fractions, the EPR extracted from IPC648 and the EPR (lab) extracted from the ethylene-propylene copolymer. The EPR was dissolved in xylene at 45 ^{o}C for 1 hour. A suspension of CNW/FITC, 2 wt% stabilizer and xylene was sonicated for 10 minutes, after which it was added to the dissolved EPR solution. The suspension of the dissolved EPR and CNW/FITC was sonicated for 10 minutes and poured into a petri dish. It is crucial that the suspension is poured immediately into the petri dish before the whiskers start to agglomerate and settle down in the suspension. The suspension was left until all the xylene was evaporated. The weight percentages of the CNW/FITC incorporated were 4 wt%, 5 wt% and 6 wt% respectively, and the above method was used for the incorporation of all three mentioned weight percentages. It is important to note that the different weight percentages were only evaluated to determine the most sufficient percentage, and this was only conducted on the

EPR extracted from IPC648. The 2 wt% stabilizer refers to the overall weight percentage, meaning that the ratio of stabilizer to labelled EPR film is 2 wt% to 98 wt%.

The EPR extracted from the IPC648 was also labelled with CNW/RhB for the evaluation of the miscibility of two different molecular weight EPRs. The miscibility will be visible by evaluating the fluorescent signals from the two different molecules present. The same procedure of incorporation was followed as above, but only 4 wt% of CNW/RhB was used.

3.2.6 Mobility test of the labelled cellulose nanowhiskers in the ethylene propylene rubber

The mobility of the CNW/FITC within the EPR was evaluated using two methods. These tests were done because if the labelled CNW shows movement or mobility in the EPR solution at room temperature, the likelihood of migration occurring at elevated temperatures is very high. The second reason for the tests was to show that the CNW/FITC will stay in the EPR and not migrate into the crystalline fraction, by showing the lack of movement between layers of labelled EPR and unlabelled EPR. Molecules are less likely to move between different phases with different densities than between similar phases with similar densities.

The first method entailed the evaluation of the movement of the CNW/FITC in the EPR while the sample was still in solution. The second method followed a layer-by-layer approach evaluating the mobility of the CNW/FITC in EPR.

3.2.6.1 Mobility of the labelled whiskers in wet form

The movement of the CNW/FITC was monitored using CFM. The CNW/FITC were incorporated into the EPR as described in Section 3.2.5, but solvent casting did not take place. The sonicated suspension was decanted into a CFM tray, which are normally used in the analysis of cell imaging.

Figure 3.4: Illustration of CFM tray filled with a suspension of EPR, CNW/FITC and xylene.

The mobility of the labelled whiskers was monitored in 10 minute time intervals. CFM images were taken every 10 minutes from above and the mobility of the CNW/FITC was monitored by the

change in fluorescence signals. The process was stopped after 80 minutes when all the xylene had evaporated.

3.2.6.2 Mobility evaluation by means of layer-by-layer approach

The second method entailed a layer by layer approach to evaluate the movement of the CNW/FITC between the EPR films. This method utilizes the fact that once the CNW/FITC has been incorporated into an EPR film it will not migrate into another layer due to the fact that the whiskers are surrounded by an organic medium.[6]

The method for the incorporation of the CNW/FITC into EPR followed the same procedure as described in Section 3.2.5, but was not left to dry completely. Two samples were prepared for analysis. The two different samples comprised of three layers each. Sample 1 had an EPR layer followed by a labelled EPR layer which was followed by another EPR layer. Sample 2 had a labelled EPR layer followed by an EPR layer which was followed by a labelled EPR layer.

Sample 1 was prepared by dissolving EPR in xylene at 45 °C for 1 hour, after which the solution was poured in a petri dish and left to dry partially. The second layer was prepared by incorporating the sonicated CNW/FITC xylene suspension into the dissolved EPR solution and the suspension was sonicated for another 10 minutes. The suspension was poured onto the partially wet EPR film in the petri dish and the suspension was left to dry partially. The third layer was prepared in the same way as layer one and the dissolved EPR was poured into the petri dish on top of the partially wet labelled EPR film. The cross sections of the dry sample were analysed by CFM. Figure 3.5 is a schematic illustration of the process used to create Sample 1.

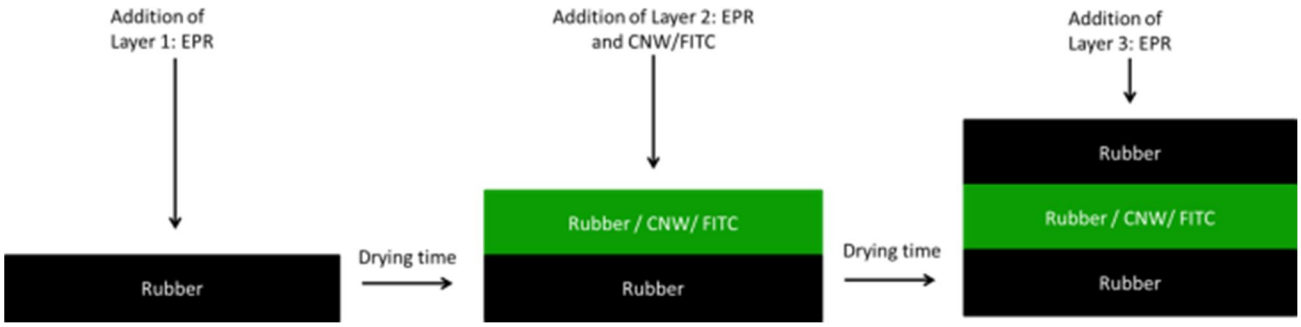

Figure 3.5: Schematic illustration of the process followed to obtain the layers in Sample1

Sample 2 was prepared in a similar manner to Sample 1, except that the first and last layers were labelled EPR, and the second layer was EPR. After the addition of the final labelled EPR layer and the drying thereof, cross sections were analysed by CFM.

3.2.7 Recombination of the labelled EPR and crystalline fraction

The labelled EPR was cut into very fine pieces and the crystalline fraction was ground into smaller, almost powder like pieces with a mortar and pestle to ensure that the sizes of the labelled EPR and crystalline fractions were similar. The fineness of the two fractions plays a role in the dispersion and flow during injection moulding. Bigger particles will take longer to melt and smaller particles which have melted already can lead to premature injection. This can cause an inconsistency in the injection moulded samples, where the different components did not have a chance to melt/flow together in the melt.

The labelled EPR and crystalline fraction was mixed together in a 17 wt% labelled EPR and 83 wt% crystalline fraction. The mix fraction was injection moulded into a dumbbell mould as described in Section 3.3.5. The dumbbell samples were microtomed to obtain cross sections of the discs and the cross sections were analysed by means of CFM.

3.2.8 Extraction of labelled EPR from the injection moulded samples

Pieces of the recombined injection moulded discs were microtomed and analysed by CFM. The injection moulded sample was then submerged in xylene. The sample was left to stir overnight at room temperature to allow the labelled EPR to dissolve in the xylene. The injection moulded sample was taken out of the xylene and the sample was microtomed again and analysed by CFM

3.2.9 Regrinding and injection moulding of samples

The injection moulded samples were broken into smaller pieces, and then ground with a mechanical blade into a powder. The powder was injection moulded into a dumbbell mould. The injection moulded sample was ground into a powder in an attempt to create a better representative sample of what happens in the mould when IPCs are manufactured.

3.3 Instrumentation and characterization techniques used in this study

3.3.1 Transmission electron microscopy (TEM)

The CNW were characterized by TEM analysis. A LEO 912 EM TEM instrument was used with lower and higher magnification for all the samples. A drop of diluted CNW (0.001 wt%) was deposited onto a carbon coated TEM grid. The CNW were negatively stained with urinal acetate and the excess solution was removed with filter paper. The TEM grid with the stained CNW was allowed to dry.

3.3.2 X-ray diffraction (XRD)

XRD was used to characterize the crystal indices of the CNW and MCC. A Bruker AXS D8 advanced diffractometer was used. The CNW and the MCC powder were compressed flat onto a XRD disc before analysis. The samples were scanned between 6.200° and 69.994° at 2θ angles. The step size was 0.028° for all the samples.

3.3.3 Polarized optical light microscopy

Suspensions of CNW were analysed by polarized optical light microscopy to observe flow birefringence patterns of the individual nanowhiskers. Two suspensions were prepared by redispersing 0.010 wt% and 0.025 wt% freeze dried CNW in deionized water. The suspensions were sonicated before the analysis to ensure that the CNW were well dispersed. If the CNW are agglomerated and not well dispersed it will lead to poor birefringence. Two polarized filters were placed at 90° to each other and a light source was shone through the filters and suspension. The images were captured while the suspension was stirred. The stirring of the suspension allowed the CNW to align in the direction of the flow.

3.3.4 Differential scanning calorimetry (DSC)

DSC analysis was done to evaluate the separation and recombination of the impact polyprolylene copolymers. A DSC Q100 TA instrument was used in the analysis. Samples (3 mg – 8 mg) were placed in the standard DSC aluminium pans. The samples were heated and cooled at a ramp of 10 °C/min for all three heating cycles. The samples were heated to 220 °C and maintained there isothermally for 5 minutes, after which the samples were cooled down to – 40 °C. A N_2 gas flow rate of 2 ml/min was used. The crystallization exotherm and melting endotherm were recorded and the analysis was done on the second and third heating cycle.

3.3.5 Injection moulding

The injection mould instrument used was a bench top HAAKE Mini Jet II from Thermo Scientific. The dumbbell mould was used for all the samples. The cylinder temperature was set at 220 °C and the mould was set at 65 °C. The injection pressure and post pressure were 250 bars. The injection time and post pressure time were 20 seconds. The samples were then removed from the mould.

3.3.6 Microtoming

The injection moulded samples were microtomed using a Leica RM2245 instrument. The dumbbell injection samples were broken into three pieces, and each section was microtomed. The sample thickness was between 10 and 16 µm in diameter. The microtomed sheets were transferred onto a microscope slide.

3.3.7. Fluorescence spectroscopy

A Perkin Elmer LS 50 B luminescence spectrometer was used for the analysis of the labelled whiskers. The labelled whiskers were suspended in distilled water and the suspension was transferred into a spectrometer cuvette. The absorbance was measured between the 200 nm and 700 nm wavelengths.

3.3.8 Confocal fluorescence microscopy

A Carl Zeiss Confocal LSM 780 Elyra S1 with SR-SIM superresolution microscopy was used to analyse the samples. The sample preparation varied for the different samples submitted. The CNW/FITC was prepared by placing a drop of the nanowhisker solution on a microscope slide. Small squares were cut out of the dry labelled EPR films as well as the layered EPR films. The squares were placed on a microscope slide, avoiding any folds or air bubbles. The movement of the CNW/FITC was measured in a CFM tray as discussed previously. The recombined samples subjected to microtoming were also placed on a microscope slide and the same was done when the extraction of the labelled EPR in xylene were investigated. All of the samples were covered with a cover slip to ensure that the sample did not move, and to protect the laser. The lasers used had wavelengths of 488 nm and 561 nm respectively, and different magnifications were applied.

3.4 References

1. Bondeson D, Mathew A, Oksman K. Cellulose 2006; 13(2):171-180.
2. Capadona JR, Shanmuganathan K, Trittschuh S, Seidel S, Rowan SJ, Weder C. Biomacromolecules 2009; 10(4):712-716.
3. JunkeráNielsen L, Eyley S, Thielemans W, Aylott J. Chemical Communications 2010; 46(47):8929-8931.
4. de Goede E, Mallon P, Pasch H. Macromolecular Materials and Engineering 2010; 295(4):366-373.
5. Van Reenen A, Basson N. Express Polymer Letters 2012; 6(5): 427-436
6. Siqueira G, Bras J, Dufresne A. Polymers 2010; 2(4):728-765.

CHAPTER 4

Preparation and characterization of cellulose nanowhiskers

4.1 Introduction

Two different experimental methods were investigated in order to produce cellulose nanowhiskers (CNW) from microcrystalline cellulose (MCC), namely acid hydrolysis and sonication. This was done in order to find the best route for the fabrication of the whiskers to use in this study. The final step for both of these CNW production methods was to isolate the whiskers by freeze drying, as was discussed in Section 3.2.1 and Section 3.2.2. The CNW obtained by means of acid hydrolysis were compared to the CNW obtained by means of sonication. The isolated CNW were labelled with a fluorescent marker, fluorescein isothiocyanate (FTIC). These nanowhiskers were also characterized and compared to the unlabelled CNW. This was done in order to ensure that the labelling reactions did not in any way influence the shape, size or morphology of the CNW. Characterization of the CNW obtained (by acid hydrolysis, sonication and after labelling) was done by transmission electron microscopy (TEM), flow birefringement and x-ray diffraction (XRD).

4.2 Transmission electron microscopy (TEM)

Images of the shape and size of the CNW produced by the various production methods were obtained by means of TEM. The images were used to determine the dimensions of the individual whiskers obtained. These results were then compared to those reported in literature.[1,2] As discussed in Section 3.2.1 and Section 3.2.2, the freeze dried whiskers were re-dispersed in deionized water to obtain a 0.01wt % suspension, after which the sample was prepared for TEM analysis.

Figures 4.1 (a) and (b) show electron micrographs of CNW produced by using acid hydrolysis as discussed in Section 3.2.1. The TEM results of CNW produced by sonication are shown in Figure 4.2.

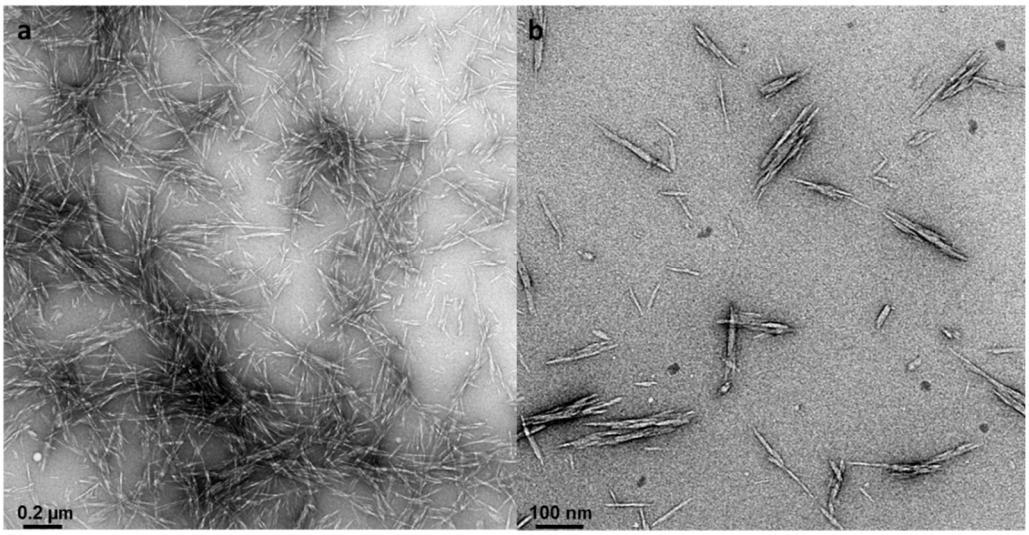

Figure 4.1: TEM images of CNW produced by means of acid hydrolysis (a) lower magnification and (b) higher magnification.

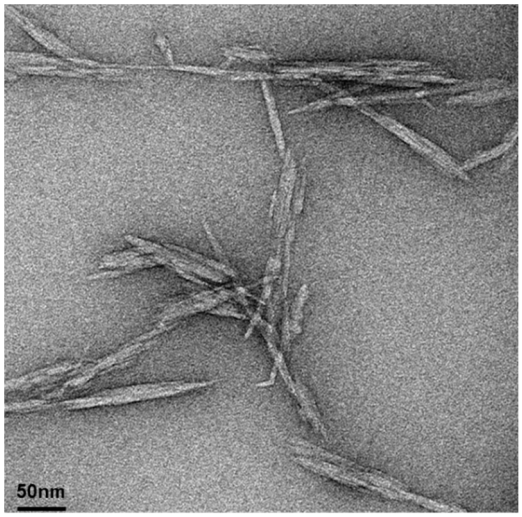

Figure 4.2: TEM image of CNW produced by sonication.

Figures 4.1 and 4.2 clearly show the rod-like structures of the whiskers, and the dimensions of the product produced by means of acid hydrolysis and sonication were in the nanometer range (nm), corresponding to what is found in literature.[1,2] The average dimensions of the CNW produced by acid hydrolysis and sonication are in the range of 5 nm – 20 nm in diameter and 120 nm – 250 nm in length. Results are given in in Table 4.1.

Table 4.1: The dimensions of CNW obtained by acid hydrolysis and sonication

Method	Average diameter (nm)	Average length (nm)
Sulphuric acid	8.31	151
Sonication	9.21	156

The percentage yield when preparing CNW from sulphuric acid was slightly higher than the percentage obtained through sonication.

Table 4.2: Comparison of percentage yield between CNW produced by means of acid hydrolysis and sonication

Method	Average yield (%)
Sulphuric acid	22.3
Sonication	20.6

Sonication, on the other hand, is a much easier process to use. As was described in Section 3.2.2, the process of producing CNW through sonication was investigated at different sonication times in an attempt to increase the percentage yield of the CNW. The time increase did result in a slightly higher percentage yield of the CNW, but the agglomeration also seemed to increase with time as shown in Figure 4.3. Figure 4.3 shows the transmission electron micrographs of the CNW obtained by sonication for (a) 6, (b) 7 and (c) 8 hours. Comparing the three micrographs in Figure 4.3, there was an increase in the amount of whiskers present as the time increased from 6 hours to 8 hours, and the whiskers appeared to be more agglomerated.

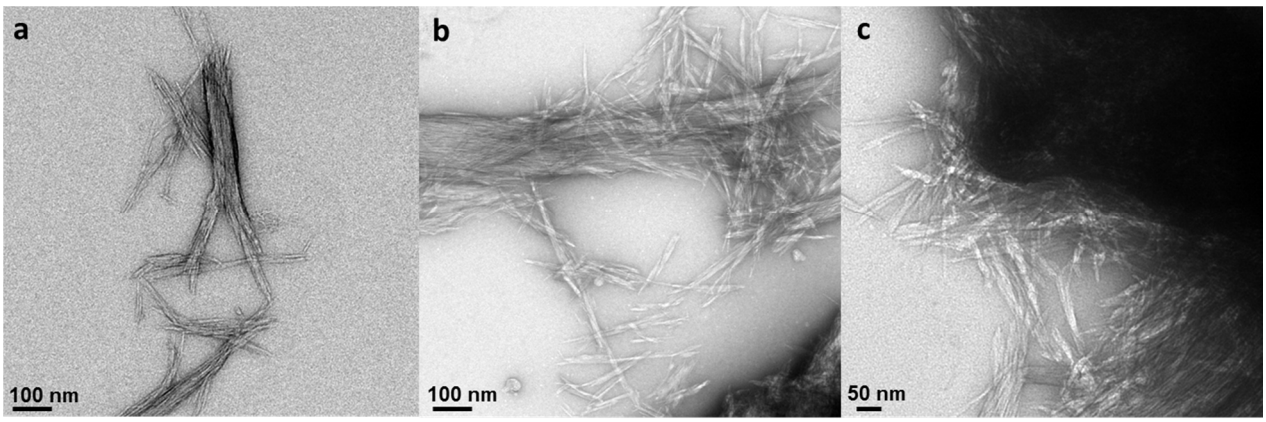

Figure 4.3: TEM images of CNW obtained through sonication after (a) 6 hours, (b) 7 hours and (c) 8 hours.

In Figure 4.4 a comparison is shown of the dispersion of the whiskers on the same scale. Figure 4.4 (a) shows the CNW produced by acid hydrolysis and Figure 4.4 (b) shows the whiskers produced by sonication. For a better visual understanding of the difference in dispersion of the CNW produced by the two methods, transmission micrographs with the same scaling are displayed below. In both cases the CNW were redispersed in deionized water after preparation and isolation.

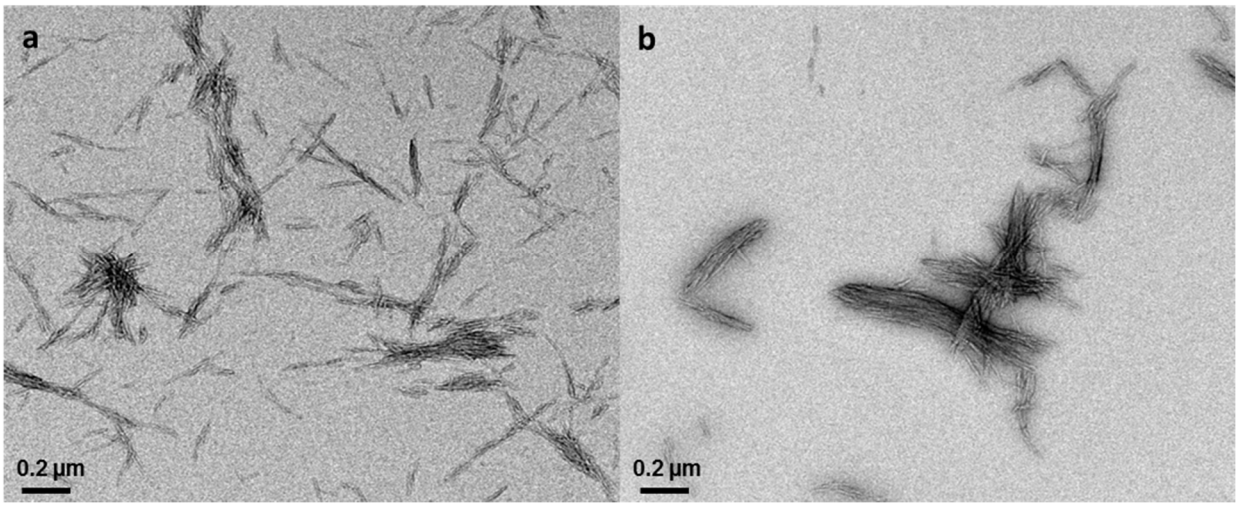

Figure 4.4: TEM images of CNW produced by means of (a) acid hydrolysis and (b) sonication.

It is clear that the CNW produced by acid hydrolysis (Figure 4.4 (a)) are more evenly dispersed than the whiskers produced by sonication (Figure 4.4 (b)). The whiskers appear to be more densely agglomerated in Figure 4.4 (b) than in Figure 4.4 (a). The CNW produced through sonication have more hydroxyl groups on their surfaces, making them more likely to form strong hydrogen bonds.[3] The CNW produced by sulphuric acid hydrolysis contain sulphate groups on the surfaces. The CNW with the sulphate groups tend to form more stable suspensions than the CNW without the sulphate groups.[4,5].

When considering which method of synthesizing CNW to pursue, it was decided to continue with hydrolysis as the resultant whiskers dispersed better in a water medium, and it is an even greater challenge to disperse the CNW in a non-polar medium. The CNW produced by means of acid hydrolysis will be characterized further and used throughout the rest of this study.

TEM analyses were conducted on the whiskers labelled with FTIC (Section 3.2.3). This was done to confirm that the presence of the fluorescent dye does not influence the dispersion of the whiskers, or their rod-like structure.[6] Figure 4.5 shows CNW/FITC redispersed in water. The same sample preparation was applied as previously for the pure whiskers.

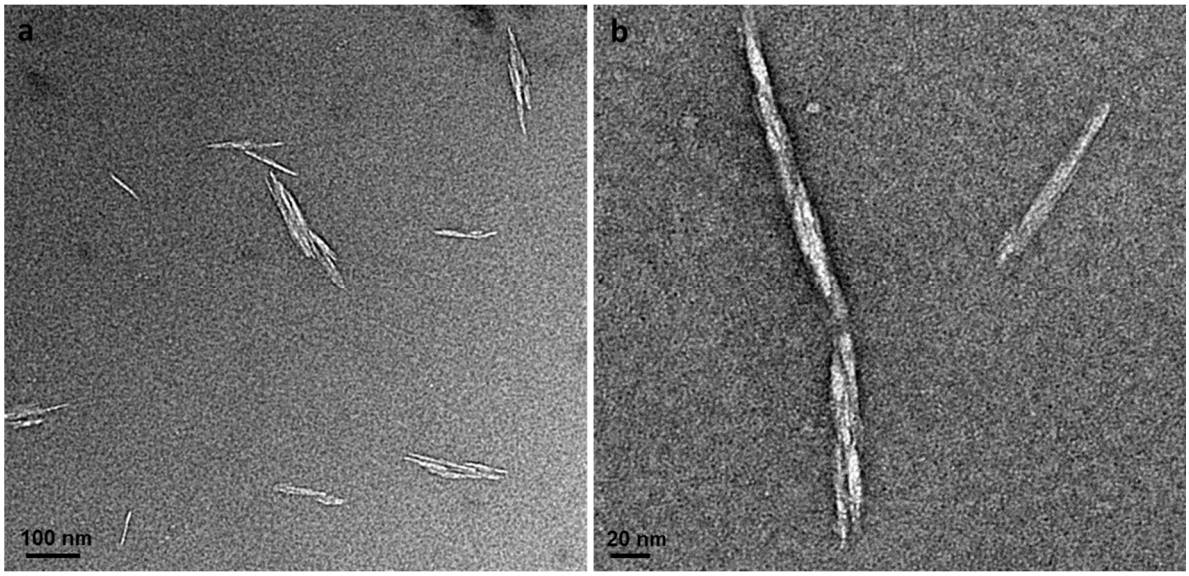

Figure 4.5: TEM images of CNW labelled with FITC at a lower magnification (a) and higher magnification (b).

From the TEM images it is clear that the dye does not influence the rod-like structure of the whiskers. The dispersion of the whiskers also seems to be good and agglomeration is minimal. We can therefore conclude that FITC does not influence the morphology or structure of the CNW used for the purposes of this study.

4.3 X-ray diffraction (XRD)

Microcrystalline cellulose (MCC) while being highly crystalline, still contains some amorphous material. The presence of both crystalline and amorphous regions within the MCC crystals makes characterization by XRD quite complicated, but XRD is still a valuable tool for confirming the isolation of the CNW from MCC.

Another important factor worth noting is the size of cellulose crystals. The cellulose crystallites are very small, typically in the range of 20 – 50 Å in diameter. These small crystals can cause peak broadening of the spectra and can be confused with the amorphous regions.[7] The degree of crystallinity is also strongly dependent on the source of origin.

The percentage crystallinity of MCC and CNW has been calculated using different methods, of which Segal's method is the most common.[8] The amorphous region has a broader peak as mentioned before, and the crystalline regions have sharp peaks. The broad peak of the amorphous regions can be subtracted from the overall spectra to produce spectra only containing the reflectance of the crystallites.[7]

The XRD spectra obtained for MCC and CNW are illustrated below in Figure 4.6 and Figure 4.7 respectively.

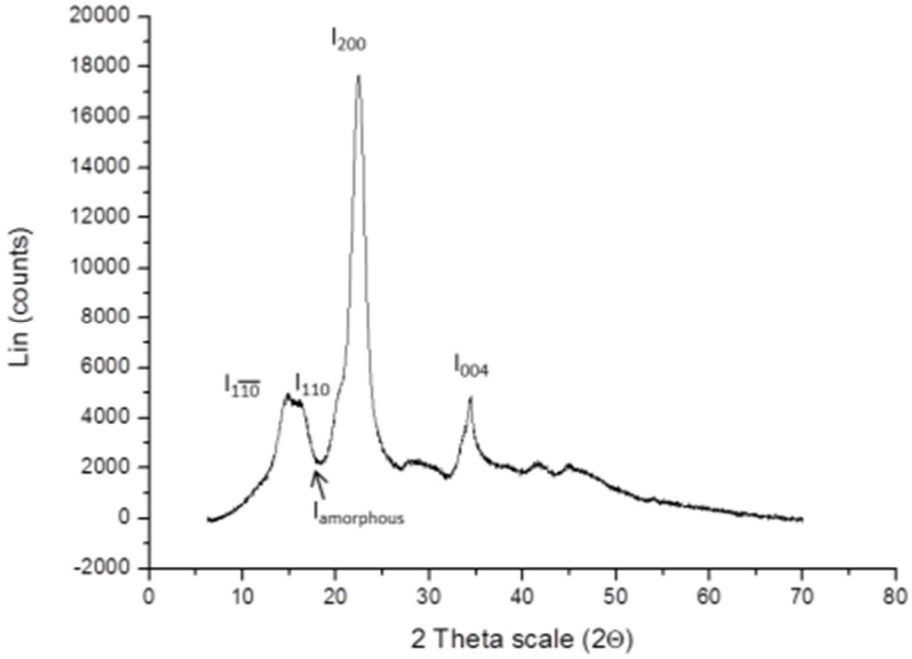

Figure 4.6: XRD diffraction pattern for pure MCC.

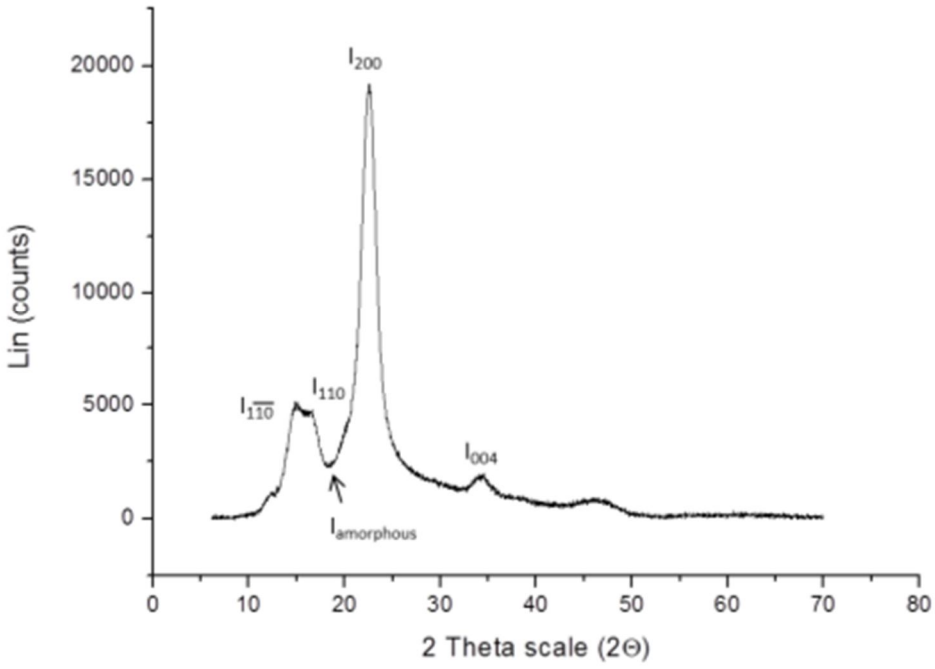

Figure 4.7: XRD diffraction pattern for CNW.

The peaks at 14° - 18° are due to the crystallite indices of $I_{11\bar{0}}$ and I_{110} and the peak at 22° is due to the I_{200} index. These peaks represent the directions perpendicular to the fibre axis, while the peak at 33° – 35° is represented by directions parallel to the fibre axis and have the I_{004} index.[7-9] Comparing Figure 4.6 and Figure 4.7 the spectra look similar, except for the intensities of the different peaks. In this study Segal's method was used to determine the crystallinity (X_c) of the CNW.

According to Segal's method, X_c is determined by using I_{200} and $I_{amorphous}$. The I_{200} index is the intensity of the crystalline peak at the maximum and $I_{amorphous}$ index is the intensity at the minimum of 14° – 18°, as indicated in the two figures. To calculate $X_{c,}$ Scherre's equation was used.[10] The values obtained for the crystallinity of the CNW and MCC are displayed in Table 4.3

$$X_c = \frac{I_{200} - I_{amorp\ hous}}{I_{200}} \times 100\%$$

Equation 4.1: Scherre's equation for determining crystallinity.[10]

Table 4.3: Summary of crystallinity indices and crystallinity

Sample	I_{200}	$I_{amorphous}$	X_C (%)
CNW	19134.5	2265.4	87.6
MCC	17180.0	2609.9	84.8

According to Segal's method and Scherre's equation, the percentage crystallinity of the CNW is higher than that of MCC, as expected. The difference in percentage crystallinity between MCC and CNW is less than one might expect, but it is important to remember that MCC is already a crystalline form of cellulose. This means that the overall crystallinity of the MCC is relatively high compared to bulk cellulose as some of the amorphous regions have already been removed.[11] The higher percentage crystallinity of the CNW compared to MCC confirms the disintegration of the amorphous regions inside the MCC when acid hydrolysis is used to produce the whiskers.

If we examine Figure 4.6 and Figure 4.7 more closely, it is apparent that there is a definite decrease in size in the I_{004} peak. This can be due to two possibilities; the removal of the amorphous region, or the size and degradation of the crystallites. The second possibility is worth mentioning because the decrease at I_{004} might not just be due to the removal of the amorphous region, but also due to the decrease in size of the MCC fibres. This is another indication that CNW were produced. Similar spectra were published by Yu *et al*.[8] Figure 4.8 illustrates the spectrum Yu *et al*. obtained for the production of CNW by using acid hydrolysis.

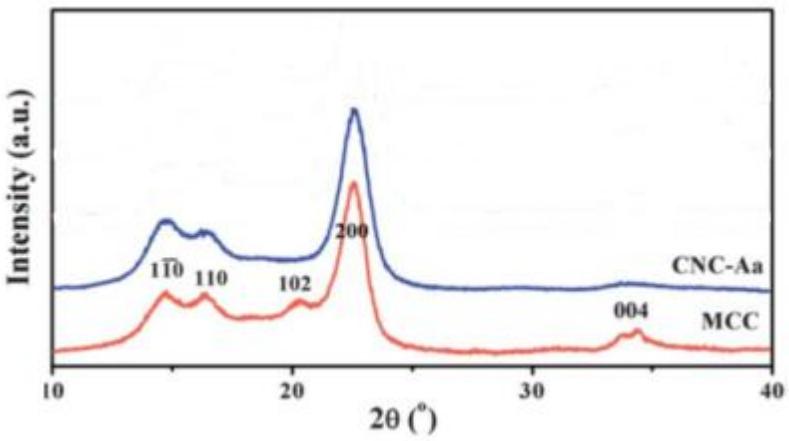

Figure 4.8: XRD diffraction patterns for MCC compared to CNW (CNC-Aa) produced through acid hydrolysis.[8]

Comparing the different patterns from Figure 4.6, Figure 4.7 and Figure 4.8, the spectra look fairly similar. The values obtained through the use of Segal's method indicated an increase in crystallinity after MCC was hydrolysed by sulphuric acid. The results found above clearly indicate that CNW were produced by means of acid hydrolysis and was successfully characterized by XRD.

4.4 Flow birefringence

The CNW were further characterized using polarized light. This was done to see if the suspensions exhibited chiral nematic behaviour. The existence of whiskers in a cellulose suspension can be confirmed when flow birefringence is observed. This is indicated by a nematic liquid, which is caused by the crystalline alignment of the whiskers.[12,13] Cross-polarized light images of the 0.01 wt% and 0.025 wt% CNW suspensions were taken after redispersing the freeze dried whiskers in deionized water. The different suspensions were prepared as explained in Section 3.3.3. The images of the two suspensions are shown in Figure 4.9 (b) and (c). The patterns are observed through the contrast between the darker patches and the lighter areas in the suspension. The darker areas are associated with the light which passes straight through the solution and the lighter areas are associated with the reflecting light caused by the aligned CNW in suspensions. The patterns can be used to confirm the presence of the whiskers and the relative amount of agglomeration.

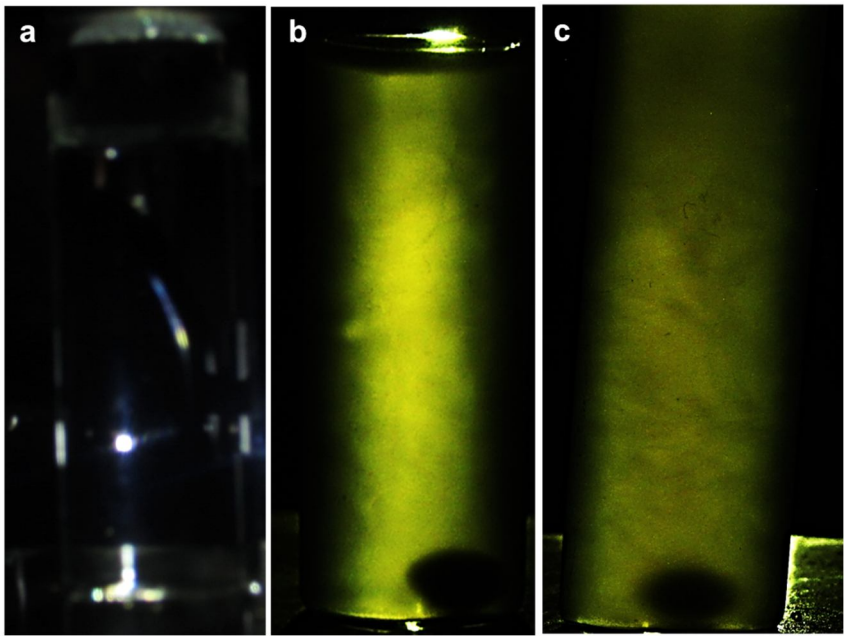

Figure 4.9: Cross-polarized light images (a) pure water, (b) CNW in suspension 0.025 wt% and (c) CNW in suspension 0.01 wt%.

The images in Figure 4.9 display birefringence of the individual nanowhiskers, as seen in images (b) and (c). The darker areas in these images create the scattering of the light, which is associated with the aligned CNW in suspension. Figure 4.9 (a) does not exhibit any birefringence, as expected. These images confirm the reasonable dispersion of the whiskers.

4.5 Fluorescence

The successful attachment of fluorescein 5/6-isothiocyanate (FITC) and rhodamine B (RhB) to the CNW was visually observed. The colour of the labeled whiskers with FITC was light orange and the colour observed for the labeled CNW with RhB was light pink. Fluorescence spectroscopy and confocal fluorescence microscopy were also conducted to confirm the visual assessment. FITC was mostly used in this study to label the CNW. RhB was only used at the end of this study, so the characterization discussed in this chapter will mainly focus on the use of FITC. The whiskers labelled with FITC will be referred to as CNW/FITC and the whiskers labeled with RhB will be referred to as CNW/RhB for the remainder of the thesis. The colour of the pure CNW and the whiskers labeled with FITC are shown in Figure 4.10.

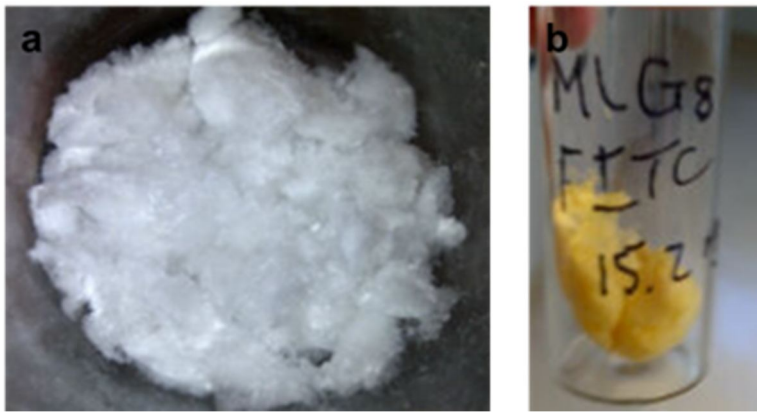

Figure 4.10: Freeze dried (a) CNW and (b) CNW/FITC.

4.5.1 Fluorescence spectroscopy

The freeze dried CNW/FITC were redispersed in distilled water by means of sonication as described in Section 3.3.7. The diluted solution of CNW/FITC was analysed with fluorescence spectroscopy to confirm the reactivity of the FITC attached to the whiskers. FITC has an absorption maximum at 490 nm and an excitation peak at 520 nm – 540 nm (511.5 nm), as illustrated by Figure 4.11.

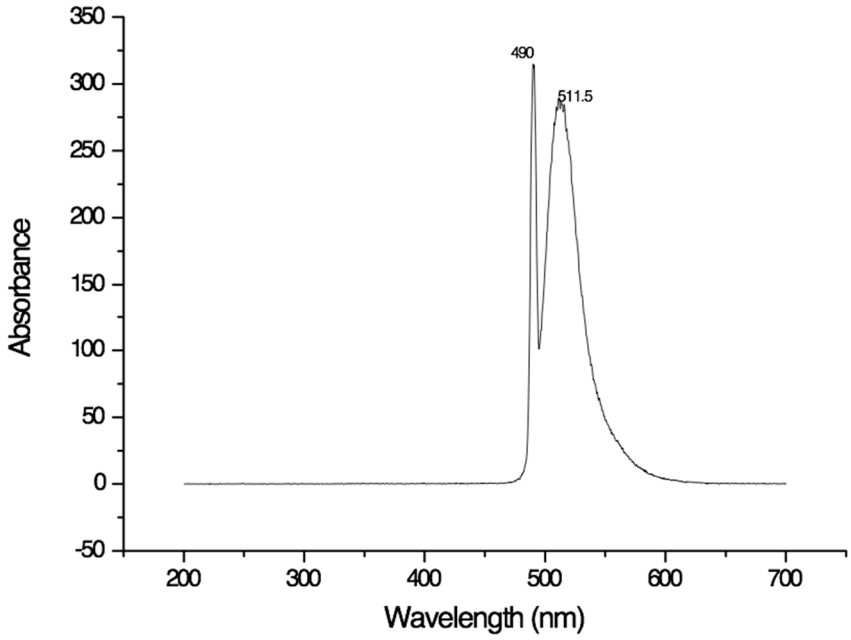

Figure 4.11: Fluorescence spectrum of pure FITC in distilled water.

Figure 4.12 shows the fluorescence spectrum obtained from CNW/FITC. The spectrum is almost identical to that of the spectrum obtained for pure FITC in Figure 4.11. The absorption maximum in Figure 4.12 is at 490 nm and the excitation is at 513.5 nm. It is important to note that the absorption maxima and excitation can be caused by excess dye trapped inside the whisker matrix. This was prevented by removing the excess dye through the process discussed in Section 3.2.3. Therefore, the only contributing factor to this spectrum in Figure 4.12 would be the successful attachment of the fluorescent dye, FITC to the whiskers.[14,15] The presence of the absorption and excitation peaks in Figure 4.12 also confirms that the reactivity of the FITC after attachment was still intact.

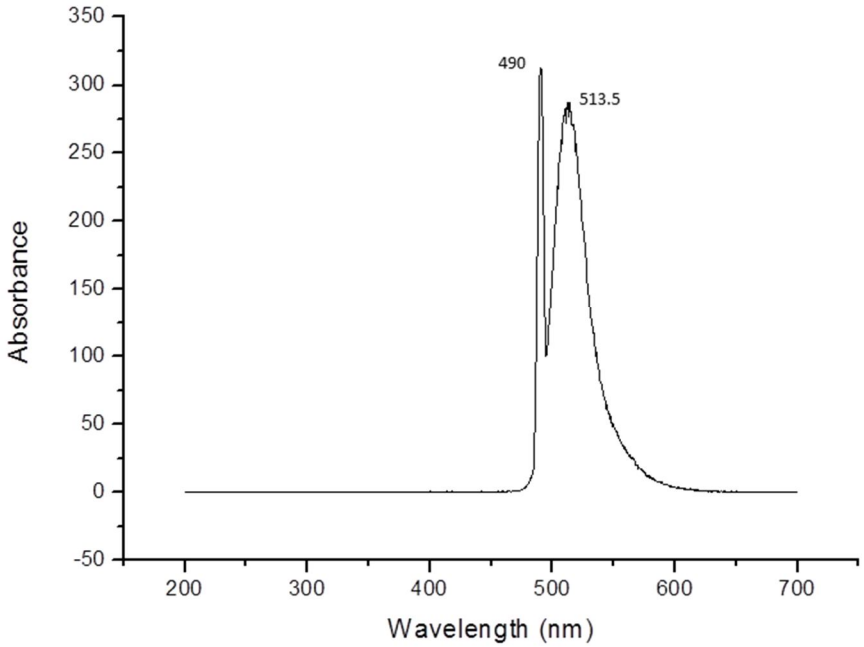

Figure 4.12: CNW/FITC in distilled water.

4.5.2 Confocal fluorescence microscopy (CFM)

The labeled cellulose nanowhiskers were also analysed with confocal fluorescence microscopy (CFM). A solution of CNW/FITC was prepared as described in Section 3.3.8 and was submitted together with a pure CNW sample. The same preparation procedure was followed for the pure freeze dried CNW as for CNW/FITC. The CNW sample was submitted to aid as a control.

The open pin-hole setting was chosen to identify the nanorod-like structure of the whiskers. An open pin-hole can detect more fluorescence signals, although the structures in the image might be more out of focus than those in images taken using a closed pin-hole. The open pin-hole also allows more light through, as is shown is Figure 4.13.

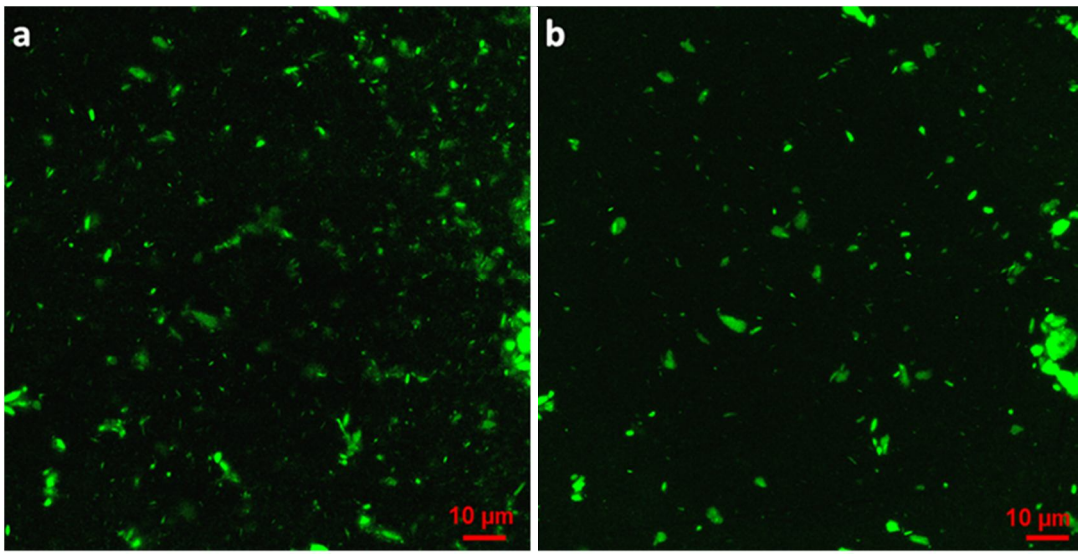

Figure 4.13: CFM of CNW/FITC illustrating the difference between (a) open pin-hole and (b) closed pin hole.

The CFM images show the presence of FITC attached to the CNW. Figure 4.14 (a) is an image of the whiskers on the background created by the TPMT filter, clearly showing the rod-like structures. Figure 4.14 (b) shows the fluorescent signals of the FITC attached to the whiskers and (c) is an overlay of the two images. The CFM images show very well dispersed labelled CNW throughout the whole sample, with some agglomeration in certain areas. As expected, pure CNW did not show any fluorescence, so we can therefore conclude that the fluorescent signals present are only as a result of the FITC.

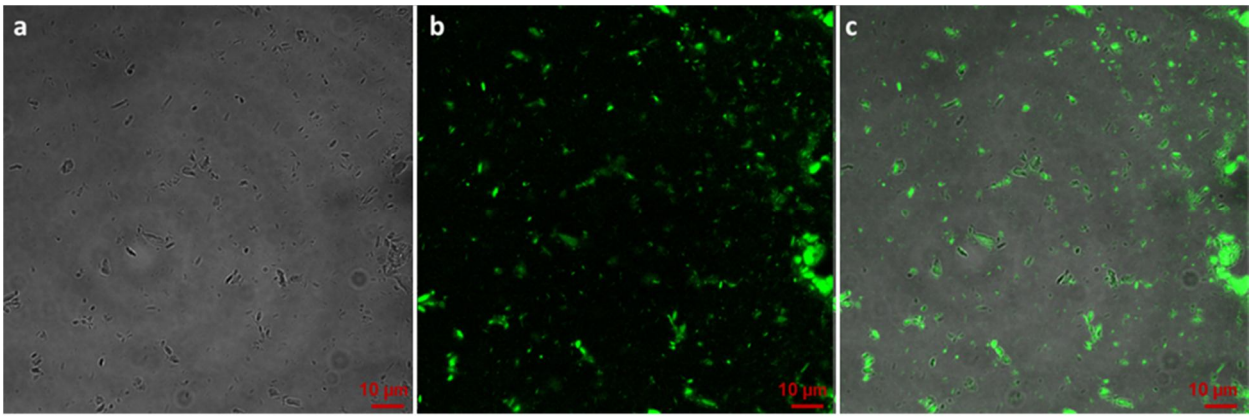

Figure 4.14: Open pin-hole CFM images of CNW/FITC dispersed in water (a) TPMT filter, (b) 488 nm and (c) is an overlay of (a) and (b).

4.6 Conclusion

The CNW were successfully produced by both acid hydrolysis and sonication. TEM analysis of the produced CNW confirmed the presence of their rod-like structures for both procedures. The percentage yield and the dispersion of the CNW produced by means of acid hydrolysis were slightly better than the CNW produced by sonication. Further proof that CNW were produced was evidenced by comparing the amorphous peaks in the MCC and CNW XRD spectra. The attachment of the FITC to the CNW was confirmed by fluorescence spectroscopy and confocal fluorescent microscopy. The labelled whiskers are easily detectable, even in diluted solutions.

4.7 References

1. Habibi Y, Lucia LA, Rojas OJ. Chemical Reviews 2010; 110(6):3479-3500.

2. Rusli R, Eichhorn SJ. Applied Physics Letters 2008; 93(3):033111.

3. Capadona JR, Shanmuganathan K, Trittschuh S, Seidel S, Rowan SJ, Weder C. Biomacromolecules 2009; 10(4):712-716.

4. Siqueira G, Bras J, Dufresne A. Polymers 2010; 2(4):728-765.

5. Hasani M, Cranston ED, Westman G, Gray DG. Soft Matter 2008; 4(11):2238-2244.

6. JunkeráNielsen L, Eyley S, Thielemans W, Aylott J. Chemical Communications 2010; 46(47):8929-8931.

7. Thygesen A, Oddershede J, Lilholt H, Thomsen AB, Ståhl K. Cellulose 2005; 12(6):563-576.

8. Yu H, Qin Z, Liang B, Liu N, Zhou Z, Chen L. Journal of Material Science 2013; 1(12):3938-3944.

9. Klemm D, Heublein B, Fink H, Bohn A. Angewandte Chemie International Edition 2005; 44(22):3358-3393.

10. Morán JI, Alvarez VA, Cyras VP, Vázquez A. Cellulose 2008; 15(1):149-159.

11. Mathew AP, Oksman K, Sain M. Journal of Applied Polymer Science 2005; 97(5):2014-2025.

12. Bondeson D, Mathew A, Oksman K. Cellulose 2006; 13(2):171-180.

13. Brinchi L, Cotana F, Fortunati E, Kenny J. Carbohydrate Polymers 2013; 94(1):154-169.

14. Dong S, Roman M. Journal of the American Chemical Society 2007; 129(45):13810-13811.

15. Dong H, Strawhecker KE, Snyder JF, Orlicki JA, Reiner RS, Rudie AW. Carbohydrate Polymers 2012; 87(4):2488-2495.

CHAPTER 5

Labelled cellulose nanowhiskers in ethylene propylene rubber: Results and discussion

5.1 Introduction

The separation of the ethylene propylene rubber (EPR) and rest of the crystalline fraction and the results thereof will be discussed first in this chapter, followed by results of the incorporation of the labelled cellulose nanowhiskers (CNW/FITC) into the EPR. The rubber phase will be referred to as EPR and the semi-crystalline and iPP phase will be referred to as the crystalline fraction throughout the remainder of the thesis. The different weight percentages of CNW/FITC incorporated into the rubber will be also be discussed.

5.2 Differential scanning calorimetry (DSC)

The IPC648 was separated into the EPR and crystalline fractions as described in Section 3.2.4. Examples of the extracted products obtained after xylene evaporation are shown in Figure 5.1. The crystalline fraction was white in colour, very brittle and hard. The EPR was opaque in colour, very flexible and rubbery.

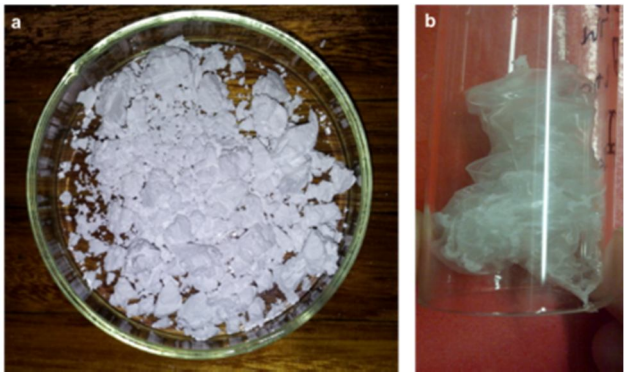

Figure 5.1: Examples of extracted samples to show the difference in appearance (a) crystalline fraction and (b) EPR.

The average weight percentages of the crystalline fraction and the EPR were 82.3 wt% and 16.5 wt% respectively, as summarized in Table 5.1. The total weight percentages of the two were

slightly less than 100 wt%, which can be ascribed to possible loss of product during the separation step.

Table 5.1: Summary of the average wt% of extracted EPR and crystalline fractions

Fraction	Average weight percentage (wt%)
EPR	16.5
Crystalline	82.3

Differential scanning calorimetry (DSC) was used to verify the separation of the EPR and crystalline fraction. The results of the EPR and crystalline fraction were compared to the DSC results obtained from the original IPC648 sample.

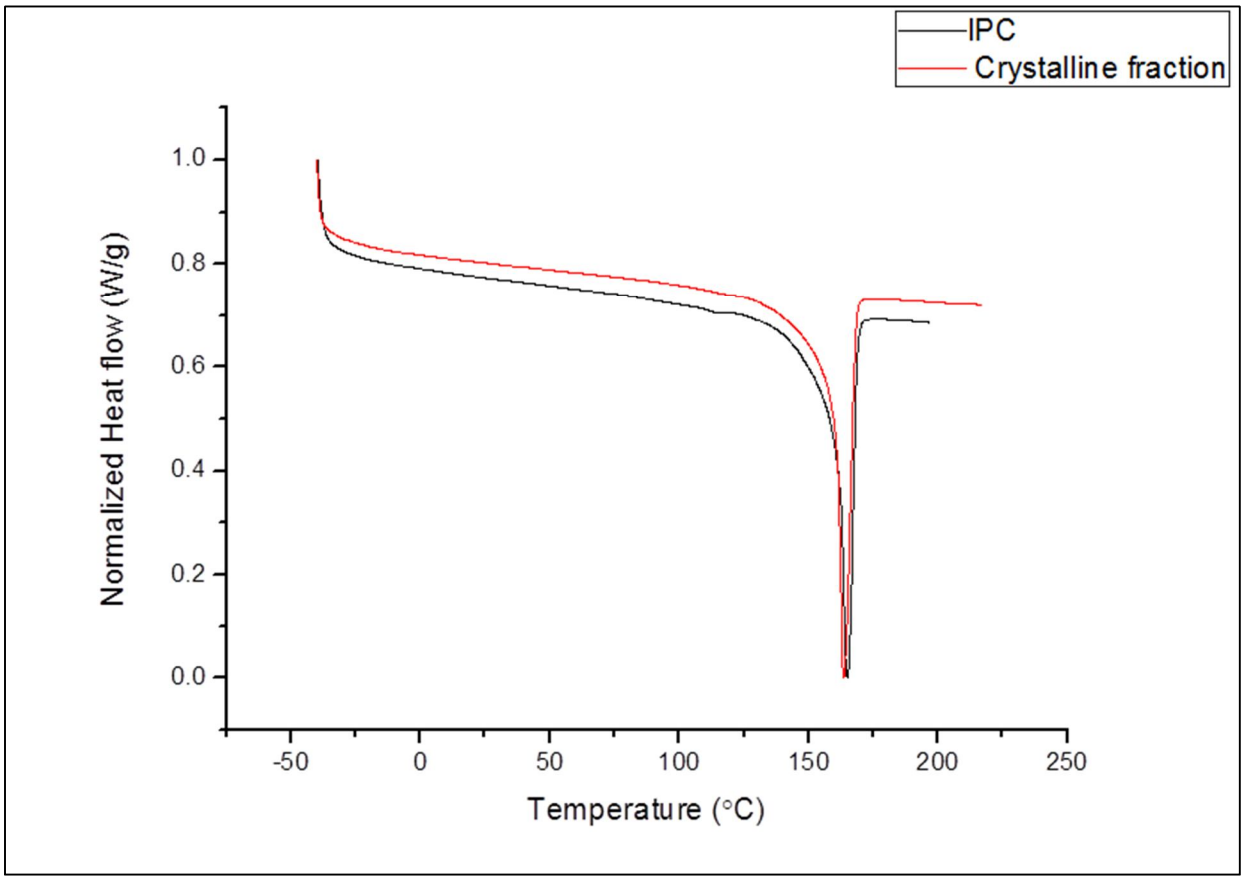

Figure 5.2: DSC thermogram of original IPC648 and crystalline fraction

Table 5.2: Summary of the DSC results for IPC 648 and crystalline fraction

Sample	(J/g)	Crystallinity percentage (%)
IPC648	73.00	35.26
Crystalline fraction	35.26	46.32

The thermograms given in Figure 5.2 show no significant difference in the crystallization and melting temperatures (T_c and T_m) of the crystalline fraction (solid line), compared to the original IPC648 sample (dashed line). Table 5.2 provides a summary of the results obtained from the DSC thermograms. The table shows that the percentage crystallinity of the crystalline fraction is slightly higher than that of the original sample, indicating that the rubbery phase was removed. This shows that the crystalline fraction extracted is similar to the crystalline fraction in the IPCs and the extraction of the rubber did not have a significant influence on the thermal properties of the remaining material. Figure 5.3 shows the DSC thermogram obtained for the extracted EPR.

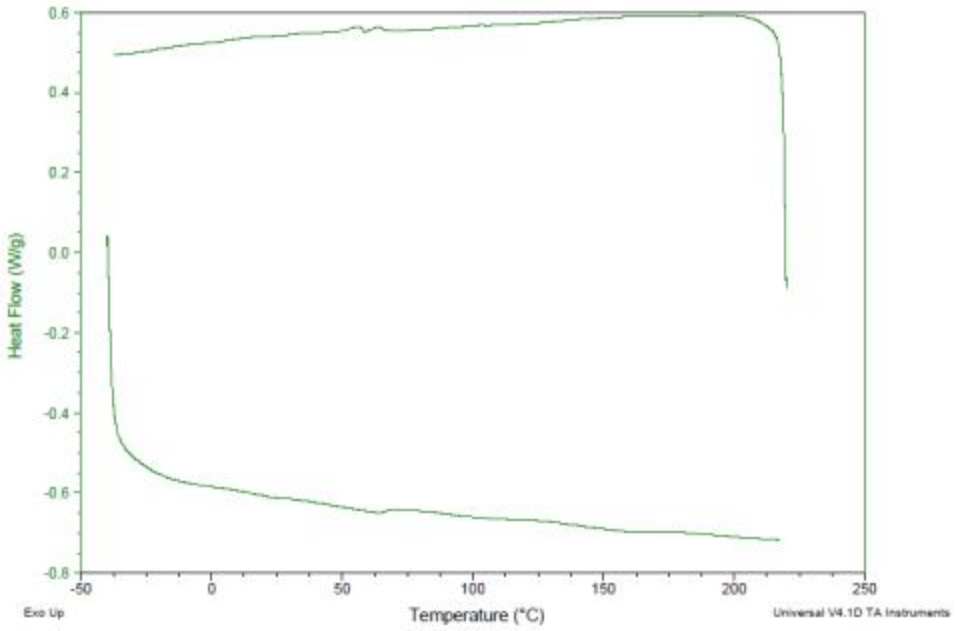

Figure 5.3: DSC thermogram of the EPR extracted from IPC648

The thermogram obtained for the extracted EPR clearly shows the absence of any significant crystallization and melting peaks. The thermogram is similar to other examples of pure EPR.[1] From Figures 5.2 and 5.3 we can conclude that the EPR fraction removed from the IPC648 sample was mostly amorphous and that the rubber fraction did not contain any crystallisable polypropylene copolymer chains. It is important to make this distinction as other studies have shown that the

rubbery fraction of these complex copolymers do in fact contain some sparingly crystalline material.

5.3 Incorporation of labelled cellulose nanowhiskers into rubber

CNW labelled with FITC were incorporated into EPR through the method described in Section 3.2.5. Neither the incorporation of CNW nor the incorporation of CNW/FITC into EPR has been investigated previously, so the method developed and the success thereof was also evaluated. The success of the incorporation was evaluated by way of investigating the dispersion of the CNW/FITC in the EPR film and the detection of the FITC.

Different percentages of labelled whiskers were incorporated into the EPR to investigate which amount would be the most efficient to use. As a first trial, 4 wt%, 5 wt% and 6 wt%.of the labelled whiskers were used. The EPR films were created by solvent casting from a xylene solution containing both the EPR and the required amount of labelled whiskers. The films containing CNW/FITC will be referred to as labelled EPR films throughout the remainder of the thesis. The labelled EPR films were analyzed using confocal fluorescent microscopy (CFM). The images obtained through CFM were analysed and the different weight percentages of CNW/FITC were compared.

In the first experiment, 5 wt% of labelled whiskers was incorporated into EPR. This value was used as a reference point to determine the necessary loading that would allow sufficient detection of the attached FITC. The dispersion of CNW/FITC throughout the EPR film was also evaluated.

Figure 5.4 shows CFM images of the labelled EPR film containing 5 wt% CNW/FITC. The images clearly show that the FITC-labelled CNW could be detected. Figure 5.4 (a) and (b) were taken from the same labelled EPR film but represent different areas in the film and are described as Area 1 and Area 2.

When comparing the two images in Figure 5.4 it is evident that the CNW/FITC was distributed throughout the film. Small areas of agglomeration are visible in both areas, but the overall distribution of the labelled whiskers inside the EPR film seems to be fairly homogenous. This indicates that the method developed for the incorporation of the labelled whiskers was successful.

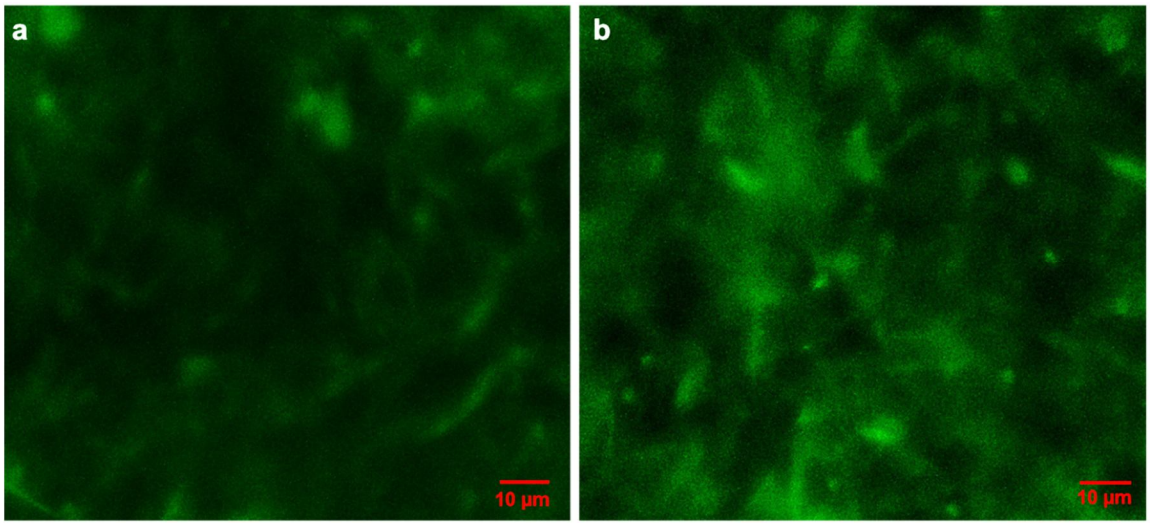

Figure 5.4: CFM images of the 5 wt% CNW/FITC incorporated into EPR. (a) Area 1 and (b) Area 2

The CFM images of the 6 wt% CNW/FITC incorporated into the EPR are shown in Figure 5.5. The figure shows very bright and clear areas of fluorescence. The increase in the intensity of the fluorescence signals of the FITC molecules can be due to agglomeration of the CNW/FITC inside the EPR. When a fluorophore is closely surrounded by other fluorophores, the intensity of the observed fluorescence increases significantly.[2] As mentioned in Chapter 2 the CNW tend to form strong hydrogen bonds due to the presence of the hydroxyl groups on the surface of the CNW.[3,4] This can lead to the formation of CNW/FITC agglomerates inside the EPR film.

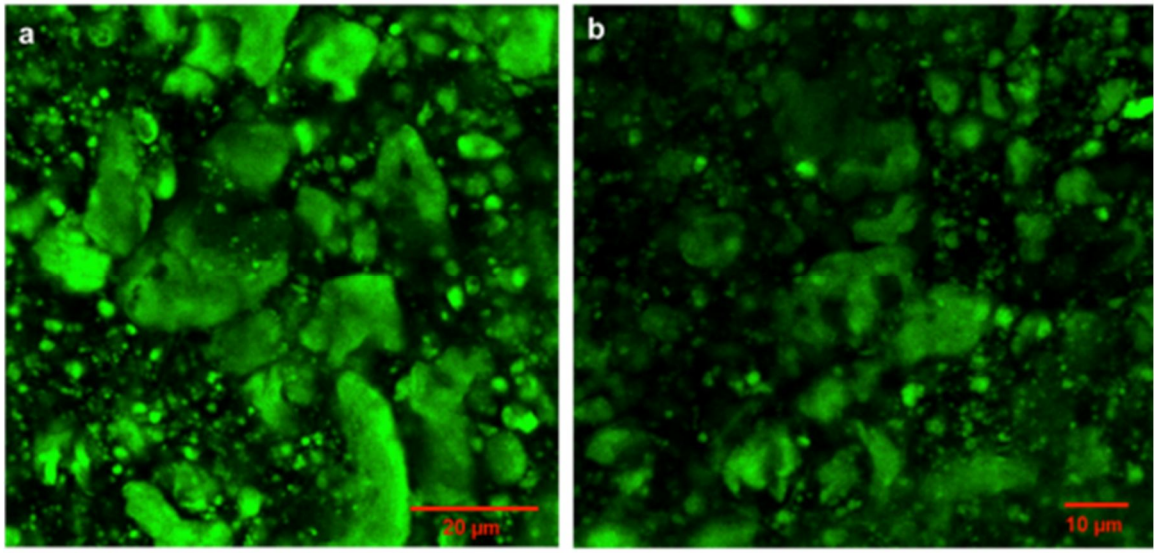

Figure 5.5: Fluorescent image of CNW/FITC 6 wt% in EPR (a) Area 1 and (b) Area 2.

Large agglomeration areas are visible in both areas 1 and 2 of Figure 5.5. Although the dispersion of the CNW/FITC in both areas is similar, and the conclusion that the whiskers have been

dispersed through the whole sample can be drawn, the extent of agglomeration of the CNW/FITC is not ideal.

Figure 5.6 below shows CFM images of EPR labelled with 4 wt% CNW/FITC. The different areas taken from the labelled EPR film indicates a uniform dispersion of the labelled whiskers. The intensity of the fluorescent signal has decreased as expected but not to the extent that the signals were too weak for detection. Less agglomeration of the CNW/FITC than was visible in the case of the sample containing 6wt% CNW/FITC (Figure 5.5) is seen in both Figures 5.6 (a) and (b).

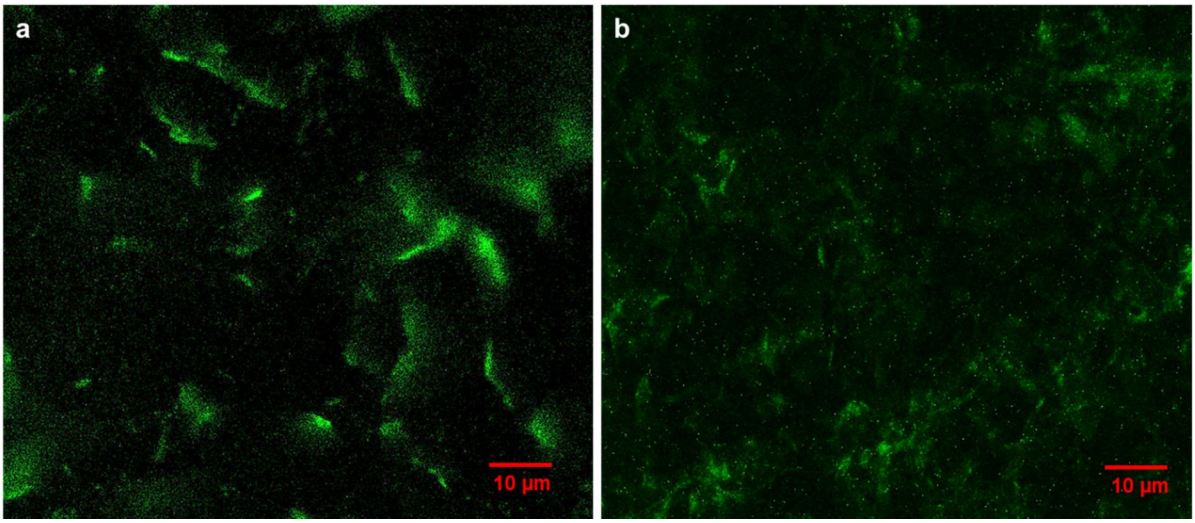

Figure 5.6: CFM images of 4 wt% CNW/FITC incorporated into EPR (a) Area 1 and (b) Area 2.

In Figure 5.7 the CFM images of the three different weight percentages of the CNW/FITC incorporated into the EPR are compared. All three CFM images shows that the CNW/FITC have been successfully incorporated into the EPR. Comparing Figure 5.7 (a) and (b), the dispersion of the labelled whiskers appears similar. The fluorescent intensity of (b) is higher than (a) as one would expect from the higher percentage of labelled whiskers incorporated. The fluorescent intensity of the 4 wt%, although lower, is still acceptable and shows that the CNW/FITC can be detected. Comparing Figure 5.7 (c) with (a) and (b) there is a definite change in the dispersion appearance of the labelled whiskers. The presence of pockets of agglomerated CNW/FITC is clearly visible in (c) and not in (a) nor (b). A possible reason for the agglomeration of the labelled whiskers for the 6 wt% could be the increase in hydrogen bonding with the higher percentage of CNW present. The strong interactions between the hydrogen bonds create a percolating network, as mentioned previously.[5]

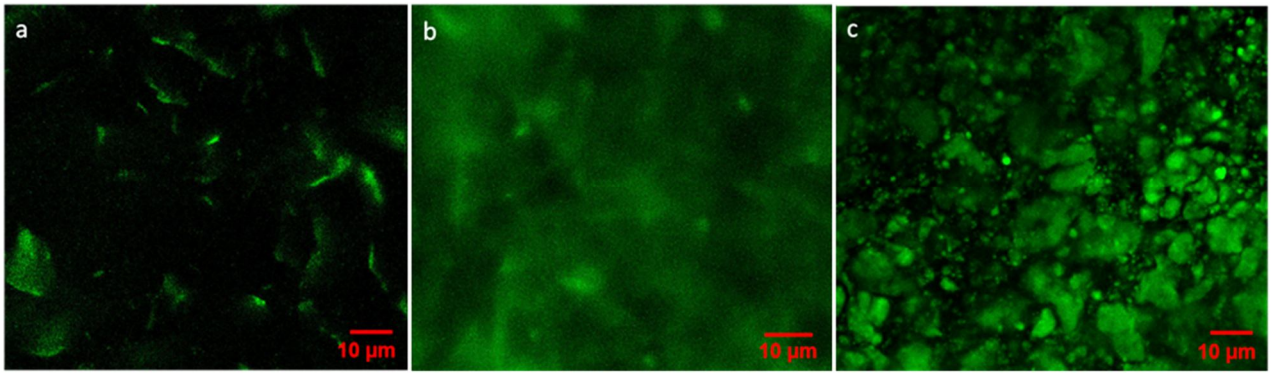

Figure 5.7: CFM images of different labelled EPR films with (a) 4 wt% CNW/FITC, (b) 5 wt% CNW/FITC and (c) 6 wt% CNW/FITC.

The CFM images containing the 4 wt%, 5 wt% and the 6 wt% CNW/FITC all show the successful incorporation of the labelled whiskers into the EPR. The agglomeration that was observed with the 6 wt% CNW/FITC would make the use of the 4 wt% and 5 wt% CNW/FITC more advisable. When comparing the 4 wt % with the 5 wt% CNW/FITC the only real difference is the fluorescence intensities. As the labelled whiskers were still detectable with the incorporation of the 4 wt% it was decided to continue the rest of the experimental work exclusively using 4 wt% of labelled whiskers.

5.4 Mobility of the labelled cellulose nanowhiskers within the ethylene propylene rubber

CNW form very stable aqueous suspensions due to their tendency to form strong hydrogen bonds. This makes it extremely difficult to disperse the CNW in non-polar and organic solvents. The tendency of the CNW to form strong hydrogen bonds is its biggest disadvantage with regards to sufficient dispersion in organic and non-polar solvents.[3-8]

In this study however, that specific disadvantage of the CNW was exploited. The mobility of the labelled whiskers after incorporation and solvent casting was evaluated and will be discussed in this section. At this point, it is important to mention that evaluating the mobility in this part of the study is crucial. The outcome of the mobility of the labelled whiskers greatly influenced the continuation of the study. As previously stated, the desired outcome of the study is to establish and develop a methodology which can help and assist in visually understanding the morphology of the rubber inside the crystalline fraction. Knowing where and how the rubber fraction distributes itself within the crystalline fraction will enable us to better understand and visualize the morphology of impact polypropylene copolymers.

The mobility of the CNW/FITC was first evaluated by monitoring the movement of the CNW/FITC by CFM, after addition of the CNW/FITC solution to the EPR solution as described in Section 3.2.6. The evaluation was conducted on the solution while film formation (solvent evaporation) occurred. The second method utilized different layers of EPR to establish the mobility of the CNW/FITC within the EPR film and between EPR films. The cross sections of these layers were analysed using CFM.

5.4.1 Mobility of labelled cellulose nanowhiskers in EPR: Method one

The movement of the CNW/FITC inside the EPR was monitored in solution as the mobility of particles is higher in solution due to Brownian motion. This was done by taking CFM images at different times. The solution was placed in a container as illustrated in Figure 5.8 and the images were taken from above. The movement of the CNW/FITC was monitored by taking the images at 10 minute intervals.

Figure 5.8: A visual illustration of the container used with the labelled whiskers and EPR solution.

The CFM images were taken from above at the different time intervals of 0 min (t0), 10 min (t10), 20 min (t20), 30 min (t30), 40 min (t40), 50 min (t50) and 60 min (t60). These images are shown in Figure 5.9. There are no real visual differences in the first 10 minutes as indicated by Figures 5.9 (a) and (b). Visual differences were observed from 20 minutes onwards as indicated by Figures 5.9 (c) – (h). In Figures (c) and (f) new CNW/FITC fluorescence structure appeared as indicated. The appearance of this structure is most definitely due to the evaporation of the xylene. The evaporation of the xylene decreases the level of the solution. The CNW/FITC will move downwards in the EPR solution as the CNW/FITC will not evaporate with the xylene. The change in the level of the solution enables the confocal microscope to detect more fluorescent signals deeper in the solution. The detection of fluorescent signals with the confocal microscope can be limited by the “thickness” of the layer being evaluated. The structure which appeared after 20 minutes in (c), moved and attached to another CNW/FITC structure during this 10 minute time interval and is shown in Figure 5.9 (d). In Figure 5.9 (e) and (f) the visual difference on the right of the image can be related to the migration of the CNW/FITC due to Brownian motion at the edges of the container.

Figure 5.9 clearly illustrates the limited movement of the CNW/FITC inside the EPR, even when the EPR is still in solution. The tendency of the CNW/FITC to move inside the EPR phase can be regarded as minimal. The movement of the CNW/FITC inside the EPR solution can mostly be ascribed to the evaporation of the xylene. The evaporation of the xylene forces the labelled whiskers to move downwards as the level of the solution decreases. It should be noted that the meniscus of the solution in the container can also contribute to the movement of the CNW/FITC. The meniscus influences the level of the solution by having slightly higher levels at the sides of the container compared to the levels at the middle of the solution. This level difference can also create movement.

Overall, however, the observation of the movement (or lack thereof) during solvent evaporation of a mixture of EPR and labelled CNW leads to the conclusion that reasonably dispersed CNW in the EPR can be achieved during film formation, and that the movement and agglomeration of the CNW during this process is minimal. An early presumption at this stage was that the movement of the CNW within the rubber phase would also be limited once film formation (solidification) had taken place. The wet sample mobility test illustrated the lack of particle movement in solution. Most particles have a higher tendency to move within a solution than in a solid. When particle movement in the solution is limited, the probability of movement in the solid state is unlikely. This can also help us to predict possible movement in the melt. The solution and melt could behave similarly in terms of flow properties, and particle movement between similar molecular structures or phases are more likely.

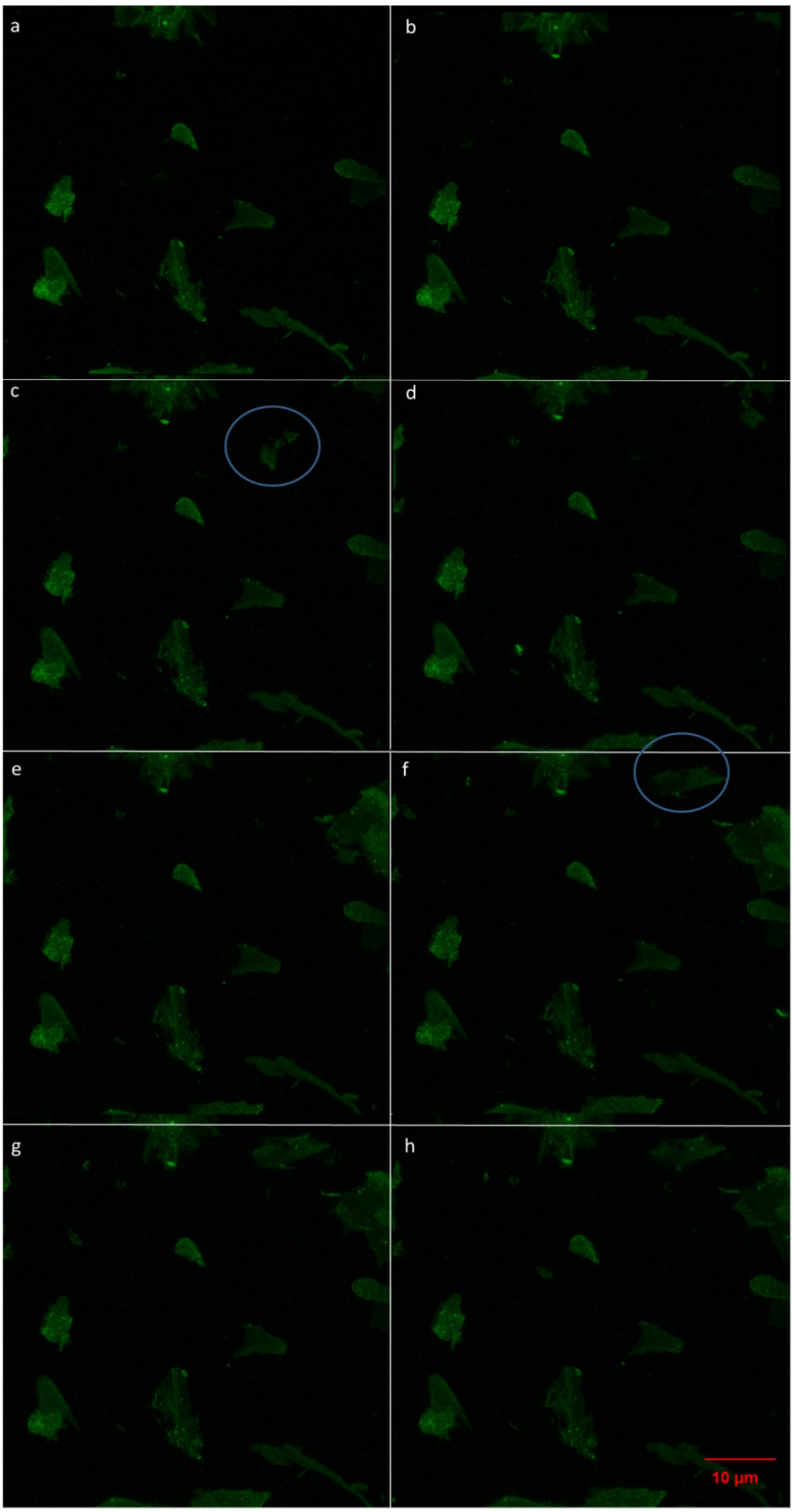

Figure 5.9: CFM images tracking the movement of CNW/FITC in EPR at (a) 0 min, (b) 10 min, (c) 20 min, (d) 30 min, (e) 40 min, (f) 50 min, (g) 60 min and (h) 80 min.

5.4.2 Mobility of labelled cellulose nanowhiskers in EPR: Method two

The second method used to evaluate the mobility of the labelled whiskers was conducted through a layer by layer approach as described in Section 3.2.6.2. This is to illustrate the minimal movement of the labelled whiskers between labelled EPR and clear EPR. Cross sections of the layered samples were submitted to CFM for imaging. The first sample submitted was an EPR film, followed by a labelled EPR film and concluded with another EPR film. The second sample consisted of a labelled EPR film, an EPR film and another labelled EPR film. The two samples are illustrated in Figure 5.10.

Figure 5.10: Illustration of the two samples created by using different layers of EPR and CNW/FITC films and pure EPR films

The CFM images obtained for Sample 1 and Sample 2 are shown below. The images were produced using a z-stack approach. This means that the images were obtained by taking pictures in small intervals (microns) moving in the z-plane. This technique can provide individual images per interval or a 3D image produced by compressing all the individual images into one image. It should be noted that the layered samples were too thick to capture the whole cross–section properly with one z-stack, so more than one z-stack was taken consecutively to produce the images shown. The images were compressed and modified to obtain an overall image of the layers.

Figure 5.11 is a 3D CFM image obtained for the layered Sample 1. The figure clearly shows three distinct regions. The three regions are divided into the bottom, the middle and the top. The top and bottom regions do not show strong fluorescent signals compared to the middle region. As illustrated in Figure 5.10 the middle area of Sample 1 contained CNW/FITC. The strong fluorescent signals observed in the middle area of Figure 5.11 correspond to the labelled EPR film in Sample 1. The fluorescent signals are largely observed in the middle area of the image. This suggests that the CNW/FITC did not migrate into the EPR films despite the introduction of the warm solution, which would partially dissolve the EPR containing the CNW/FITC. The presence of the weak or scattered fluorescent signals further away from the centre can be attributed to the way

the layers were prepared. Firstly, the weak signals towards the bottom area can be some of the CNW/FITC that settled downwards as the xylene evaporated, as explained in the previous method. Secondly, the weaker signals towards the top layer can be as a result of (a) the CNW/FITC found on the surface of the labelled EPR film or (b) the labelled EPR itself. The CNW/FITC on the surface could have been disrupted by the warm solution of EPR that was poured onto the labelled EPR film to create the third layer. The labelled layer of EPR at the surface could have been dissolved by the warm solution and the CNW/FITC inside this rubber phase could than have moved with it.

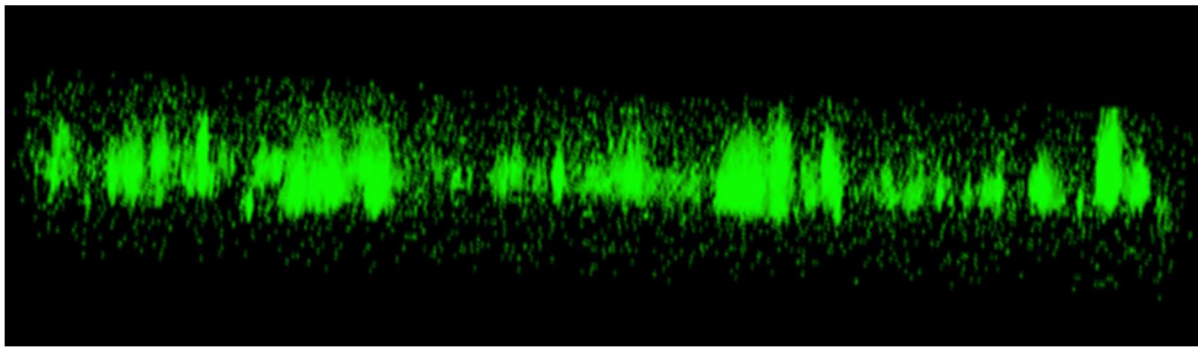

Figure 5.11: 3D confocal fluorescent microscopy image of Sample 1.

Figure 5.12 shows individual CFM images of the different layers of Sample 1 obtained from the z-stack. Image (a) was taken at the bottom of Sample 1, (b) was taken in the middle region and (c) was taken in the top area of Sample 1. Figure 5.12 (a) and (c) do not show any fluorescence compared to Figure 5.12 (b). The CFM image in (b) corresponds to the labelled EPR and the CFM images of (a) and (c) corresponds to the unlabelled EPR. The CFM images in the figure below also correspond to what is shown by the 3D image in Figure 5.11. This also indicates that the labelled whiskers did not migrate into the bottom or the top layer.

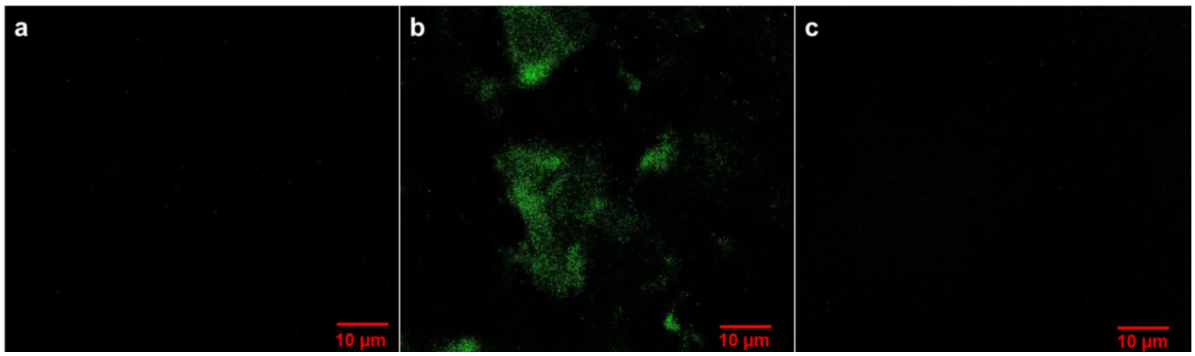

Figure 5.12: Confocal fluorescent microscopy images of Sample 1 (a) bottom layer, (b) middle layer and (c) top layer.

In Figure 5.13 the three different layers are also very clearly visible. The strong fluorescence signals at the bottom and the top of the image are associated with the CNW/FITC inside the EPR. The lack of strong fluorescent signals in the middle of the image indicates that this insertion does not contain CNW/FITC. It can therefore be said that the labelled EPR films are visible at the top and the bottom of the image and the EPR film is present in the middle. The lack of strong fluorescent signals in the middle also indicates that the labelled whiskers did not migrate from the labelled EPR films to the EPR. The weak fluorescent signals in the middle can be described by the same reasons as discussed for Figure 5.11. The presence of the CNW/FITC on the surface of the bottom layer or the EPR itself could have been disrupted by the warm EPR that was poured onto the film to create the second layer. The warm solution of EPR and xylene can dissolve some of the labelled EPR after casting.

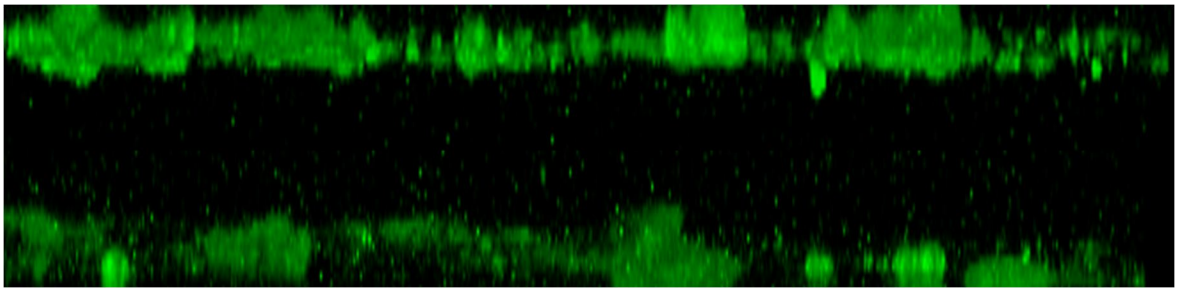

Figure 5.13: 3D confocal fluorescent microscopy image of Sample 2.

Figure 5.14 show the individual CFM images obtained from the z-stack of Sample 2. Figure 5.14 (a), (b) and (c) represents the bottom, the middle and the top respectively. Images (a) and (c) show strong fluorescent signals compared to image (b). This also correlates to the labelled and unlabelled EPR of Sample 2 as indicated by Figure 5.10.

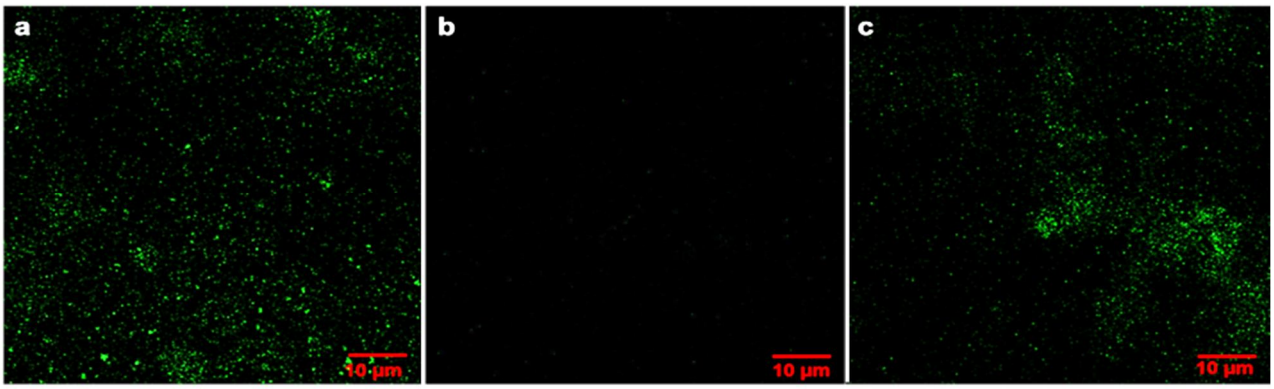

Figure 5.14: Confocal fluorescent microscopy images of Sample 1 (a) bottom layer, (b) middle layer and (c) top layer.

From the figures above it is clear that the mobility of the CNW/FITC inside the EPR is limited and that the labelled whiskers do not migrate freely from the one layer to the next, even in the presence of warm solvent. Both methods, the wet and the layer by layer approach, clearly show that the labelled whiskers largely stay within the EPR phase in which they were placed and do not migrate throughout the whole sample. After incorporation into a specific EPR, the CNW/FITC tend to stay in the EPR and do not move around. Proving this concept allows us to predict with reasonable confidence that the CNW/FITC will possibly stay in the EPR and will not migrate into the crystalline fraction when the fractions are melt-recombined. This said, recombination occurs at elevated temperatures, which can increase the mobility of the whiskers and which might lead to migration into the crystalline fraction. Illustrating the lack of movement of the whiskers between the EPR films do not exclude the possibility of migration to the crystalline phase in the melt but it does show that the possibility is far lower.

5.5 Recombination of ethylene propylene rubber and the crystalline fraction

The EPR and the crystalline fraction were separated by the method described in Section 3.2.7. This was done in order to label the EPR film with CNW/FITC. As discussed previously, different weight percentages of CNW/FITC were incorporated into EPR, after which it was analysed. After evaluation it was decided to use 4 wt% of CNW/FITC and 96 wt% EPR. The labelled EPR and crystalline fraction was recombined through injection moulding. The ratio in which the fractions were recombined was 17 wt% labelled EPR and 83 wt% crystalline fraction. The labelled EPR contained 4 wt% CNW/FITC and 2 wt% stabilizer. The stabilizer was incorporated to prevent the degradation of the sample during injection moulding, which can occur when a sample is exposed to high temperatures.

A labelled EPR film containing 2 wt% stabilizer was analysed by CFM. This was done to evaluate the influence of the stabilizer on the dispersion of the labelled whiskers inside the EPR film.

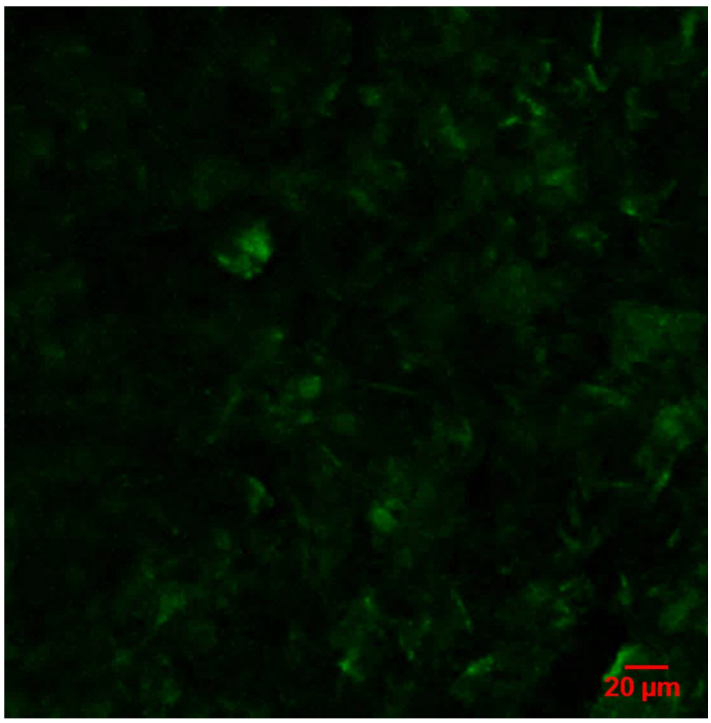

Figure 5.15: CFM image of the labelled EPR film containing 2 wt% stabilizer

The figure above indicates that the dispersion of the labelled whiskers is homogenous. The incorporation of the 2 wt% stabilizer into the EPR film did not influence the dispersion of the CNW/FITC inside the EPR film.

The crystalline fraction and unlabelled EPR were first recombined using injection moulding. DSC was used to analyse the sample and to determine the crystallinity of the recombined sample. This was done to verify the technique and percentages (17 wt% EPR and 83 wt% crystalline fraction) used for the recombination step and the accuracy thereof.

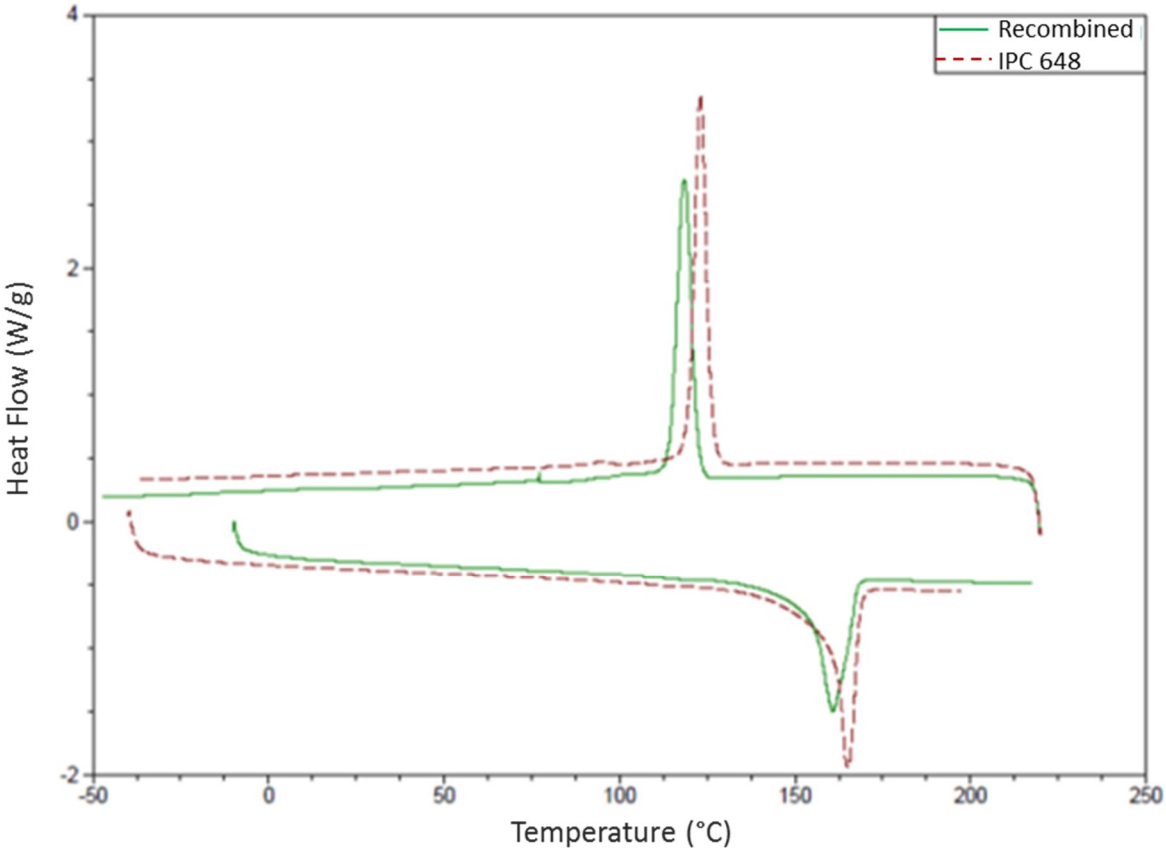

Figure 5.16: DSC thermograms overlay of recombined EPR, crystalline fraction and IPC648

The obtained thermograms in Figure 5.16 indicate that there is a small difference in the T_c and T_m values. There is also a slight decrease in crystallization as summarized in Table 5.2. This indicates, as could be expected, that recombination results in a material that is similar, but not identical to the original, unextracted IPC.

Table 5.3: Summary of the DSC results for IPC 648 and recombined

Sample	(J/g)	Crystallinity percentage (%)
IPC648	74.08	35.79
Recombined	69.04	33.35

This is probably due to the fact that a limited amount of sample degradation and molecular weight breakdown is inevitable during the extraction and recombination processes. Both these processes involve either elevated temperatures or friction or both, and this will lead to degradation.

5.5.1 Injection moulding of labelled ethylene propylene rubber and crystalline fraction

The labelled EPR and crystalline fraction were recombined through injection moulding. The injection moulded samples were microtomed to create cross sections through the samples. Three different cross sections were taken as representatives of the whole injection moulded sample. The three different cross sections are labelled a, b and c as indicated by Figure 5.17.

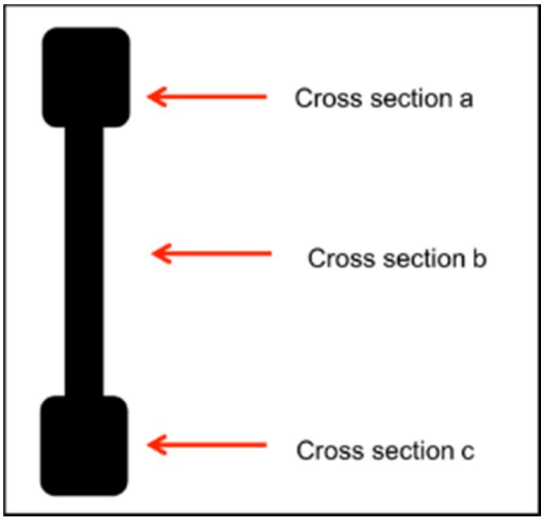

Figure 5.17: Illustration of the three microtomed cross sections

The microtomed cross sections were submitted to CFM to evaluate the distribution of the labelled EPR in the injection moulded sample.

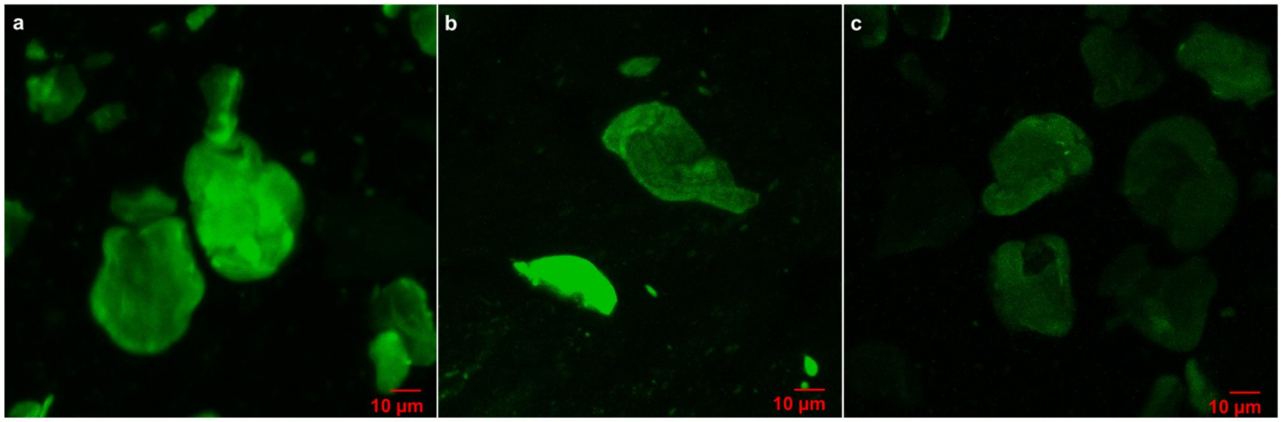

Figure 5.18: CFM images of the injection moulded samples (a) Cross section a, (b) Cross section b and (c) Cross section c.

In Figure 5.18 the CFM images of the three cross sections taken from the injection moulded sample are shown. All three images show similar fluorescent structures indicating that the three sections can be taken as an overall representation of the rest of the injection moulded sample. The fluorescent signals present can only be attributed to the labelled EPR inside the recombined fraction. As the EPR and the crystalline materials will phase separate, it is expected that discrete rubber particles should be present in the final product. It is fair to assume that the structures visible in Figure 5.18 represent these rubbery particles.

The fluorescent signals, however, are relatively strong compared to the CFM images shown previously. This could be attributed to the fact that EPR films are really thin compared to the thickness of the injection moulded samples. Another possible reason for the strong fluorescent signals observed could be sample folding, which occurred during the microtoming of the cross sections.

The images show that the labelled whiskers did not migrate throughout the whole sample but stayed within the EPR. This is shown by the fluorescent structures observed in images (a) to (c). These fluorescent structures are relatively large, as the scale bar indicates, and significantly larger than the incorporated labelled whiskers. That said, it is important to remember that when analysing fluorescent images the exact size can be misleading due to the scattering pattern of the fluorescent light, making labelled structures appear larger than what they are.

Due to the size of the injection moulded EPR two methods were conducted in an attempt to create a more accurate representation of the morphology of these commercially available impact polypropylenes.

The first method was to cut the EPR before recombination into even smaller pieces than the labelled EPR used previously. The second method involved the grinding of the obtained injection moulded disc. The results of the two methods are shown in Figure 5.19 and Figure 5.20 respectively. Figure 5.19 and Figure 5.20 clearly show strong fluorescent signals but with a decrease in the overall size of the fluorescent structures compared to Figure 5.18. The smaller sized EPR incorporated seems to have better distribution of the labelled EPR inside the injection moulded sample. In both samples the three cross sections seem to have a better distribution in terms of the particle size of the labelled rubber within the injection moulded sample. When comparing the CFM images obtained in Figure 5.19 and Figure 5.20 there was no significant visual difference in the overall distribution, so it was decided to only make use of the very finely cut labelled EPR.

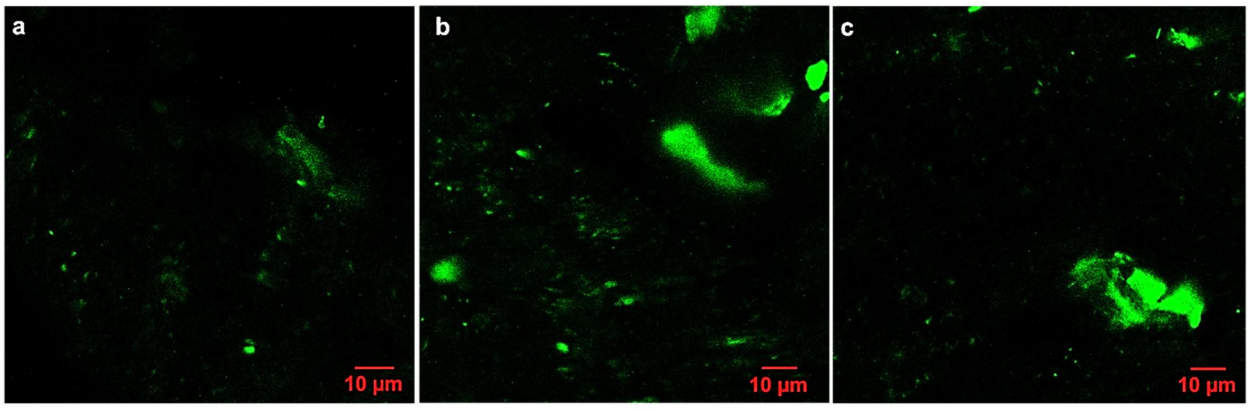

Figure 5.19:CFM images of the three cross sections obtained from the injection moulded sample produced by the finely cut EPR (a) Cross section a, (b) cross section b and (c) cross section c.

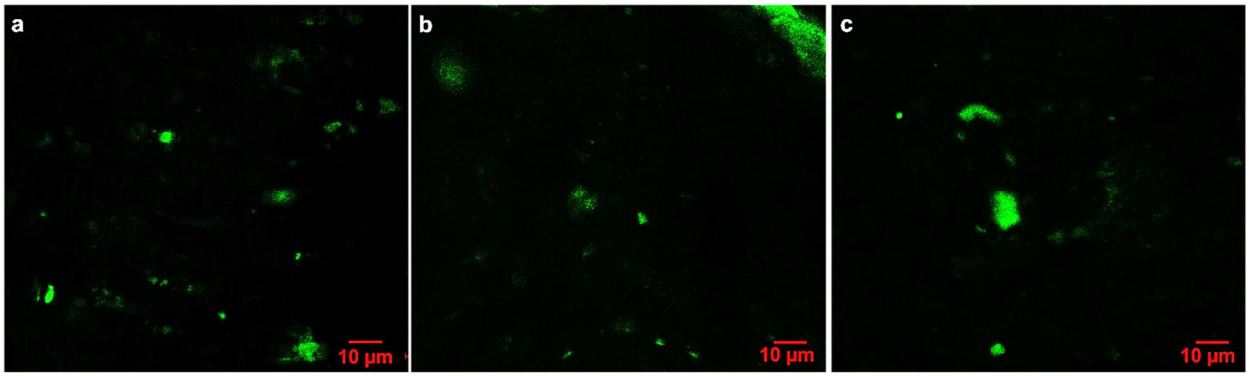

Figure 5.20: CFM images of the three cross sections obtained from the finely ground injection moulded sample (a) Cross section a, (b) Cross section b and (c) Cross section c.

From the above three figures it can be concluded that the recombination of the labelled EPR and the crystalline fraction was successful and the smaller the particles sizes before injection moulding the better the dispersion of the EPR. Most importantly, the results shown in Figures 5.18, 5.19 and 5.20 indicate that the use of labelled CNW as probes to visualize morphology in complex polymer systems is viable.

5.5.2 Extraction of the labelled ethylene propylene rubber

The mobility of the fluorescently labelled whiskers proved to be limited in the EPR film in which they were incorporated during the wet sample and layer by layer approach. These tests provided the necessary platform to continue the study of labelling the EPR with the fluorescently labelled whiskers. The CFM images of the injection moulded samples showed strong fluorescence signals, which could be associated with the labelled EPR. A study was conducted on an injection moulded sample to confirm that the labelled whiskers did not migrate into the crystalline fraction during the

process of injection moulding. The fluorescent signals of the injection moulded sample were compared to the injection moulded sample after being exposed to xylene for 24 hours. Xylene is s solvent for the EPR, but not for the crystalline fraction. Figures 5.21 and 5.22 show the CFM images of the untreated and treated sample respectively. A tiling z-stack image was compiled for both samples. This was done to create an overall view of the injection moulded sample and the distribution of the labelled EPR within the sample. Figures 5.21(a) to (c) show the CFM images obtained by using the 488 nm laser (a), the T PMT filter (b) and both in (c). The T PMT filter was used as it allows light to passes through the sample, creating a contrast between the amount of light passing through and the light reflected by the sample creating an image. The same CFM setup was used for the xylene treated sample and the CFM images generated as shown in Figure 5.22.

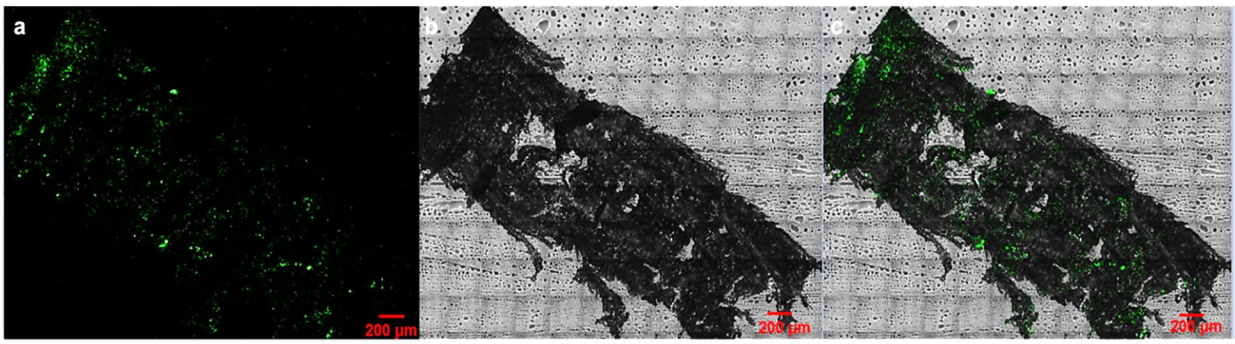

Figure 5.21: Z-stack tile CFM image of the untreated injection moulded sample at (a) Laser 488 nm, (b) T-PMT filter and (c) 488 nm laser and T PMT filter.

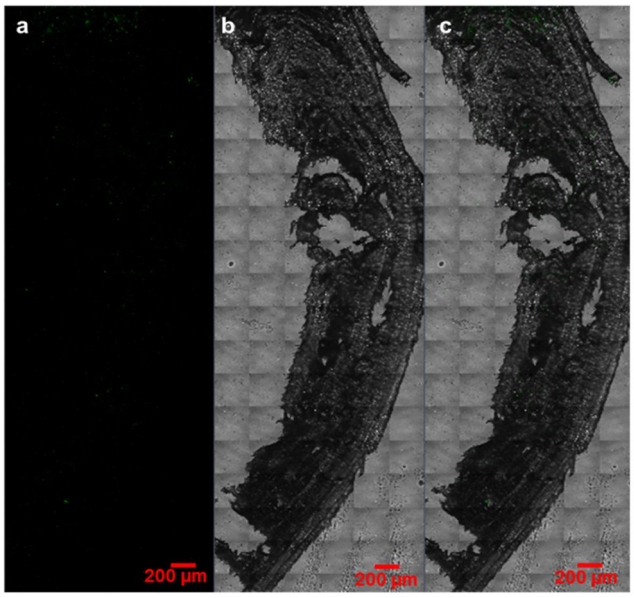

Figure 5.22: Z-stack tile CFM image of the xylene treated injection moulded sample at (a) Laser 488 nm, (b) T-PMT filter and (c) 488 nm laser and T-PMT filter.

Comparing the treated injection moulded sample with the untreated injection moulded sample, there is a definite decrease in the fluorescent signals. This is clearly visible when comparing Figure 5.21 (a) with Figure 5.22 (a). In Figure 5.22 (a) some very weak fluorescent signals are present. This can be ascribed to some of the labelled EPR towards the middle of the sample, which was not directly exposed to the xylene. This is confirmed by the 3D CFM images below.

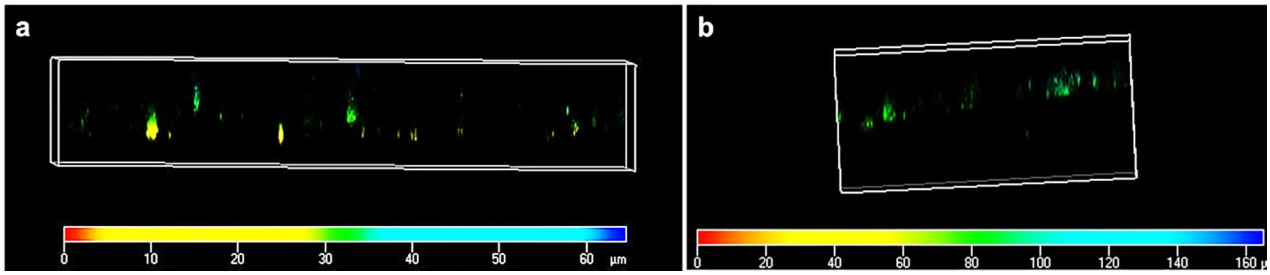

Figure 5.23: 3D CFM images of (a) untreated and (b) treated injection moulded samples

Figure 5.23 (b) does not show fluorescent signals until deeper down in the sample, at approximately 60 µm to 80 µm. Comparing the distribution of the fluorescent signals in Figure 5.23 (a) with Figure 5.23 (b) it is clear that there are no fluorescent signals at the surface. This proves that the CNW/FITC was extracted with the EPR as the CNW/FITC will not dissolve in xylene.

5.6 Conclusions

The IPC648 sample was successfully fractionated into an EPR fraction and crystalline fraction. The separation of the two fractions was confirmed by DSC thermograms. The percentage crystallinity was slightly higher for the crystalline fraction compared to the normal IPC648. The labelled CNW were successfully incorporated into the EPR film for all three weight percentages used. All three weight percentages showed an even distribution of the labelled CNW within the EPR film. The 6 wt% fraction seemed to cause agglomeration of the CNW/FITC due to the strong hydrogen bond interactions between the whiskers. The 4 wt% CNW/FITC showed detectability and evenly distributed fluorescent signals and was therefore used throughout this study. The movement of the labelled whiskers inside the EPR film was also evaluated by CFM and showed that the overall movement of the CNW/FITC is very limited. The labelled EPR and crystalline fraction were recombined successfully by means of injection moulding. The DSC thermograms of the recombined sample and original IPC648 were compared and revealed a slight shift in the crystallization and melting temperatures with a slight decrease in the overall percentage crystallinity. The CFM images showed that the labelled EPR can be easily detected after recombination and that the labelled EPR is dispersed through the whole injection moulded sample.

However the CFM images obtained showed very large EPR particles and the recombination of the labelled EPR and crystalline fraction were evaluated. The evaluation of the recombined samples did not show significant visual differences between the two new methods evaluated, but compared to the original method used for recombination there was a significant improvement. The smaller sized particles showed a better distribution of the EPR inside the injection moulded sample. The injection moulded sample from which the labelled EPR was extracted did show a decrease in the fluorescent signals on the surface, which indicates that the labelled whiskers did not migrate into the crystalline fraction, but stayed within the EPR.

5.7 References

1. Xue Y, Fan Y, Bo S, Ji X. European Polymer Journal 2011; 47(8):1646-1653.

2. Gonçalves MST. Chemical Reviews 2008; 109(1):190-212.

3. Siqueira G, Bras J, Dufresne A. Polymers 2010; 2(4):728-765.

4. Eichhorn S, Dufresne A, Aranguren M, Marcovich NE, Capadona JR, Rowan SJ, Weder C, Thielemans W, Roman M, Renneckar S. Journal of Material Science 2010; 45(1):1-33.

5. Siqueira G, Tapin-Lingua S, Bras J, da Silva Perez D, Dufresne A. Cellulose 2011; 18(1):57-65.

6. Habibi Y, Lucia LA, Rojas OJ. Chemical Reviews 2010; 110(6):3479-3500.

7. Li Y, Ragauskas AJ. Algae 2011; 75(80):10-15.

8. Capadona JR, Shanmuganathan K, Trittschuh S, Seidel S, Rowan SJ, Weder C. Biomacromolecules 2009; 10(4):712-716.

CHAPTER 6

Evaluation of labelled ethylene propylene rubber

6.1 Introduction

It has been proposed (without proof) that the properties of propylene impact copolymers can be altered by the addition of more rubbery material. The work presented in this chapter seeks to see if two rubber samples that appear to be chemically similar (but not identical) but differing in molecular weight will in fact mix when they are melt-blended with the semicrystalline/crystalline fraction of the IPC. To this end, an ethylene-propylene copolymer (Mw 724000 g/mol) sample was obtained from an industrial source. The molecular weight of this sample is higher than that of the IPC648. The sample was mostly comprised of EPR, but also contained some semi-crystalline copolymers. The reason for using this sample for further studies was to obtain an ethylene-propylene rubber sample, (EPR (lab)), from a source other than the one extracted from the IPC648 polymer. This would allow for further studies with regards to the miscibility of rubbery materials during blending experiments.

The EPR fraction was isolated according to the method described in Chapter 3 to obtain an ethylene propylene rubber fraction, and a crystalline fraction. The isolated fractions will be referred to as EPR (lab) and crystalline fraction (lab) respectively. The fractions were analysed by means of DSC. The extracted EPR (lab) was labelled with 4 wt% CNW/FITC. The labelled EPR (lab) film was analysed using CFM. The labelled EPR (lab) and the crystalline fraction (lab) were recombined after the addition of a 2 wt% stabilizer and compared to the recombined labelled IPC648 sample.

The miscibility of the two different molecular weight rubber fractions was then evaluated. The rubber fractions used were the EPR, which was extracted from IPC648, and the EPR (lab) extracted from the industrial ethylene-propylene copolymer sample. The two EPR samples were labelled with two different fluorescent markers, FITC and RhB, to detect the miscibility. The labelled EPR (lab) with 4 wt% CNW/FITC will be referred to as EPR/FITC for the remainder of the thesis.

6.2 Differential scanning calorimetry (DSC)

The ethylene-propylene copolymer sample was separated into two fractions: the EPR (lab) and crystalline fraction (lab). DSC analyses were done on both fractions to evaluate the success of the separation. The DSC thermograms obtained are shown in Figure 6.1 and Figure 6.2.

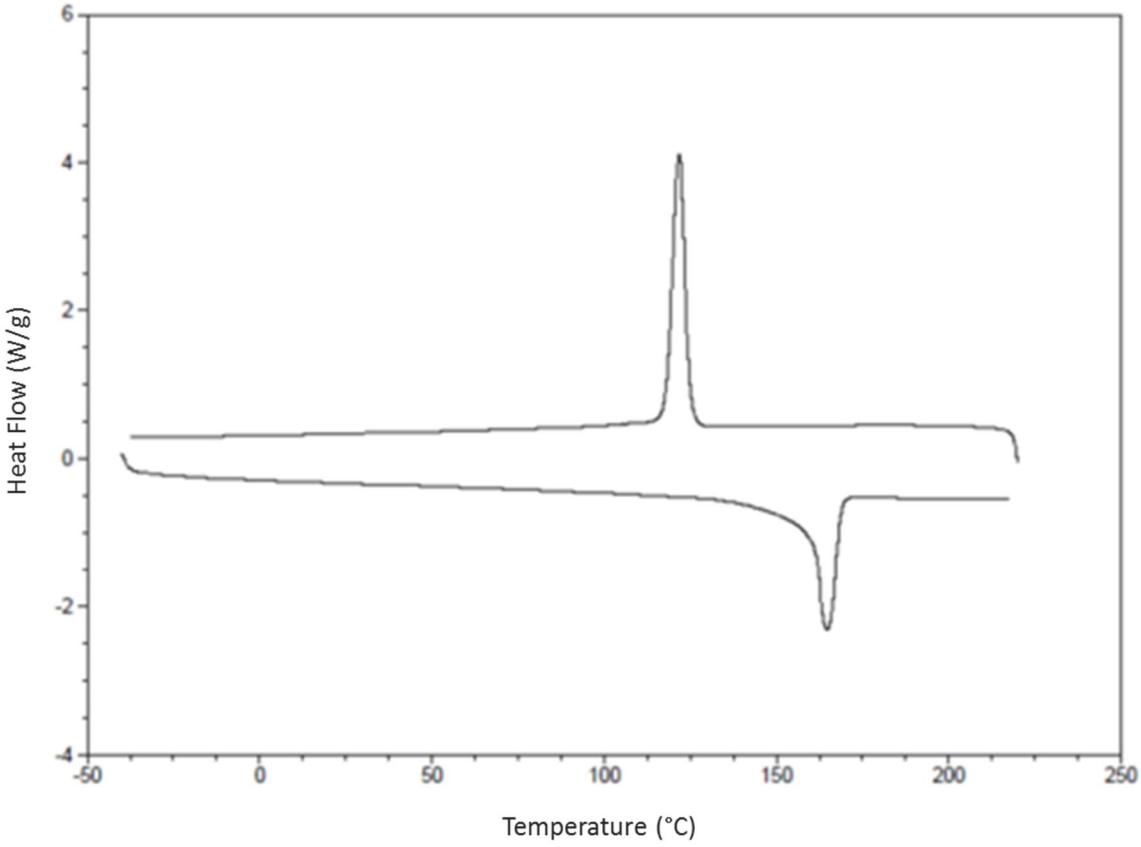

Figure 6.1: DSC thermogram of crystalline (lab) fraction.

The DSC thermogram in Figure 6.1 shows a very strong crystallization and melting peak. The T_m and T_c values, of 165 °C and 125 °C respectively, are the temperatures associated with isotactic polypropylene. This is an indication that the removal of the EPR (lab) did not have an effect on the remaining the crystalline fraction (lab).

The DSC thermogram in Figure 6.2 shows a very small crystallization peak. The crystallization peak seen is very small, and is caused by poly(ethylene) chains inside the EPR (lab). If this sample contained any isotactic polypropylene chains, a strong and prominent crystallization peak would be visible in Figure 6.2. Therefore it can be concluded that the EPR (lab) was mostly removed from the crystalline fraction (lab), but that the EPR (lab) fraction still contained some crystalline PE. It is important to remember that the ethylene-propylene copolymer has a synthetic

rubber phase which contains a higher amount of poly(ethylene) content compared to IPC648, which can contribute to some crystallization. From Figures 6.1 and 6.2 it is clear that the sample was separated into the two fractions.

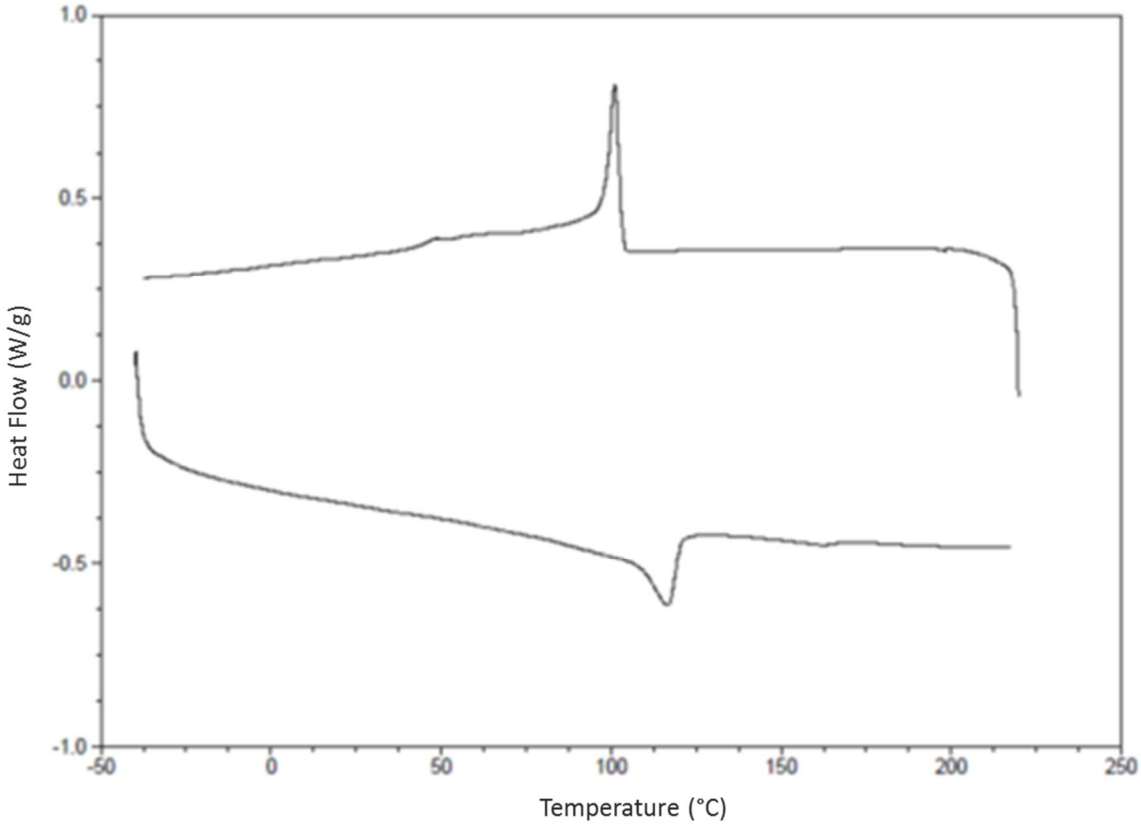

Figure 6.2: DSC thermogram of EPR (lab) fraction.

6.3 Incorporation of labelled cellulose nanowhiskers into ethylene propylene rubber extracted from the ethylene-propylene copolymer

Labelled CNW were incorporated into the EPR (lab) following the same procedure used for the IPC648 EPR sample, as described in Chapter 3. The labelled whiskers were incorporated into the EPR (lab), in a 4:96 wt% ratio. The labelled EPR (lab) with the 4 wt% CNW/FITC will be referred to as EPR/FITC, as mentioned earlier. CFM was used to analyse the incorporation of the 4 wt% CNW/FITC into the EPR (lab) film.

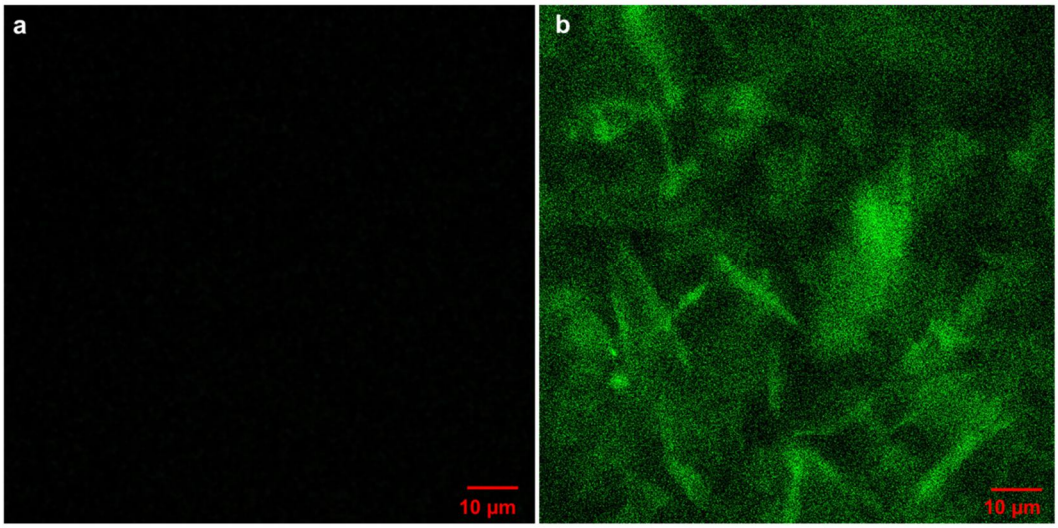

Figure 6.3: CFM images of (a) ERP (lab) and (b) EPR/FITC.

Figure 6.3 show the CFM images obtained from the unlabelled EPR (lab) and the labelled EPR (lab). Figure 6.3 (a) shows no signs of fluorescence, while Figure 6.3 (b) shows strong, well dispersed fluorescent signals. The only difference between the samples in (a) and (b) are the presence of the incorporated CNW/FITC in the EPR (lab) film. From Figure 6.3 (b) it is clear that the incorporation of the labelled whiskers into the EPR (lab) was successful.

Different areas of the EPR/FITC film were cut out and analysed by means of CFM. The different areas were taken to evaluate the overall incorporation and dispersion of the CNW/FITC in the EPR/FITC film.

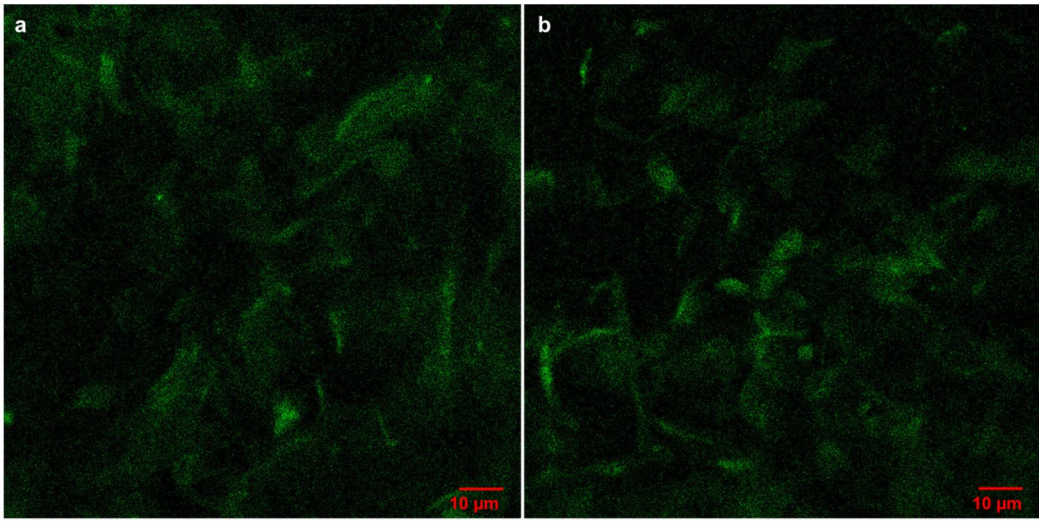

Figure 6.4: CFM images of the EPR/FITC (a) Area 1 and (b) Area 2

The CFM images in the above figure show that the CNW/FITC were successfully incorporated into the EPR (lab). The CNW/FITC are evenly dispersed in the EPR/FITC film as seen in the above figure. This is shown by the homogenous distribution of the fluorescent signals in Figure 6.4 (a) and (b). Both images have a uniform dispersion of labelled whiskers inside the EPR (lab) film. Section 1 and Section 2 represent different areas of the EPR/FITC film. The fact that both sections show similar distributions of the labelled whiskers inside the EPR (lab) film confirms the fact that the CNW/FITC were incorporated and dispersed evenly throughout the whole EPR/FITC film.

6.4 Recombination of the two fractions from the ethylene-propylene copolymer sample after the labelling by means of injection moulding

The EPR/FITC fraction was recombined with the crystalline fraction (lab) by means of injection moulding. The recombined injection moulded sample was evaluated by means of DSC and CFM. The DSC was done to evaluate the success of the recombination of the EPR/FITC with the crystalline fraction (lab). The EPR/FITC and crystalline fraction (lab) was recombined in a 17 wt% EPR (lab) and 83 wt% crystalline fraction (lab). A stabilizer (2 wt%) was added to prevent degradation from occurring while the EPR/FITC and crystalline fraction were exposed to elevated temperatures inside the heating cylinder. Different sections of the injection moulded samples were microtomed and submitted to CFM to determine the dispersion of EPR/FITC inside the injection moulded sample. The fluorescent images of CFM will be discussed.

6.4.1 Differential scanning calometry (DSC)

DSC analysis was done on a recombined sample to evaluate the effect (if any) of the recombination procedure. The DSC thermogram is shown in Figure 6.5. The thermogram shows two crystallization peaks and two melting peaks. The peak temperatures for both the crystallization and melting peaks correspond to the T_c and T_m temperatures obtained from the individual samples. This indicates that both fractions were present in the recombined sample and that the recombination of the two fractions did not affect the thermal properties of the materials.

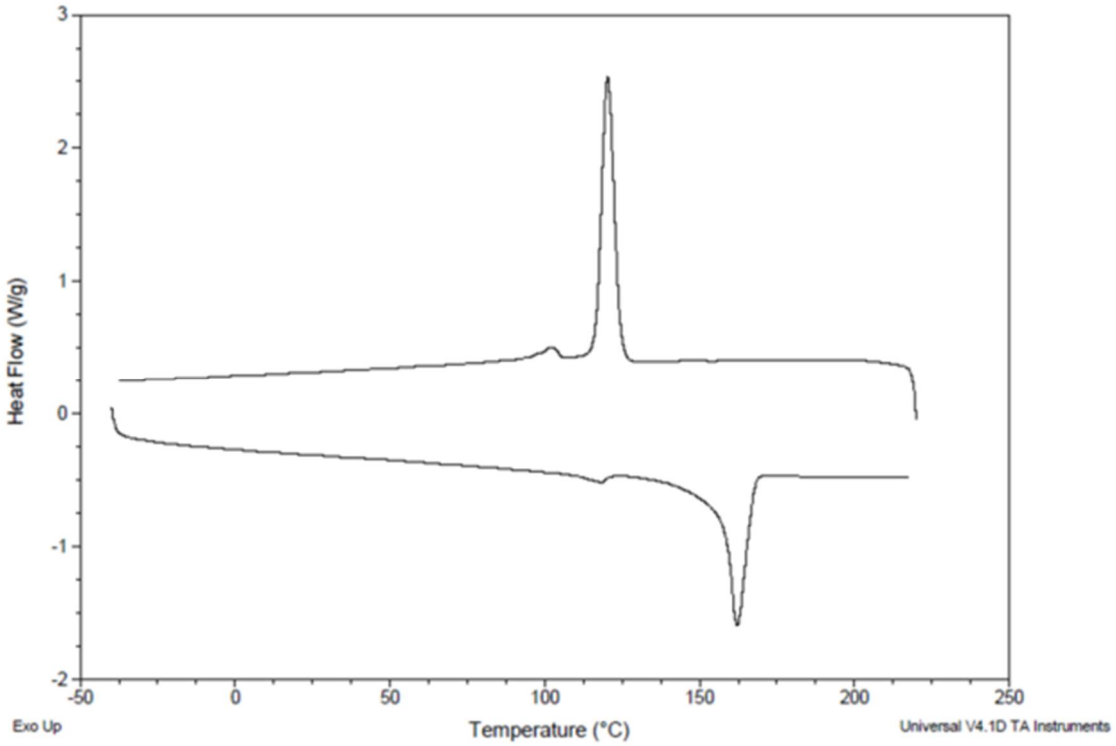

.

Figure 6.5: DSC thermogram of the injection moulded crystallization fraction (lab) and EPR/FITC.

6.4.2 Confocal fluorescent microscopy of injection moulded samples

The injection moulded samples were microtomed in three sections, after which the sections were submitted to CFM. The microtomed samples were submitted to CFM to evaluate the dispersion of the EPR/FITC fraction in the overall injection moulded sample. Different sections of the injection moulded samples were evaluated and used to compile an overall representation of the injection moulded sample. The same method was used, as described in Section 5.5.1, and the illustration of the different sections used for CFM are seen below.

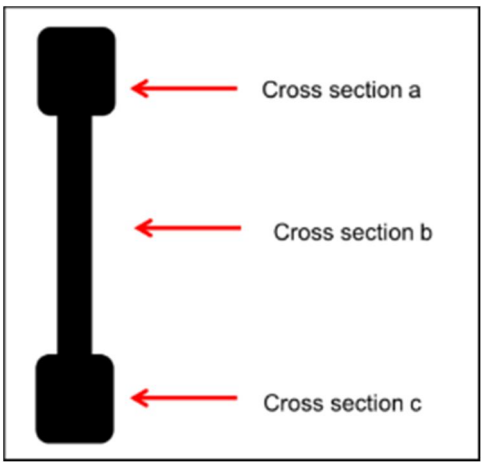

Figure 6.6 : Illustration of the cross sections taken from the injection moulded samples.

The CFM images obtained from the different cross sections are illustrated below in Figure 6.7. All three sections show fluorescent signals. The fluorescent signals are caused by the presence of the incorporated labelled whiskers. The incorporated labelled whiskers will most likely stay in the EPR (lab) (as discussed in Chapter 5), although there is a small possibility that they might still migrate into the crystalline fraction (lab). The mobility of the whiskers was discussed and proved in Chapter 5, but it was only applicable to the IPC648 rubber fraction. Taking the scaling of the images into account, the fluorescent structures are in the range of 10 µm. This does indicate that the dispersion of the EPR/FITC occurred during the mixing and injection moulding. This is a clear indication that the fluorescent structures seen below are caused by the labelled rubber, and not by migrated CNW/FITC.

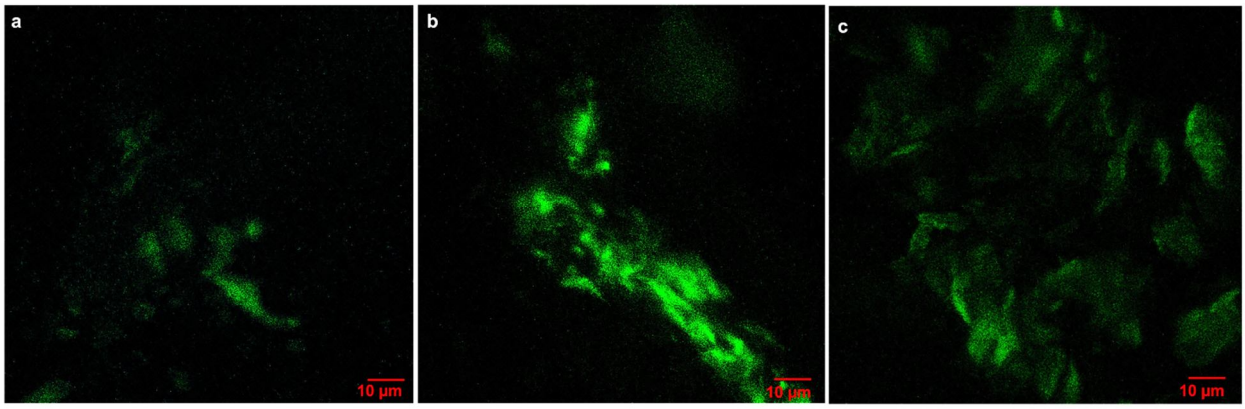

Figure 6.7: CFM images of the injection moulded recombined samples (a) Section a, (b) Section b and (c) Section c.

Figure 6.7 also shows that the EPR/FITC is dispersed throughout the sample. The CFM images confirm that the labelled rubber (lab) and crystalline fraction (lab) were successfully recombined.

Although no conclusion can be drawn about the actually morphology of the ERP inside the injection moulded sample at this point, the possibility of using the labelled CNW was confirmed.

6.5 Miscibility of different rubber fractions

In this section the miscibility of two rubber fractions with different molecular weights were evaluated. The rubber fractions used were the EPR extracted from IPC648, and the EPR (lab). The molecular weight of the EPR, is the lower of the two. The two EPR samples were labelled with two different fluorescent markers, FITC and RhB respectively, to evaluate the miscibility. The labelled markers used were attached to CNW, after which the CNW/FITC and CNW/RhB were incorporated into the two EPRs using 4 wt% ratios. The fluorescently labelled rubber fractions were mixed together using different ratios. The different ratios of EPR were recombined with the crystalline fraction obtained from the IPC648 by means of injection moulding. The elevated temperatures used during injection moulding caused the polymer samples to melt and flow together before injection. After injection the sample cooled down in the mould. This relatively slow cooling should allow for any separation of the rubbery phases to occur. The molecular weight of the polymer plays significant role in this step as the molecular weight influences the mobility of the polymer chains, which could contribute to phase separation. If the two EPRs are miscible in the melt, separation would be limited. The separation (or lack thereof) was evaluated by means of CFM.

6.5.1 Incorporation of fluorescently labelled cellulose nanowhiskers into rubber

Previously, there was no method available which could visually show miscibility of two different EPRs. Labelling of the EPR extracted from IPC648 and EPR (lab) extracted from the ethylene-propylene copolymer enables us to use different fluorescent molecules to differentiate between the two EPRs. This knowledge can provide a better understanding of EPR for further studies or industrial processes.

The cellulose nanowhiskers were labelled with FITC and RhB respectively, as discussed in Section 4.5. The visual observation of the light orange and light pink whiskers after freeze drying confirmed the attachment of the fluorescent dyes to the CNW for CNW/FITC and CNW/RhB respectively. The isolated freeze dried labelled whiskers are shown in Figure 6.8.

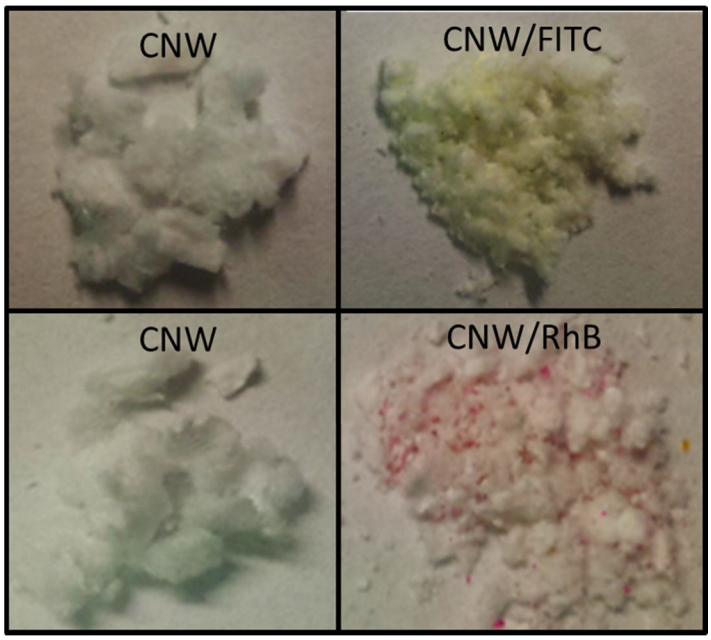

Figure 6.8: Pictures of freeze dried CNW, CNW/FITC and CNW/RhB.

The CNW/FITC were incorporated into the extracted EPR (lab) and the CNW/RhB were incorporated into the EPR extracted from IPC648. Both samples were prepared by incorporating 4 wt% of the labelled whiskers into the rubber. The EPR labelled with CNW/RhB will be referred to as EPR/RhB for the remainder of the thesis and, as previously mentioned, the labelled EPR (lab) with CNW/FITC will be referred to as EPR/FITC. Different areas of the EPR/FITC and EPR/RhB individual films were analysed by means of CFM. As the labelling of EPR/FITC was already discussed earlier in this chapter, only the incorporation of the 4 wt% CNW/RhB will be discussed in this section.

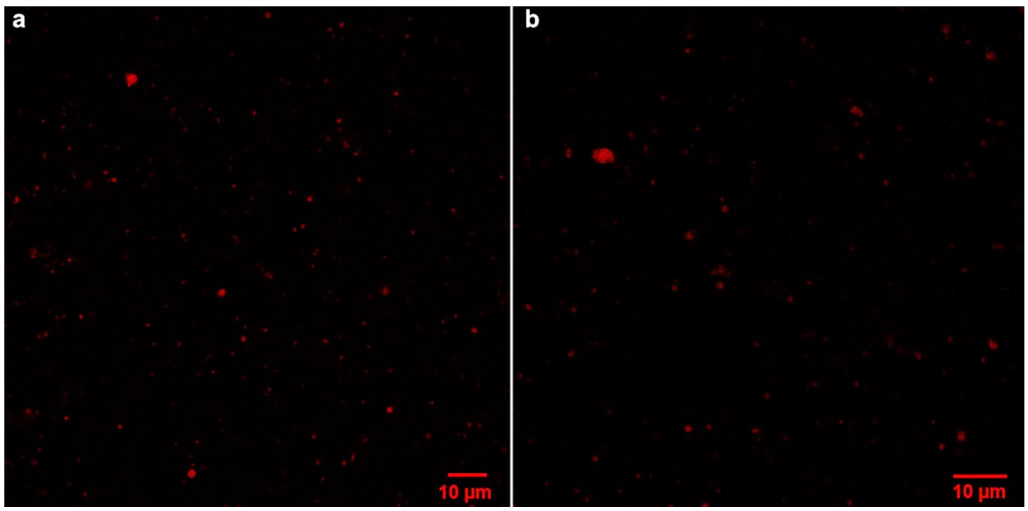

Figure 6.9: CFM images of EPR/RhB (a) Area 1 and (b) Area 2.

The CFM images obtained from the labelled EPR/RhB are shown in Figure 6.9. The two images (a) and (b) in the above figure are very similar. Both images show an even dispersion of the labelled whiskers within the EPR. This means that the CNW/RhB were dispersed throughout the film evenly and not just in certain areas. The even distribution of the labelled whiskers is an indication of the successful incorporation of the CNW/RhB into the EPR.

6.5.2 Recombination of the crystalline fraction extracted from IPC648 with the two labelled rubbers by means of injection moulding and investigating the miscibility of the two different ethylene-propylene rubbers

The two labelled EPRs were mixed together in different ratios to evaluate the miscibility of the different EPRs during injection moulding. The elevated temperatures to which the samples are exposed during the process of injection moulding cause the polymer to melt and flow together before injection. A stabilizer (2 wt%) was added to prevent degradation from occurring while the samples were exposed to the elevated temperatures in the heating cylinder. After injection the samples cooled down in the mould and were allowed time for fractionation to occur, as explained previously. The injection moulded samples were microtomed and analysed by CFM.

Three different samples were used for injection moulding. The ratios of the labelled rubber fractions used in the three samples are shown in Table 6.1.

Table 6.1: The different ratios of the labelled rubber used for recombination

Sample	EPR/RhB	EPR/FITC
Sample 1	50	50
Sample 2	75	25
Sample 3	25	75

Each of the three different samples were recombined with a crystalline fraction from IPC648. The weight percentages used for the recombination were 83 wt% crystalline fraction and 17 wt% rubber fraction. The recombined samples will be referred to as Sample 1, Sample 2 and Sample 3, according to the ratios listed in in Table 6.1 for EPR/RhB and EPR/FITC. The injection moulded samples were microtomed and the different cross sections were analysed by CFM.

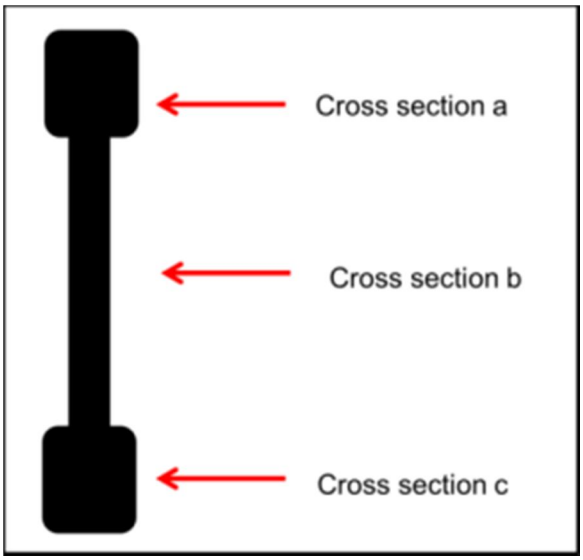

Figure 6.10: Illustration of the microtomed cross sections of the injection moulded samples

The CFM images of the three different cross sections of Sample 1 are shown below in Figure 6.11. The images in (a), (d) and (g) were taken when the sample was excited at 561 nm, (b), (e) and (h) were taken when the sample was excited at 488 nm and the images in (c), (f) and (i) were taken when the sample was excited at wavelengths of 488 nm and 561 nm.

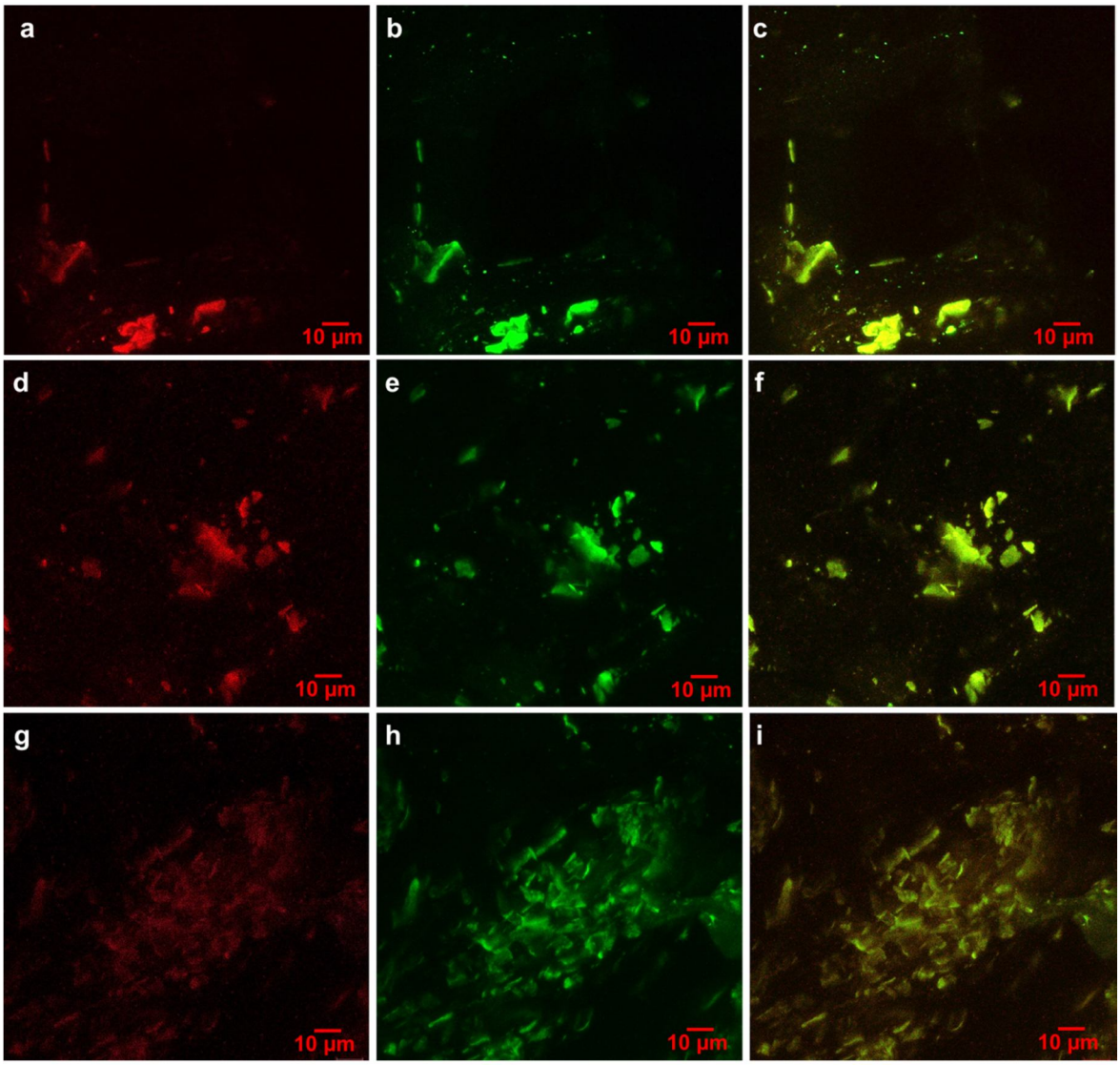

Figure 6.11: CFM images of the three cross sections of Sample 1, (a) – (c) cross section a, (d) – (f) cross section b and (g) – (i) cross section c. The CFM images of (a), (d), (g) excited by 561 nm, (b), (e), (h) excited by 488 nm and (c), (f), (i) excited by both wave lengths 488 nm and 561 nm.

Figure 6.11 (a), (d) and (g) clearly shows the fluorescent signals associated with the EPR/RhB while Figure 6.11 (b), (e) and (h) show the fluorescent signals associated with EPR/FITC. Figure 6.11 (c), (f) and (h) show the presence of both EPRs, as indicated by the slight yellowish colour. The images in (c), (f) and (h) clearly show the fluorescent signals produced by the EPR/FITC, while the fluorescent signals associated with EPR/RhB appear to be fairly weak, thus giving rise to a more yellowish appearance rather than orange.

Comparing the three different cross sections represented in the above figure, it is clear that an even distribution of the EPRs did occur throughout Sample 1. When comparing Figure 6.11 (a) with (b), the fluorescent structures seem similar. The same can be observed when comparing

Figure 6.11 (d) with (e) and Figure 6.11 (g) and (h). This indicates that the EPR/FITC and EPR/RhB are in the same vicinity and can either lie closely on top of each other, or can occupy the same space.

It is necessary to note that the EPR/RhB signals were very weak compared to the EPR/FITC and that the images obtained from the 561 nm laser in Figure 5.11 were slightly enhanced to see the structures better. At this point it can be concluded that both EPRs were present, but no definite conclusion regarding the complete miscibility of the two EPRs can be made. That said, it can be concluded that the distributions of the two labelled rubbers through Sample 1 are similar.

It was decided after analysing Sample 1 that Sample 3 will not be analysed by CFM, as in the 1:1 ratio of the EPR/FITC to EPR/RhB, the EPR/FITC signals are already too strong compared to the signals obtained for EPR/RhB . The strong signal of the EPR/FITC at a 50:50 ratio would make the likelihood of detection of the EPR/RhB in Sample 3 very low.

From Figure 6.11 it can be concluded that the recombination of the 50:50 rubber fractions and crystalline fraction using injection moulding was successful, and that the distribution is evenly spread throughout the whole sample.

The figure below shows the CFM images of the cross sections taken from Sample 2. The images were taken with the different lasers as indicated by Figure 6.12. The three cross sections show strong fluorescent signals. Images (a), (d) and (g) shows the fluorescent signals associated with EPR/RhB and images (b), (e) and (h) show the fluorescent signals associated with the excited ERP/FITC. The images shown in Figure 6.12 (c), (f) and (i) show the fluorescent signals of both the EPR/FITC and the EPR/RhB. The different cross sections all show very good fluorescent signals for both EPR/FITC and EPR/RhB. This shows that both the EPR/FITC and the EPR/RhB were successfully distributed throughout the injection moulded sample. The morphology of the fluorescent structures in Figure 6.12 (a), (d) and (g) corresponds to the morphology of the fluorescent structures in Figure 6.12 (b), (e) and (h). This is an indication that the EPR/FITC and EPR/RhB are in the same vicinity and can be due to the fact that they occupy the same space or that they are laying on top of each other, as mentioned previously. The presence of both labelled rubbers indicates that the recombination was successful.

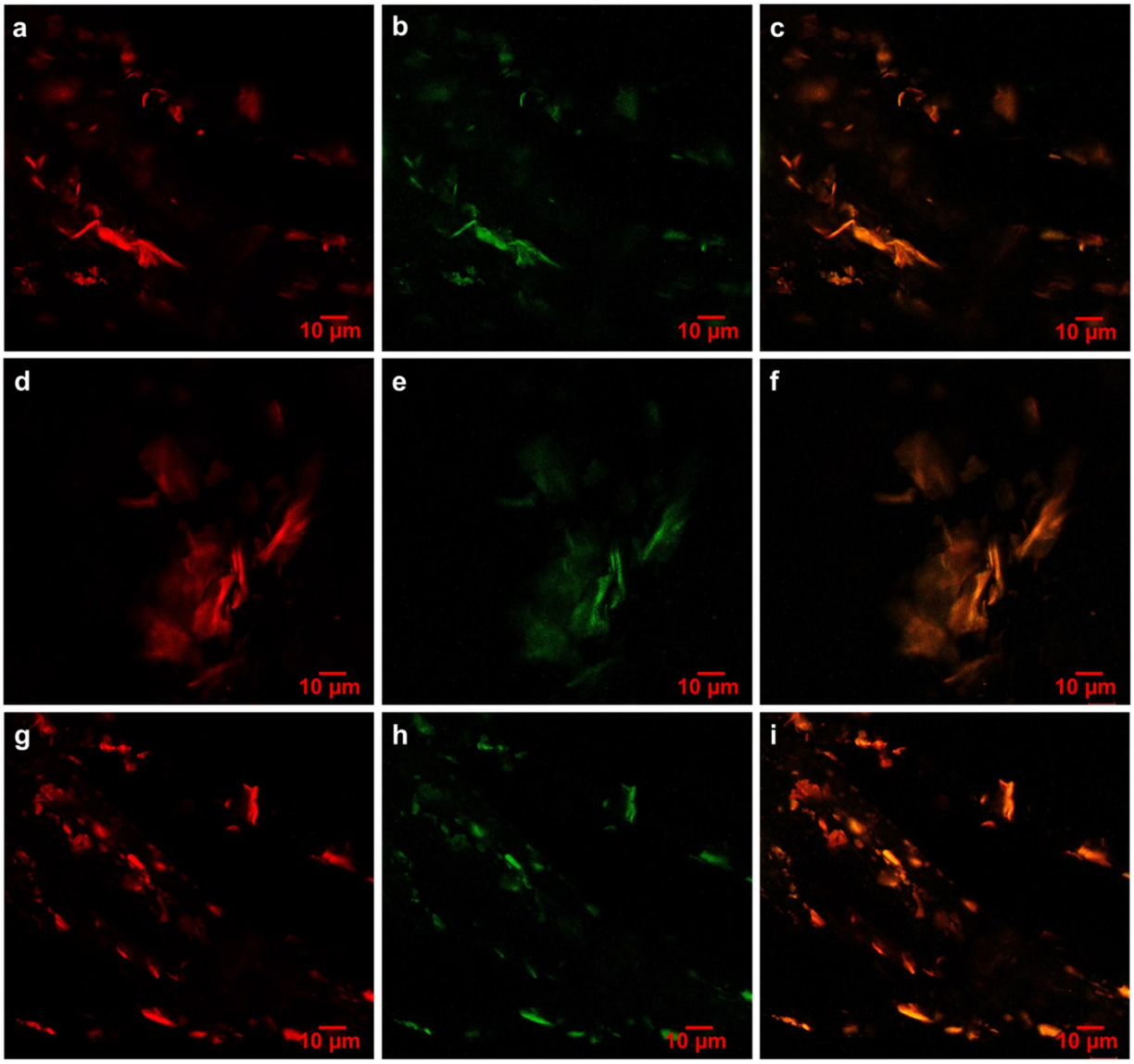

Figure 6.12: CFM images of the three cross sections of Sample 2, (a) – (c) cross section a, (d) – (f) cross section b and (g) – (i) cross section c. The CFM images of (a), (d), (g) excited by 561 nm, (b), (e), (h) excited by 488 nm and (c), (f), (i) excited by both wave lengths 488 nm and 561 nm.

The miscibility of the two EPRs is important for future studies which involves the replacement of commercial rubber with synthetic rubber. The miscibility of the two different EPRs were further investigated by CFM. Z-stack images were used to generate a 3D image of the sample. The 3D image was analysed to determine the spatial orientation of the fluorescent signals, which will enable us to draw a conclusion with regards to the miscibility of the two EPRs. The fluorescent signals present in the 2D image can be correlated with the 3D image as to where on the z-plane the signals originate from. Two different fluorophores can only give the same reading if they are bonded or coming from the same source; i.e., if the signals in the z-plane occupy the exact same space. Figure 6.13 show the 3D generated CFM images. Figure 6.13 (a) and (d) were excited by the 488 nm laser while the images in (b) and (e) were excited by the 561 nm laser. The images

obtained in Figure 6.13 (c) and (f) were excited by both lasers. Images (c) and (f) clearly shows that the fluorescent signals observed are caused by fluorophores present in the same structure. The fluorophores in this case would be the EPR/FITC and EPR/RhB, which indicates that the two labelled rubbers are present in the same structure. The two cross sections show that for the specific areas indicated in the 2D images, the EPR/FITC and EPR/RhB occupy the same area in the z-plane. If this was not the case the images obtained in (a) and (b) would not have exhibited identical fluorescent signals. The fact that there are no individual fluorescent signals from either the EPR/FITC or the EPR/RhB indicates that these labelled rubbers had to have blended together in the melt flow process and did not fractionated into the different EPRs or phase separated, once injection moulded. This is a strong indication that the EPR extracted from the commercial sample and IPC648 are miscible in the melt flow.

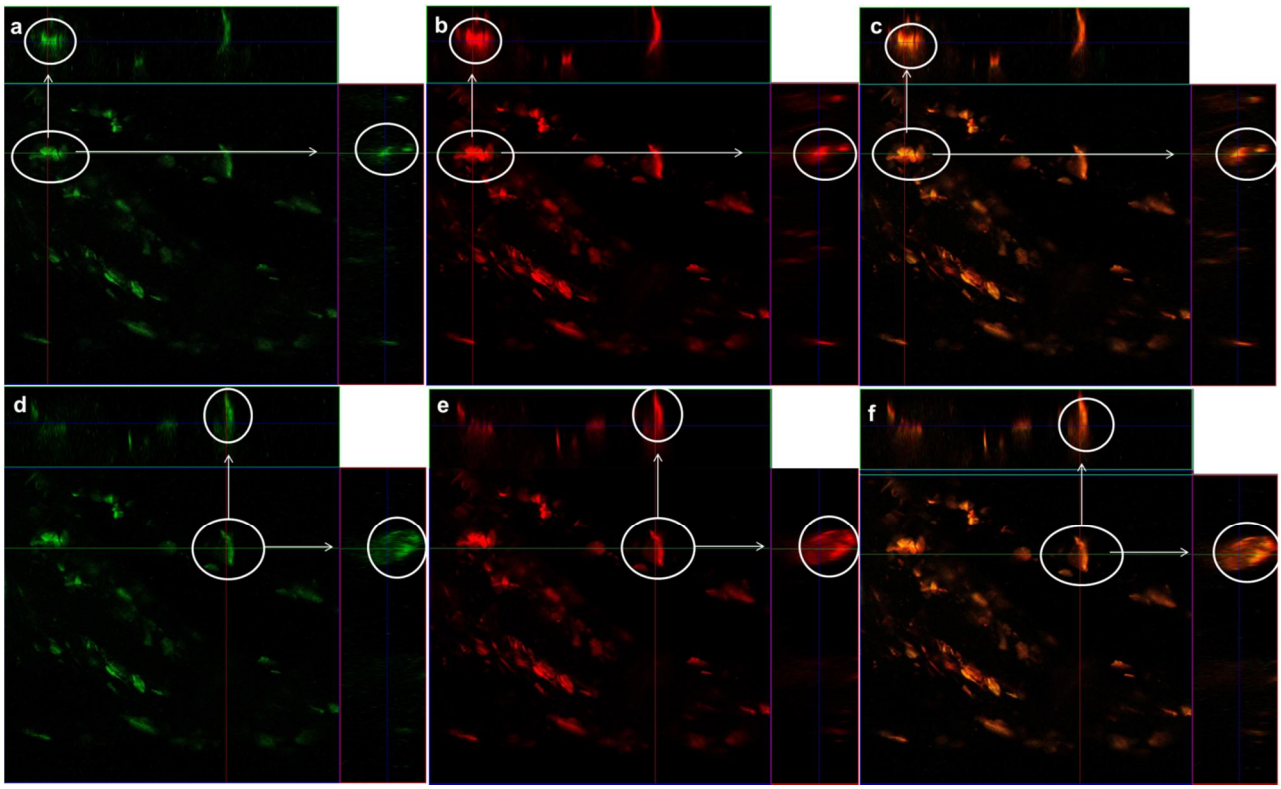

Figure 6.13: Z- stack CFM images taken from one of the injection moulded cross sections (a) and (d) 488 nm laser, (b) and (e) 561 nm laser, (c) and (f) 488 nm and 561 nm laser.

6.6 Conclusions

The DSC thermograms showed that the EPR (lab) fraction and the crystalline fraction (lab) were separated. The EPR (lab) fraction did not contain any isotactic polypropylene chains. The labelled cellulose nanowhiskers were successfully incorporated into the EPR (lab) fraction. It was possible to incorporate CNW/RhB into the EPR by following the same procedure as used for the

CNW/FITC. The CFM images showed that the CNW/FITC and CNW/RhB were evenly distributed throughout the EPR (lab) and EPR film respectively. The recombination of the EPR/FITC film and the crystalline fraction (lab) by means of injection moulding was successful. The success of the recombination of the two fractions was confirmed by the DSC analysis and CFM. The evaluation of the EPR/FITC film and the mobility of the CNW/FITC after injection moulding were analysed and confirm by CFM. The CNW/FITC stayed in the EPR/FITC film and did not migrate into the crystalline fraction.

The mixing of the EPR/FITC and EPR/RhB was successful and different ratios of labelled EPR can be used. The labelled rubbers and crystalline fractions were successfully recombined in a 17 wt% EPR and 83 wt% crystalline fraction. CFM showed that the fluorescent intensity of the FITC is stronger than RhB and therefore higher percentages would be advisable when mixing the EPR/FITC and EPR/RhB. The sample with the 75 wt% EPR/RhB and 25 wt% EPR/FITC showed better results for identifying the miscibility of the two EPR's once injection moulded. 3D CFM images showed that the two EPRs with different molecular weights are in fact miscible to some extend during injection moulding.

CHAPTER 7

Conclusions and future recommendations

7.1 Conclusion

The CNW were successfully produced by both acid hydrolysis and sonication. The dimensions and rod-like structures of the CNW were confirmed by TEM analysis. The TEM images showed better dispersion of the CNW produced by acid hydrolysis than the CNW produced by sonication. The percentage yield obtained for the CNW produced by sonication was slightly lower than for the whiskers obtained by acid hydrolysis. The XRD spectra confirmed that these nanowhiskers were produced when the amorphous regions of the MCC were compared with the amorphous regions of the CNW sample. Flow birefringence showed the chiral nematic motion of the CNW in suspension. Fluorescent spectroscopy and CFM confirmed the attachment of the FITC to the CNW. Confocal fluorescence microscopy also illustrated that the labelled whiskers are easily detectable, even in diluted suspensions.

The DSC thermograms confirmed that two fractions were obtained during separation: an EPR fraction and a crystalline fraction. The DSC did not show big differences in the T_m and T_c values indicating that removing the EPR did not affect the crystalline structure of the polypropylene. The incorporation and dispersion of the labelled CNW into the EPR was confirmed by CFM. The CFM images for all three weight percentages of the labelled CNW used showed an even distribution throughout the whole EPR film. The 6 wt% fraction seemed to cause agglomeration of the CNW/FITC due to the strong hydrogen bond interactions between the whiskers. An evaluation of the three weight percentages of the CNW/FITC (4 wt%, 5 wt% and 6 wt%) concluded that the 4 wt% was the best suited for the research. The 4 wt% CNW/FITC was easily detectable and displayed evenly distributed fluorescent signals with the lowest tendency to agglomeration. Confocal fluorescent microscopy confirmed that the overall movement of the labelled whiskers inside the EPR film was very limited.

The recombination of the labelled EPR and crystalline fraction by means of injection moulding proved to be successful. When compared, the DSC thermograms of the recombined sample and the original IPC648 revealed a slight shift in the crystallization and melting temperatures. An investigation into the mobility of the labelled whiskers showed very limited movement, and the whiskers seemed to stay in the EPR in which they were incorporated.

The CFM images showed the well dispersed fluorescent signals throughout the injection moulded sample. Upon further investigation, the CFM images obtained before and after the extraction of the labelled EPR from an injection moulded sample confirmed that the whiskers stayed in the EPR. The decrease in fluorescent intensity confirmed that the labelled whiskers were extracted along with the EPR, which indicates that the labelled whiskers stayed within the EPR phase, and confirmed that the labelled EPR was dispersed throughout the injection moulded sample.

The ethylene-propylene copolymer sample was separated into the EPR (lab) fraction and the crystalline fraction (lab), which was confirmed by the DSC. The CNW/FITC were incorporated into the EPR (lab) fraction. An even distribution of the labelled whiskers throughout the EPR film was observed.

The recombination of the EPR/FITC film and the crystalline fraction (lab) by means of injection moulding was successful. The distribution of the EPR/FITC inside the injection moulded sample was analysed by CFM, which confirmed that the rubber was evenly distributed throughout the whole sample. The evaluation of the EPR/FITC film and the mobility of the CNW/FITC after injection moulding were also analysed and confirmed by CFM. The CNW/FITC stayed in the EPR/FITC film and did not migrate into the crystalline fraction.

Rhodamine B was successfully attached to the CNW and the CNW/RhB were evenly and well dispersed in the EPR. The EPR (lab) fraction and the EPR fraction were labelled successfully with CNW/FITC and CNW/RhB, as the CFM images showed. The mixing of the EPR/FITC and EPR/RhB was successful and the recombination of the labelled rubbers and crystalline fraction was confirmed by means of CFM. The CFM images showed that the fluorescent intensity of the FITC is stronger than RhB and therefore higher percentages of CNW/Rhb would be advisable when mixing EPR/FITC and EPR/RhB. The sample with the 75 wt% EPR/RhB and 25 wt% EPR/FITC showed better results for identifying the miscibility of the two EPRs once injection moulded. The 3D images obtained from CFM indicated that the EPRs were miscible.

7.2 Recommendations

The method of recombination can be improved by optimizing the EPR particle size closer to a powder form.

Use other ethylene-propylene copolymers for the extraction of EPR to create a better reference point of miscibility. It is also advisable to determine optimum ratios for the mixing of the two labelled rubbers.

7.3 Future work

Labelling a semi-crystalline fraction with a fluorescent marker can contribute to the understanding of the distribution of this fraction with regards to isotactic polypropylene and EPR. It will also be feasible to investigate the phase interaction of the different fractions. This can be done by labelling the EPR and semi-crystalline fraction with two different fluorescent molecules like FITC and RhB. Confocal fluorescent microscopy can be used to analyse the recombined samples to investigate the different distribution patterns of the two fractions. This can be of great value in understanding the interaction between the different phases.